REMODELLING THE CAVITY OF A TRANSMEMBRANE PORE BY GENETIC ENGINEERING

A Dissertation

by

YUN HEE JUNG

Submitted to the Office of Graduate Studies of
Texas A&M University
in partial fulfillment of the requirements for the degree of

DOCTOR OF PHILOSOPHY

May 2005

Major Subject: Medical Sciences

REMODELLING THE CAVITY OF A TRANSMEMBRANE PORE BY GENETIC ENGINEERING

A Dissertation

by

YUN HEE JUNG

Submitted to the Office of Graduate Studies of
Texas A&M University
in partial fulfillment of the requirements for the degree of

DOCTOR OF PHILOSOPHY

Approved as to style and content by:

Hagan Bayley (Co-Chair of Committee)	Nick Pace (Co-Chair of Committee)
Arthur E. Johnson (Member)	David Giedroc (Member)
	J. Martin Scholtz (Interim Head of Department)

May 2005

Major Subject: Medical Sciences

ABSTRACT

Remodelling the Cavity of a Transmembrane Pore

by Genetic Engineering. (May 2005)

Yun Hee Jung, B.S., Seoul National University;

M.S., Seoul National University

Co-Chairs of Advisory Committee: Dr. Hagan Bayley
Dr. Nick Pace

The cavity within the transmembrane staphylococcal α-hemolysin (αHL) pore is roughly a sphere of diameter ~45 Å (volume ~32,600 $Å^3$). The alpha-hemolysin gene was modified to introduce exogenous polypeptide sequences between positions 105 and 106 of αHL. These modified αHLs were assembled either by themselves or with wild-type (W) subunits to form stable homoheptamers and heteroheptamers, respectively. First, the ability to accommodate Gly/Ser-rich polypeptide sequences in the central cavity was tested. Concatemerized Gly/Ser-containing sequences ("loops", L; L(10n + 5), n = 0 to 21) were inserted by genetic approaches. Detailed analysis of bilayer recordings and electrophoretic migration patterns of assembled pores indicate that the upper capacity of the cavity is ~175 amino acids. Then two different polypeptides were placed in the cavity to introduce novel functional properties to the αHL pore. By introducing tandem repeats of elastin-like polypeptide sequences (VPGGG), αHL pores ($E10_1W_6$) that featured a temperature-responsive gating mechanism were obtained. The temperature-dependent properties of $E10_1W_6$ pores were monitored by single-channel

current recording in planar lipid bilayers. The amplitude and the frequency of the transient blockades increased as the temperature increased, while their duration decreased. The hydrophobic collapse of the inserted ELP loop is proposed for the source of the observed sigmoidal two-state transition for normalized closed states of $E10_1W_6$ pores. Lastly, an αHL pore was designed to detect proteins from the cis side of the membrane. The heat-stable protein kinase inhibitor (PKI) sequence was inserted into the mid-position of the Gly/Ser loop, which was generated by previous project (L105 construct). The heteromeric pore with the PKI-containing loop ($P115_1W_6$) was able to detect cAMP-dependent protein kinase catalytic subunit (PKA) at single molecular level. These engineered αHL pores provide numerous possibilities as tools for drug delivery, cryopreservation, or molecular sensing.

ACKNOWLEDGEMENTS

I would like to express a deep gratitude and admiration to my advisor, Dr. Hagan Bayley, for his guidance in both scientific and non-scientific areas during my graduate study. I would also like to thank the senior members of the lab, Dr. Stephen Cheley and Dr. Orit Braha, for their time and expertise to discuss every day experimental difficulties I encountered. I would like to thank Drs. Liviu Movileanu and Hongzhi Xie for collaborations on biophysical experiments. I treasure my past and present members of the Bayley lab, who all have contributed to my graduate work, either by engaging in helpful discussions or by giving me the other life I needed to finish my research. The staffs of the Medical Biochemistry and Genetics Department have been a valuable service over the years, especially true for Janis Chmiel, who helped me to go through the graduation requirements. Finally, I would like to thank to my families for all their support over the years.

TABLE OF CONTENTS

CHAPTER Page

LIST OF FIGURES

FIGURE Page

FIGURE Page

LIST OF TABLES

CHAPTER I

INTRODUCTION

The α-hemolysin (αHL) pore is an exotoxin secreted by *Staphylococcus aureus*. It is secreted as a water soluble monomeric form and assembles into a mushroom-shaped pore with known three-dimensional structure (*1*) on susceptible cell membranes (*2*). The pore has been useful for fundamental studies of membrane protein assembly and function. Furthermore, it can be applied in biotechnology to prepare sensors (*3*) or to make for tools to permeabilize cells for the introduction of cryoprotectants (*4*). The pore has also been used as a nanoreactor to observe covalent chemistry at the single molecule level (*5*).

αHL is a robust pore, e.g. it is stable up to 65ºC in the presence of SDS (*6*). This characteristic simplifies purification procedures for assembled αHL pore for single channel recordings. The structure of the heptameric pore is known in detail and the monomeric structure can be predicted from the structures of leukocidins, which are in the same class of β-barrel pore forming toxins (*7-10*). Furthermore, single channel electrical recordings are capable of analysing events on the microsecond time-scales, even with a minute amount of the protein. These features suggested αHL as the best

---

This dissertation follows the style and format of *Biochemistry*.

candidate for the present study, which involves redesigning a membrane pore.

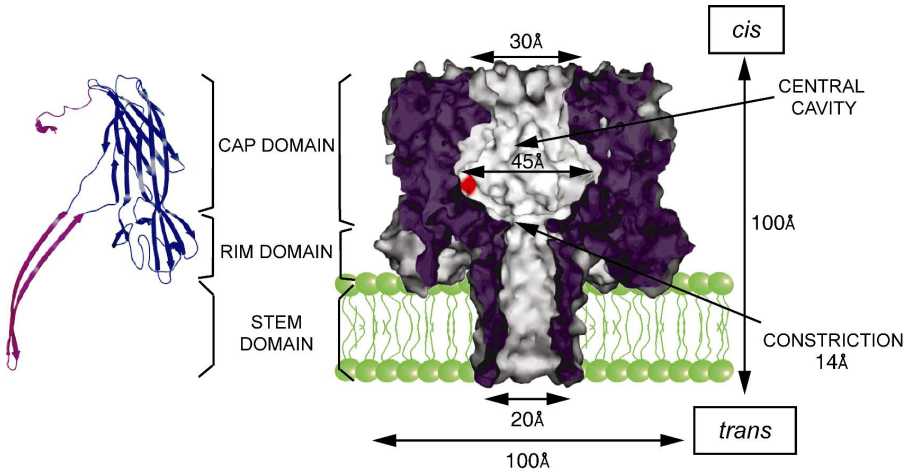

Figure 1. Structure of alpha-hemolysin and dimension of heptameric pore.

Left. αHL protomer from the fully assembled pore consists of three domains, cap, rim and stem domains. The cap and rim domains reside on the extracellular surface of the membrane. The stem domain is composed of a 14-strand antiparallel β-barrel and defines the transmembrane domain of the pore. *Right*. A transverse section through the heptameric pore (7AHL) in a lipid bilayer. The widest region of the central cavity is ~45 Å in diameter while the narrowest region, 'the constriction', is only 14 Å in diameter. One of the seven Ser residues at position 106, where all the insertional mutations were generated for this study, is shown in red.

Alpha-Hemolysin (αHL)

Structures of αHL: fully assembled heptameric pore and water-soluble monomer

The structure of the heptameric, active form of alpha-hemolysin (αHL) has been determined in the presence of detergent micelles (*1, 11*) at ~1.6 Å resolution. αHL is secreted as a monomeric water-soluble protein and assembles into a mushroom shaped heptameric pore on susceptible membranes (*2, 12*). The alpha-hemolysin pore comprises

cap, rim and stem domains (Figure 1) (*1*). The cap domain consists of β sandwiches and amino latches, one of each contributed by each protomer. The rim domain (three β strands per protomer) lies just beneath the cap domain and in direct and/or indirect contact with the outer leaflet of the membrane bilayer. The cap and rim domains reside at the extracellular surface of the membrane. The stem domain is composed of a 14-strand antiparallel β-barrel and defines the transmembrane domain of the pore. A water-filled channel runs through the pore with non-cylindrical shape along the axis of molecular symmetry (*11*). The diameter of the channel ranges from 45 Å for the widest region in the cap to 14 Å for the narrowest region, known as the constriction (Figure 1). The opening of the pore at the cis side of the bilayer measures 30 Å in diameter and on the trans side 20 Å.

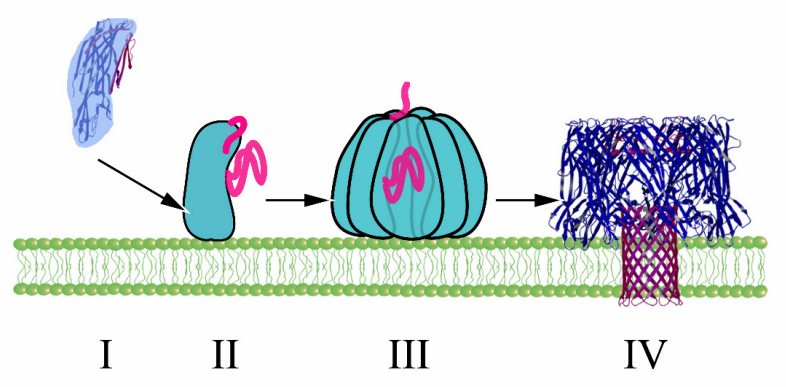

Figure 2. Assembly process model of αHL pore.

Assembly from a secreted soluble monomer to membrane-bound hemtameric pore. αHLs assemble from a soluble monomer (I) to form a putative membrane bound monomer state (II). This is followed by the formation of a prepore (III), which is finally transformed into the fully assembled pore (IV). The stem domain (residues 110-150) and the N-terminus (pink) are illustrated in pink where major conformation changes occur during assembly. The structures of water soluble-monomeric state is modeled with leukocidin monomer structure (1PVL). The heptameric pore structure (7AHL) was generated by SPOCK . This model was adapted from the work by Montoya M and Gouaux E.(*2*).

Assembly process

Several studies support the idea that the mechanism of αHL assembly is in four stages (Figure 2) (*2, 13-15*). There is no structural information for the water-soluble monomeric form of αHL. But taking into account the fact that the core (i.e. excepting amino-latch region and pre-stem domain) of the water-soluble monomeric form of both leukocidin F (LukF) and leukocidin S (LukS) subunit are very similar to the αHL protomers (*9, 16, 17*), the structures of these monomers (Figure 3) are generally presumed to resemble the monomeric structure of αHL, even though the sequence identity is only ~20-30%(*18*) between the αHL and the leukocidin monomers (*9*). αHLs are secreted as water-soluble monomers (I). Upon binding to a susceptible membrane bilayer, membrane-bound monomers (II) associate to form the pre-pore (III). The pre-stem region of the pre-pore then extends through the bilayer to generate the SDS-stable heptameric pore. The amino-latch and pre-stem region are sensitive to proteolysis, at Lys-8 and Lys-31, respectively. During the assembly pathway, the pre-stem region in the pre-pore state (III) shows resistance to proteolysis, indicating encapsulation of the pre-stem region inside cap domain. However, the amino-latch remains sensitive in the pre-pore state (III) (*15, 19*). The pre-pores can be dissociated to monomers by sodium dodecyl sulfate (SDS), even at room temperature (*13*). In contrast, fully assembled heptameric pores are stable in SDS even at elevated temperature (~ 65ºC) (*13*). In the heptameric state, both the amino-latch and stem regions are resistant to proteolysis (*13*). Biophysical studies with covalently attached fluorescent probes (*12, 13*) and

biochemical studies on site-directed cysteine αHL mutants (*20, 21*) also confirmed this assembly mechanism model.

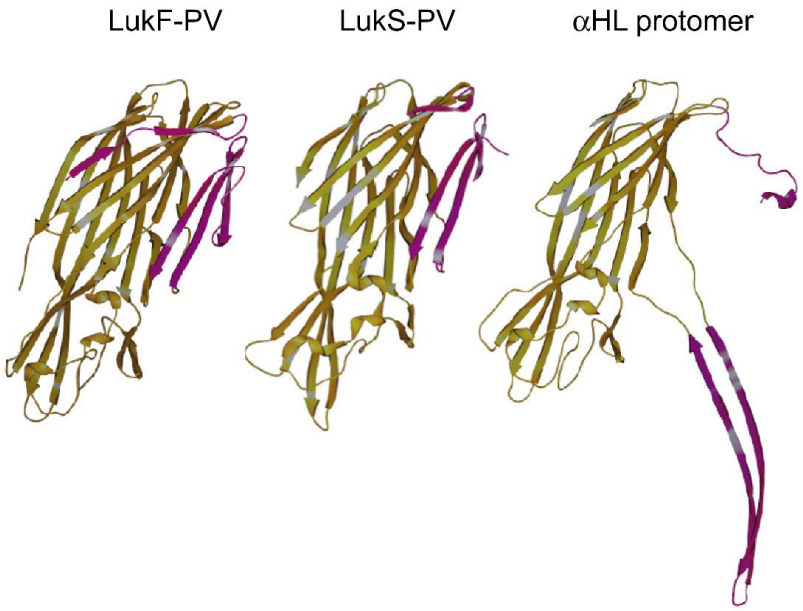

Figure 3. The structures of a αHL protomer and leukocidin monomers.

The Panton-Valentine leukocidin monomers, LukF-PV (1PVL) and LukS-PV (1T5R), from *Staphylococcus aureus* share very similar structure with an αHL protomer removed from the structure of the fully assembled αHL heptamer. The amino latch and the stem (prestem for the leukocidin monomers) domains are illustrated in violet.

Protein engineering of αHL and applications in biotechnology

αHL has been used for a variety of applications in the biotechnology. Placement of a pentahistidine sequence at stem region (130-134) of αHL created a gating mechanism, controlled by the presence of divalent metal ions (*22*). αHL-H5 mutant (*15*), together with H35C mutant (*6*), were further studied to elucidated the assembly process.

αHL-H5 mutant was arrested at the prepore state when Zn(II) ions were presented. The prepore was proved to be a heptamer. This was the first time that an intermediate state in an assembly process had been achieved by the simple introduction of a metal binding motif (pentahistidine) into the stem domain. Related metal-binding αHL mutants were developed for stochastic sensing of divalent metal ions (*23*). Various divalent metal ions bind reversibly to four engineered histidine residues near the turn of trans opening (residues 123, 125, 133 and 135) producing characteristic electrical traces. This behavior allowed the sensing of different concentrations of the metal ions simultaneously. αHL has also developed as a sensor for organic molecules. One or two cyclodextrin lodged in the β-barrel can detect a variety of guest molecules, (*24, 25*) at single molecular level. In another case, the simple introduction of seven or fourteen arginine residues near the constriction region, allowed αHL to be used to detect the important cellular second messenger inositol 1,4,5-trisphosphate with nanomolar affinity (*26*).

Most of these modifications were placed at or near the β-barrel region. Recently, cysteine residues were placed near the cis-opening of the pore for the attachment of single strand DNA. The resulting DNA-αHL pore can sense duplex formation between the tethered DNA and the complementary DNA strand by changes of ionic current flow (*27*). In another approach, Gal-β-1,3-GalNAc was attached at the cis-mouth of the pore at position 9, to detect a lectin protein (*28*). Through single channel current recordings, divalent binding events could be distinguished from monovalent binding.

Other positions engineered for the detection of molecules are the cap domain of the αHL pore, which is directly related to the present work. A single flexible biopolymer chain, polyethylene glycol 5.0 kDa (PEG 5K) was tethered at the Ser106Cys position through a disulfide bond (*8*). Interestingly, heptamers with two or more PEG chains did not form.

Besides chemical modification or point mutation, more drastic genetic engineering has also been performed on the αHL protein. The residues (25 residues) of the stem domain have been reversed by cassette mutagenesis (*29*). The pore with the reversed transmembrane domain (retro-αHL) exhibited a slightly reduced conductance and a symmetrical behavior with current-voltage relationships. The slightly assymetrical current-voltage relationship is one of the characteristics of the αHL pore. In other words, the αHL pore exhibits slightly high current amplitude at postive voltage than at negative voltage. Furthermore, when entire 25 amino-acid stem residues were removed, the mutant αHL (TCM) would still assemble into heptamers as confirmed by atomic force microscopy (*14*). The retro-αHL and TCM mutants suggested an extraordinary plasticity of alpha-hemolysin which might be very useful for the redesign of the αHL pores.

Other non-covalent modifications of the pore were designed as tools for single molecule DNA sequencing (*30*). Furthermore, the αHL pore has also been used as a nanoreactor to observe covalent chemistry at the single molecule level for the first time (*5*).

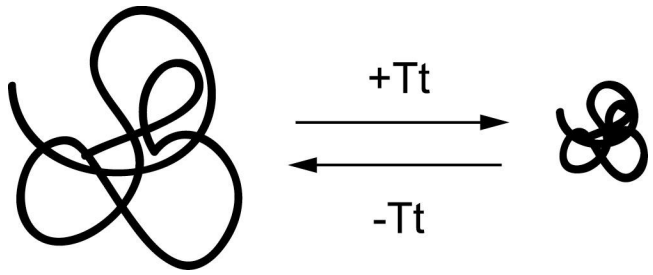

Figure 4. Elastin phase transition with temperature.

ELP is known to undergo phase transition with temperature. At higher than transition temperature, ELP changes into dense structure, due to hydrophobic collapse. At below transition temperature, ELP changes into bulky ball by swelling.

Elastin-like Polypeptide (ELP) Repeats

The protein elastin is well known for its elasticity and resilience, which is used in many tissues. Native elastin motif VPGVG repeats more than eleven times in the native elastin polypeptides (*31*). Based on the native elastin pentapeptide, many designed elastin-like polypeptides (ELPs) have been made, which are composed of tandem repeats of the pentapeptide motif Val-Pro-Gly-X-Gly (where the 'guest' residue can be any amino acid except Pro) (*32, 33*). ELPs are known to undergo inverse temperature transitions, that they aggregate above a transition temperature (Tt) but remain in solution at below Tt (Figure 4) (*34, 35*). Tt is defined as the temperature at which the half-maximal turbidity is observed. A proposed model for the inverse transition is based on a hydrophobic collapse which bound water is shed (*33, 36, 37*).

The inverse transition temperature can vary with intrinsic and extrinsic parameters (*32*). Intrinsic factors can be the identity of the guest residue, or the length of

the polymer chain. If alanine is introduced instead of valine as guest residue, Tt becomes higher than that recorded for native repeats with same length (*38, 39*). For polar amino acids (e.g. asparate) as the guest residues, a drastic increase of Tt (~45ºC) was observed (*38, 40*). The same increase in Tt was observed with longer polymers with same guest residue (*33, 41*). Extrinsic factors are salt concentration, pH, or pressure (*38, 42, 43*). By adding sodium chloride to solution, it lowered the Tt value by 14ºC per 1N of NaCl. If the guest residue is an ionizable amino acid, such as Asp, Glu, or Lys, the pH of solution can change Tt. Lowering the pH to protonate a carboxyl side chain favors hydrophobic collapse of the polymer even at lower temperature. Based on these fascinating characteristics of elastin-based polymers, numerous applications of ELP in biotechnology and medicine have been proposed (*44-47*).

Cyclic AMP-dependent Protein Kinase and Inhibitor

Reversible protein phosphorylation is involved in many processes that occur in the cell. The most important role of phosphorylation is regulatory mechanisms to respond to external stimuli or stress. cAMP dependent protein kinase (PKA) is one of the most well-studied of a very diverse protein kinase family. It is composed of two components, two regulatory subunits and two catalytic subunits, which dissociate upon activation by cAMP (*48*). Cooperative binding of cAMP to regulatory subunit triggers a conformational change that releases the catalytic subunits. The heat-stable protein kinase inhibitor (PKI) serves as a physiological inhibitor of the catalytic subunit. PKI is a small protein that is unstructured in solution (*49*). There are several tissue-specific and cell-

cycle specific isoforms (*50, 51*). It binds to the catalytic subunit with high affinity (the dissociation constant = 0.2 nM), in the presence of ATP (*52*).However, PKI has a dissociation constant (Kd) of 230 nM in the absence of ATP (*53*). The tight binding of PKI in the presence of ATP also requires divalent metal ions (Mn(II), Mg(II)) to mediate interactions between ATP and side chains of the catalytic subunit (*54*).

The inhibitory binding sites are localized at the N-terminus of PKI (positions 5-24). The identification of this high affinity peptide fragment facilitated the crystal structure determination of PKA catalytic subunit-PKI complexes with 2.0-2.9 Å resolution (Figure 5A) (*55-57*). PKI is believed to be disordered in solution based on circular dichoism, fluorescence (*58*), and NMR (*49*) (Figure 5B). There are only two helical regions, 5-12 and 35-47. The N-terminal helix (inhibitory binding helix, 5-12, red) forms a hydrophobic patch (Tyr 7, Ile 11, Phe 10), which is important residues for tight binding to PKA catalytic subunit. The patche is followed by consensus Arg-rich sequences (Arg 15, Arg 18, and Arg 19) for active site binding (Figure 5B, pink) (*59, 60*). This region undergoes confirmational changes upon binding to the catalytic subunit (*49*).

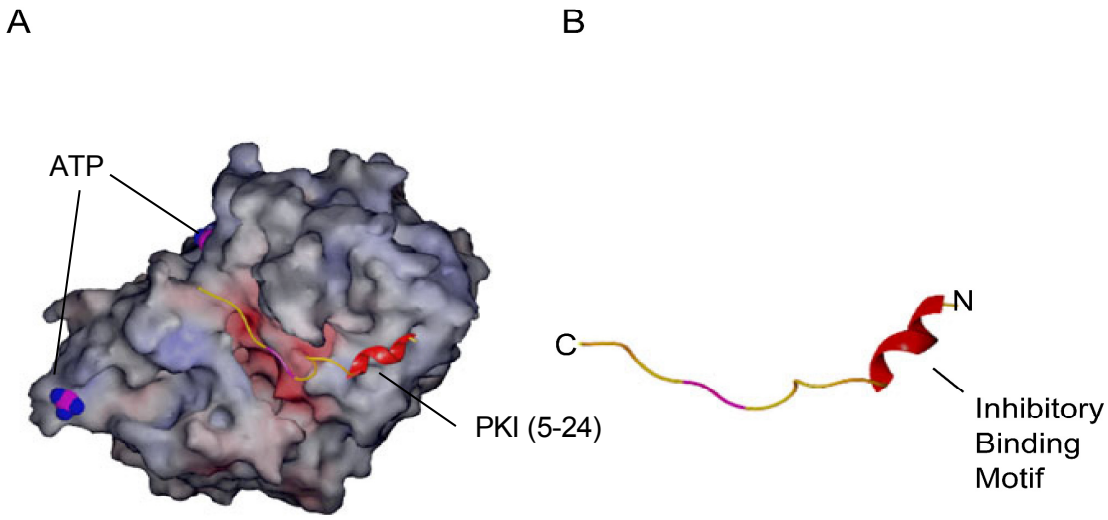

Figure 5. Structure of cAMP-dependent protein kinase catalytic subunit complexed with protein kinase inhibitor peptide.

(A) The strucutre of the PKA catalytic subunit (1ATP) with a bound PKI fragment (5-24) and ATP. The heat-stable PKI is shown as ribbon structure. (B) The tight inhibitory binding modif of the PKI fragment is represented in red, and conserved arginines (Arg 15, Arg18, and -Arg19) are in pink.

Recently in Dr Bayley's group, the interaction between a PKI fragment tethered to αHL and the PKA catalytic subunit was demonstrated in detail at single molecular level (*61*). The PKI polypeptide was attached to Thr129Cys of αHL pore, located near the trans mouth, by chemical modification. Ionic flow through the modified pore was monitored in single molecular level. Upon binding of the PKA catalytic subunit, transient blockade of electrical currents were observed. The dwell time, frequency, and amplitude of the blockade revealed a binding affinity of PKI to the PKA catalytic subunit with a comparable value to that obtained by traditional measurement. This

approach demonstrated another way to sense protein anlalytes at the single molecular level by using engineered αHL pores.

Staphylococcus aureus

Staphylococci are Gram-positive bacteria, which are normally found on the nasal passage or the skin of normal humans, and mammals (*62*). Based on the pigments produced by the bacteria, there are two species, *Staphylococcus aureus* (yellow) and *Staphylococcus epidermidis* (white). *Staphylococcus aureus* is the most commonly isolated species from affected rabbits and is a major cuase of hospital acquired infections of humans (*63*). It can be spread by direct contact or by aerosol and can reside in the nasal sinuses or lungs without showing any apparent disease. Even though the staphylococci infections are common, it usually retained at the entry points (skin, or nasal passage) by the host defense mechanisms. However serious infection can be caused through invasion to the blood stream, which quickly leads to skin lesions, infections in the lung, kidney, or heart. *S. aureus* produce many virulence factors which are mostly extracellular proteins that promote adherence, degrade host compounds, or damage host cells. The mechanism of pathogenesis for the disease caused by *S. aureus* is multifactorial (*63*). Therefore the mode of virulence factors is not yet fully understood.

S. aureus express several different types of membrane-damaging toxins, which are probably serve as the mechanism for the host invasion. There are three types of toxins secreted, alpha, delta, and leukocidins. Some are hemolytic on susceptible cells

(platelets, monocytes) which do not correlate to the virulence in vivo. For example, leukocidins, which are found mostly in the severe dermonecrotic lesions, cause membrane damage to leukocytes, but they are not hemolytic (*64*).

Other clinically important information about Staphylococci is the resistancy to various antibiotics with the hospital strains of *S. aureus*. The methicillin resistant *Staphylococcus aureus* (MRSA) develop drug resistance, which refer to "Superbug" (*65*). The mode for the drug resistance is by either mutation in the chromosomal mutation or by acquisition of extrachromosomal DNA inserts (transposons, plasmids), which is triggered by unknown factors. MRSA are responsible for the half of the hospital related infections (*66*). With more concern, *S. aureus* gained resistance to many common antibiotics, even the most powerful drug, vancomycin, within 60 years of penicillin introduction. Therefore urgent need for new drug molecules were evident to fight against MRSA. Recently, RNAII-inhibiting peptide (RIP) was tested on several animal models to test the inhibition of the MRSA strain infections (*67*). RIP is preventing the signal transduction pathway of the bacteria extracellular communication system (quorum sensing system), which is essential for the initial colonization of bacteria and for the downstream virulence factor activation (*68, 69*).

Other Pore-forming Bacterial Toxins

Membrane proteins, which span across the lipid bilayer to create a pathway for molecules across the membrane barrier, are usually referred to either pores or ion-

channels. Strictly speaking, the ion-channels represent pores that are highly specific to a particular ion. On the other hand, the pores are lack of the permeant specificities. Here, the pores (mainly pore-forming toxins) will be discussed.

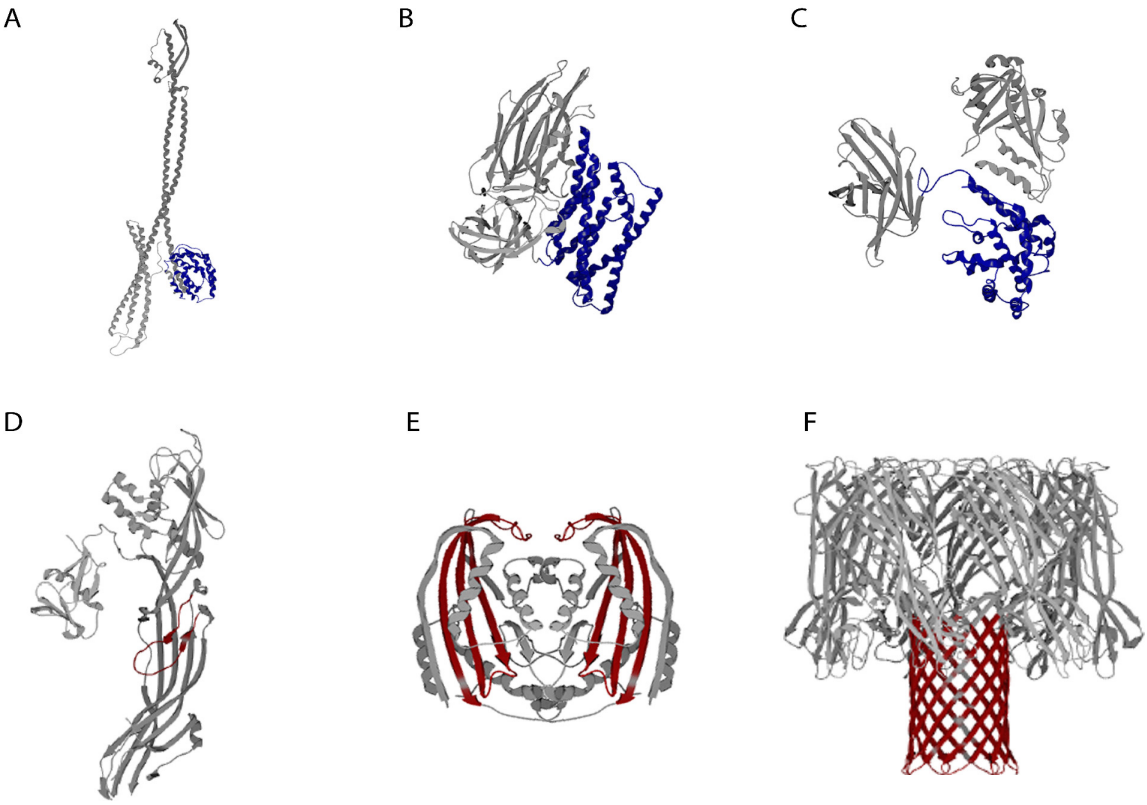

Figure 6. Ribbon representation of PFT structures.

The putative transmembrane domains are colored in blue (α-PFT) and in red (β-PFT). α-PFTs are (A) Colicin Ia, (B) Cry insecticidal δ-endotoxin, and (C) Diphtheria toxin. β-PFTs are (D) Proaerolysin monomer from *Aeromonas hydrophila*, (E) CytB δ-endotoxin dimmer from *Bacillus thuringiensis*, and (F) α-hemolysin heptamer from *Staphylococcus aureus*. All figures were generated by SPOCK.

Based on the structural feature of the transmembrane domain, pore-forming toxins (PFTs) are classified into two types, α-PFTs and β-PFTs, which are composed of

alpha helices and beta-barrel, respectively. Some of the α-PFTs are colicin (Figure 6A) from various *E. coli* (*70*), insecticidal δ-endotoxin (Figure 6B) from *Bacillus thuringiensis* (*71*), and diphtheria toxins (Figure 6C) from *Corynebacterium diphtheriae* (*72*).Also an apoptic protein of Bcl-2 family forms a pore in similar mechanism as α-PFTs (*73*). The other pore-forming toxins are β-PFTs. These toxins are mainly composed of β-sheets. Aerolysin (Figure 6D) from *Aeromonas* species (*74*), *Bacillus thuringiensis* CytB δ-endotoxin (Figure 6E) (*75*) and *Staphylococcus aureus* α-hemolysin (Figure 6F) are some of the β-PFTs.

These PFTs are secreted as water-soluble monomeric forms and then targeted to the susceptible cells using the host cell surface molecules (sugar, protein, or lipids) as their receptor. It is generally thought that the receptors serve as anchor to concentrate the toxins on the cell surface, and further facilitate the toxins to oligomerize and finally puncture holes in the membrane. The transmembrane domain of α-PFTs is hydrophobic which is hidden inside of the protein at the water-soluble state. However the transmembrane domain of β-PFT is amphiphillic. Therefore during the pore-forming step, it is logical to assemble as oligomers and enclose the polar edges of β-hairpins to generate a β-barrel. The actual mechanisms of the transmembrane domain penetration to the lipid bilayer are not fully understood for α-and β-PFTs. For α-PFT, the α-helices spread over the membrane surface and then insert to the membrane, which is called the umbrella mode (*76*). For β-PFT, the membrane spanning pre-stem (β-hairpin) region form extensive hydrogen bonding to generate a β-barrel. A few structures of these PFT

are illustrated in Figure 6.

Besides PFT and ion-channels, there are ionophores, which transports certain ions across the membrane. Ionophores are produced by bacteria to protect themselves against other bacteria. Therefore, they are used as antibiotics. There are two types for ionophores, carrier and channel. The carrier is the molecule encapsulate the ions and carry them from one side of the membrane to the other side of the membrane (Figure 7A). The channel is the molecule that spans the membrane and transports ions (Figure 7B). Valinomycin and Gramicidin are the best characterized carrier and channel type ionophores, respectively (Figure 7A,B).

Valinomycin is a cyclic dodecadepsipeptides, cyclo[-(L-Valine-D-Lactic acid-L-Valine-D-Hydroxy-isovaleric acid)$_3$-] from *Streptomyces*, which carries selectively potassium ions across the membrane (*77*). The alternating amino acid and hydroxy acid sequences compose a bracelet shaped ring. The potassium ion is placed in the center of the cyclic peptide ring and coordinates with six carbonyl oxygens of the amino acids (Figure 7A) (*78-80*). On the other hand, the exterior surface of the valinomycin-K^+ complex is hydrophobic, which facilitates the valinomycin to enter the lipid bilayer freely. By changing the sequence of the valinomycin resulting the ring expansion, larger ion specificity was introduced (*81*).

Antibiotic gramicidin is secreted from *Bacillus brevis* to make channels on Gram-positive bacteria membrane for defense mechanism. It translocates monovalent cations specifically, such as H^+, Tl^+, and alkali metals (*82*), which is composed of alternating D and L amino acids. Two molecules of gramicidins form the channel, which

undergo alignment change for open and close state-transition (Figure 7B,C) (*83*).

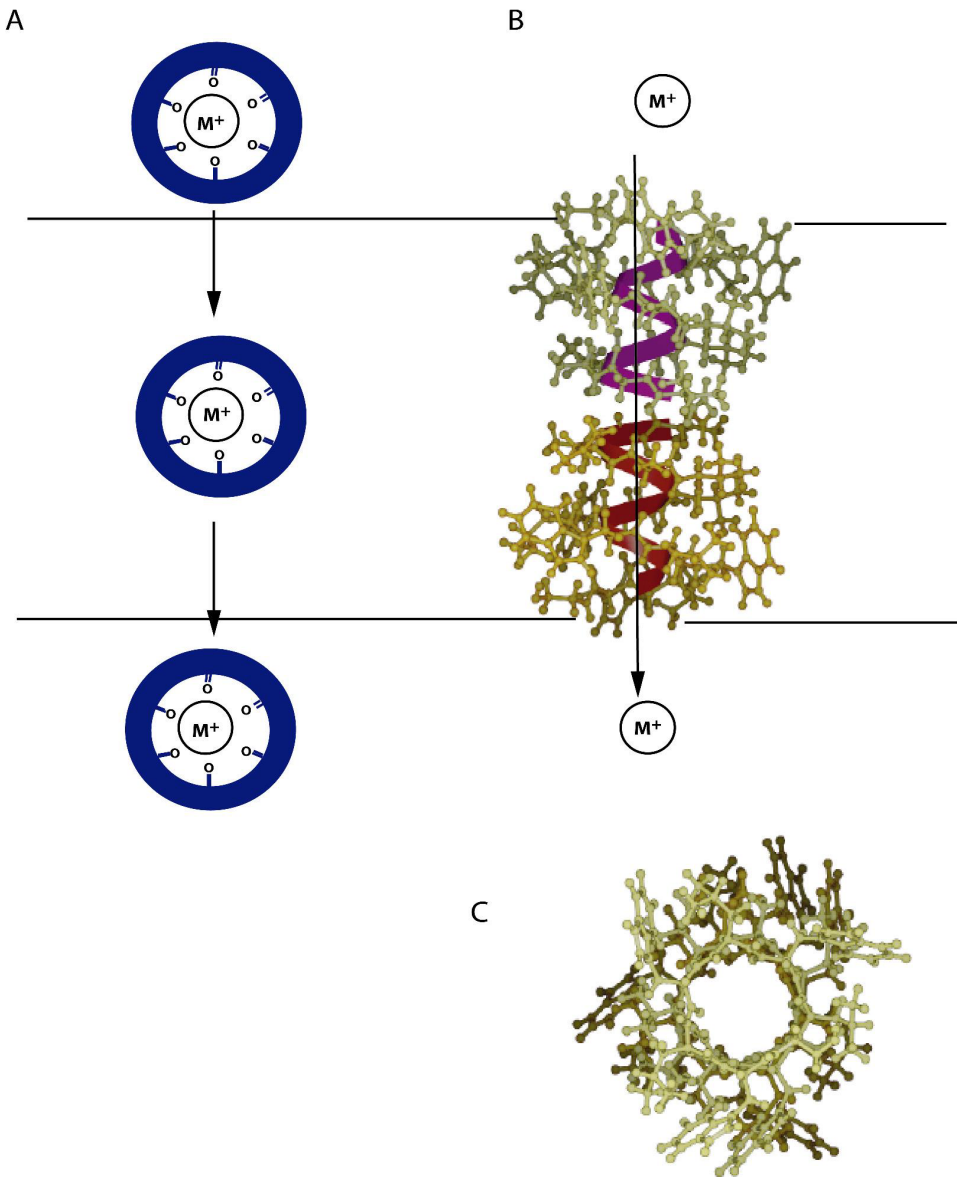

Figure 7. Diagrams of ionophores.

(A) Catoon figure of typical carrier type ionophores transporting monovalent metal ions across the lipid bilayer. (B) Graphic model of a channel type (gramicidin) is depicted. Note that two molecules of gramicidin compose a channel. The open form is shown here. (C) Saggitical view of the gramicidin dimer. All the molecular graphics of gramicidin (1MAG) is prepared by SPOCK.

Research Objectives

The αHL pore is consisted with the water-filled cavity with dimensions ranging from 14 Å to 45 Å in diameter, with approximate volume of 32,600 $Å^3$. Previously the pores have been successibly modified with one polyethylene polymer (3.5 kDa or 5.0 kDa) at Ser 106 position. Furthermore from the examination of the prepore to the pore transition, the central cavity is accommodating seven chains of the prestem domain (25 residues).

In this present project, the proposal of the cavity capacity with polypeptide chain will be tested by genetic engineering, which will be further developed to introduce novel functions. For initial project, the capacity of the central cavity will be estimated to contain flexible Gly/Ser linker polypeptide sequences and the dynamics of the inserted Gly/Ser loops will be examined with the electrical current recordings through αHL pores. Then with these results, two different approaches will be attempted. One involves the mechanism of polypeptide chain inside of the lumen (temperature responsive phase change of elastin-like polypeptide) and the other involves the detection of protein analytes from outside of the lumen (protein kinase interaction with protein kinase inhibitor fragment). Long term goal of this research is to introduce a folded functional protein, probably enzyme, into the cavity for active transport, or compartmentation of substrate and product.

CHAPTER II

MATERIALS AND METHODS

Strains

XL10-Gold ultracompetent cells (Stratagene, La Jolla, CA) were used as recipients for PCR- in vivo recombination. To prepare XL10-Gold competent cells, cells were streaked out onto 1% agar containing fresh Luria broth (LB, 1% w/v tryptone, 1% w/v NaCl, 0.5% w/v yeast extract) from a glycerol stock. After overnight growth at 37°C, a single colony was inoculated into 100 ml LB media and and grown at 37°C for 8-9 h until the OD_{600} reached 0.5. The cells were collected by centrifugation (1000 g), and resuspended in 10 ml ice-cold TSS solution (10% w/v PEG 8000, 5% v/v DMSO, 25 mM $MgCl_2$ in LB). The cells were aliquoted in 200 µl portions and immediately frozen in an ethanol-dry ice bath. Prepared competent cells were stored in –80°C and used within ~6 months.

For plasmids with repetitive DNA sequences, Sure 2 supercompetent cells (Stratagene, La Jolla, CA) were used to reduce homologous recombination in vivo. Sure 2 strains have recA, recB and recJ mutations, which provide a recombination-deficient phenotype.

Transformation

Circularized DNA was transformed into cells using a heat shock protocol (*84*). Plasmid DNA (10-100 ng) was gently mixed with 100-200 μl of freshly thawed competent cells. The cells were then incubated on ice for 30 min before heat shock at 42°C for 30 s. The cells were transferred back into ice and incubated for 5 min. The cells (50-100 μl) were then plated on LB agar containing ampicillin (100 μg/ml).

DNA Analysis and Isolation

DNA was analyzed by agarose gel electrophoresis. Electrophoresis was carried out in a Tris/borate/EDTA buffer in agarose gels (1% or 2% (w/v)) containing ethidium bromide (5 μg/ml). DNA was visualized by illumination on a short wave UV light box. Small scale DNA isolation was carried out using the QIAprep Spin Miniprep Kit (Qiagen, Valencia, CA). A 10 ml culture was grown to saturation, for 12-16 h at 37°C, harvested and processed according to the manufacturer's instructions. Miniprep DNA was used for restriction digests and sequencing when screening for clones. Large scale DNA isolation was carried out using a Qiagen Maxiprep Kit. A 200 ml culture was grown to saturation (12-16 h at 37 ºC), harvested and processed according to the manufacturer's instructions. Plasmid DNA was quantitated by measuring the A_{260} of 100-fold diluted DNA in water ([DNA] = $A_{260} \bullet 100 \bullet 50$ μg/ml). The concentration of DNA was adjusted to 400 μg/ml and the plasmid was stored at -20°C. Maxi prep DNA was used for in vitro transcription/translation reactions or for sub-cloning.

DNA fragments from PCR reactions and restriction digests required gel purification. If the wanted DNA fragment length was longer than 70bp, samples were resolved in an appropriate percentage agarose gel containing ethidium bromide. Any DNA fragment shorter than 70bp (DNA coding the repeat unit for Gly/Ser loop mutant) was resolved in a 20% polyacrylamide gel followed by staining with ethidium bromide. Gel slices containing the desired DNA fragments were excised over a long wave UV light source to minimize DNA damage. DNA was extracted from the gel slices (agarose or polyacrylamide) using the QIAquick Gel Extraction Kit (Qiagen, Valencia, CA).

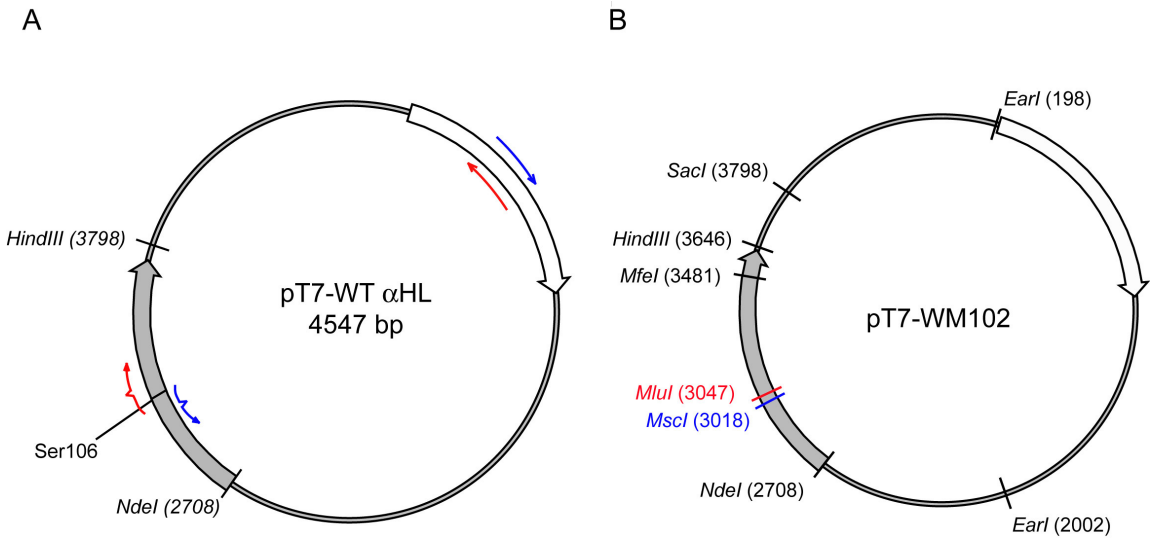

Figure 8. Generation of pT7-WM102 and its restiction enzyme map.

(A) PCR-in vivo recombination was used to generate pT7-WM102, which contains unique MscI and MluI sites. Mutagenic primer dM102-1(red with notch) and non-mutagenic primer uNM-2 (red) were used to incorporate a MluI site into NdeI-linearized pT7-WT αHL. Mutagenic primer uM102-2 (blue with notch) and a non-mutagenic primer (dNM-1, blue) produced the N-terminal half of the αHL gene with MscI site, on HindIII-linearized pT7-WT αHL template. (B) Restriction map of the resulting vector (pT7-WM102) is illustarated. Only the enzyme sites that are relevant for this work are shown. The newly incorporated MscI (blue) and MluI sites (red) are flanking the Ser 106 position of the αHL gene.

Mutagenesis

Incorporation of new restriction enzyme sites near the insertion position of the Gly/Ser loop coding DNA

Individual MscI and MluI sites were introduced into the central region of the αHL gene by a recombination-PCR protocol (*85*). In vivo recombination takes advantage of the fact that, if a plasmid is amplified as two overlapping separate halves, these halves can be assembled by *E. coli*, if the complementary ends are of sufficient length. Two sets of PCR were performed on the pT7-WT αHL template (Figure 8) (*86*). Mutagenic primer dM102-1 (red with notch) and non-mutagenic primer uNM-2 (red) pair was used for PCR on NdeI-linearized pT7-WT αHL, generating 3' half of the plasmid (Table 1). For the other half of the plasmid, mutagenic primer uM102-2 (blue with notch) and non-mutagenic primer dNM-1 (blue) were used on the HindIII-linearized pT7-WT αHL template. The overlaps of the mutagenic primers and the non-mutagenic primers wer 12 bp and 23 bp, respectively. The Expand high fidelity polymerase (Roche, Indianapolis IN) was used to minimize PCR induced errors. Each reaction contained water (40.5 μl), 10x reaction buffer (5 μl), 10 mM dNTP mix (1 μl), 100 mM primers (1 μl each), template (2 μl) and Expand polymerase (0.5 μl). The reactions were heated for 2 min at 94ºC, prior to polymerization reactions. PCR conditions were 20 cycles of denaturation at 95°C for 2 min, annealing at 52°C for 30 s, and polymerization at 72°C for 1 min. A final incubation at 72ºC for 5 min was included to ensure the extension was complete.

TABLE 1. List of plasmids and primers for generation of Gly/Ser loop-containing αHL.

Plasmid/ primer	Description of construct	Reference
pT7-WT αHL	T7 vector with wild-type alpha-hemolysin gene (αHL)	(86)
pT7-WM102	Y102W, M113A, and K288E point mutation on αHL gene, pT7 vector background	In this work
pT7-L(10n+5)	Gly/Ser loop insertions in between N105 and S106 residues, n=number of repeat units (SGSGSGGSGS) 0, 1, 2,…, 9, 10, 14 or 21, pT7-WM102 background	In this work
pT7-WT αHL D4	Wild type αHL with a tail of four aspartates on the C terminus	(87)
dNM-1	5'-ATAAAGTTGCAGGACCACTTCTG-3'	(87)
uNM-2	5'-CAGAAGTGGTCCTGCAACTTTAT-3'	(87)
dM102-1	5'-TCGATTGATACAAAAGAGTAcgcGtcTACTTTAACTTATGGA-TCC-3'	In this work
uM102-2	5'-TGTATCAATCGAATTTCTTGGccAGTAATCAGATAT-TTGAGCTAC-3'	In this work

Footnote: underlining indicates the newly introduced MluI and MscI sites in dM102-1 and uM102-2, respectively (Figure 8). The small letters denote base changes.

The PCR products were mixed together and used to co-transform E. coli XL10 Gold (Stratagene, La Jolla, CA). The cells were grown for 16 h on LB-ampicillin plates. Colonies were picked and the DNA was isolated. MluI digestion was used to screen for the new MscI and MluI-containing vector (pT7-WM102). The entire αHL gene in pT7-WM102 was sequenced to confirm the mutation. A fortuitous Lys-288 to Glu mutation was discovered, which later proved useful for the separation of heteromeric pores. Positive clones were transformed back into XL-10 Gold cells and large scale plasmid

preparations were made. To revert this mutation, Lys-288Glu, in pT7-WM102 and the genes encoding the loop-containing mutants, a gel-purified NdeI-MfeI fragment of each construct was inserted into a vector comprising the large NdeI-MfeI fragment (~4.3 kb) of pT7-WT αHL. All the revertants were sequenced.

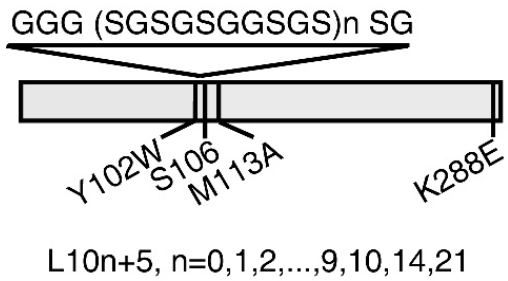

Figure 9. Diagram of Gly/Ser loop-containing αHL gene.

Schematic of the L subunits. The glycine-serine loops were inserted before residue Ser-106.

Construction of Gly/Ser-loop containing alpha-hemolysin genes

Genes encoding alpha hemolysin subunits containing various length of Gly/Ser-rich loops were constructed in three steps; Generation of the repeat unit, concatemerization of repeats, and ligation into the αHL gene. The loop-containing subunits (L) were designated by the length of inserted polypeptide chain (10n+5, where n is the number of repeat units) (Figure 9). The first loop-containing mutant, L15, was generated by ligation of two double-stranded oligonucleotides, formed from the single strands YI001, YI002, YI003 and YI004 (Table 2), into the vector pT7-WM102 from which the central MscI-MluI fragment had been removed, as illustrated (Figure 10). This

DNA encodes the amino acid sequence PRN*GGGSGSGSGGSGSSG*SIDTKEYA, where the exogenous Gly/Ser loop sequence is in italics. The AvaI sites, which flank the repeat unit, are underlined in the oligonucleotide sequences.

TABLE 2. List of synthetic oligonucleotides used for L15 generation and concatemer formation.

DNA	Sequence	Description
YI001	5'-CCAAGAAATGGCGGGGGCTCGGGGTC-CGGAAGCGG-3'	5' half for Gly/Ser loop of L15 mutant (sense). AvaI site is underlined
YI002	5'-CGGATCAGGCTCCTCGGGTTCGATTGATA-CAAAAGAGTA-3'	3' half for Gly/Ser loop of L15 (sense) with AvaI site (underlined), 5'-phosphorylated
YI003	5'-CGCGTACTCTTTTGTATCAATCGAACCCG-AGGAGCCT-3'	5' half for Gly/Ser loop of L15 (antisense) with AvaI site (underlined), 5'-phosphorylated
YI004	5'-GATCCGCCGCTTCCGGACCCCGAGCCCCC-GCCATTTCTTGG-3'	3' half for Gly/Ser loop of L15 (antisense), AvaI site is underlined
AC003	5'-TCGGGTTCGATTGATACAAAAGAGTA-3'	'Cap' DNA, sense strand,
AC004	5'-CGCGTACTCTTTTGTATCAATCGAAC-3'	'Cap DNA, antisense strand

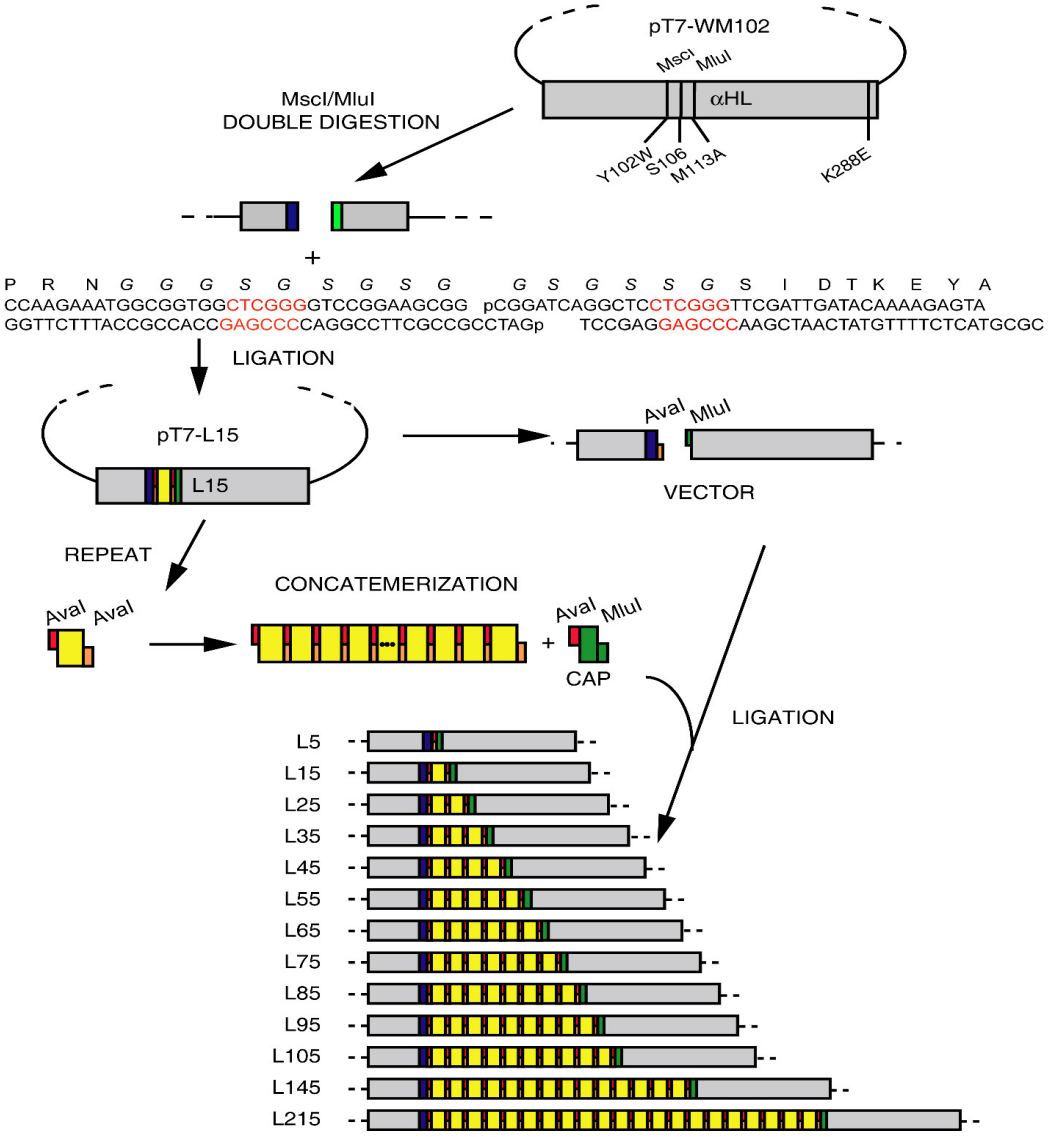

Figure 10. Construction of αHL genes containing concatemeric DNA sequences encoding internal polypeptide loops.

To introduce MscI and MluI sites for cassette mutagenesis, Y102W and M113A mutations were introduced by PCR-in vivo recombination. The K288E mutation was fortuitously generated during this process. The resulting vector, pT7-WM102, was digested with MscI and MluI, and then ligated with a synthetic duplex encoding PRN*GGGSGSGSGGSGSSG*SIDTKEYA. The italics indicate the inserted Gly/Ser-loop of mutant L15. The underlined red nucleotides indicate non-palindromic AvaI sites. The repeat unit was purified after AvaI digestion of L15. Tandem ligation of the repeat was performed in the presence of unphosphorylated cap oligonucleotides to control concatenation (cap to repeat, 1: 20). Concatemers were purified and ligated to a vector comprising the L15 plasmid from which the AvaI-MluI fragment had been removed. The nomenclature of the L subunits is L(10n+5), where n is the number of repeat units.

A substantial amount of the repeat unit (~0.5μg) was prepared by AvaI digestion (300 U) of the L15 plasmid (170 μg DNA, 37°C for 16 h), followed by TBE-polyacrylamide gel purification. The cap DNAs were AC003 (sense) and AC004 (antisense), which code *G*SIDTKEYA (Table 2). The initial Gly is an additional exogenous residue. The remaining amino acids are from the wild-type sequence except for the final Ala, which is from the mutation Met-113 to Ala mutation. The repeat unit was mixed with "cap" DNA (the cap to repeat molar ratio was 1:20) and T4 DNA ligase (400 U), and incubated at 16°C for 16 h (Figure 10). The cap oligonucleotides served to control the length of the concatemers, and to allow direction cloning without self ligation. A series of DNA concatemers was generated by tandem ligation of purified repeat units in the presence of cap oligonucleotides (Figure 11). Head-to-tail oligomerization was ensured by flanking the repeat units with non-palindromic AvaI sites (*88,89*). The cap duplex was unphosphorylated to prevent dimerization.

The concatemers were purified from preparative 2.5% agarose gels by using the QIAEX II gel extraction kit procedure (Qiagen, Valencia, CA). The concatemers (~10 pmol) were ligated into a recipient vector (100 to 150 fmol) prepared by digestion of the pT7-L15 plasmid with AvaI and MluI. The ligated products were transformed into E. coli Sure2 cells (Stratagene, La Jolla, CA), to prevent corruption of the repetitive genes by recombination. The constructs were screened by MscI and MluI digestion. Despite repeated attempts, L85 was not formed in this process and it was eventually produced by limited digestion of L105 with AvaI (0.2 U/ μg DNA, 37°C, 1 h), followed by

purification of the 8-fold repeat and its ligation into the recipient vector (100 to150 fmol of the pT7-L15 plasmid's AvaI-MluI fragment) in the presence of cap DNA (2 pmole).

All DNA ligation reactions were performed with 400 U of T4 DNA ligase (New England Biolabs, Beverly, MA) for 16 h at 22°C in 20 µL buffer, unless otherwise indicated. DNA was sequenced by Lone Star Labs Co. (Houston, TX). Synthetic oligonucleotides were produced by Integrated DNA Technologies (Coralville, IA).

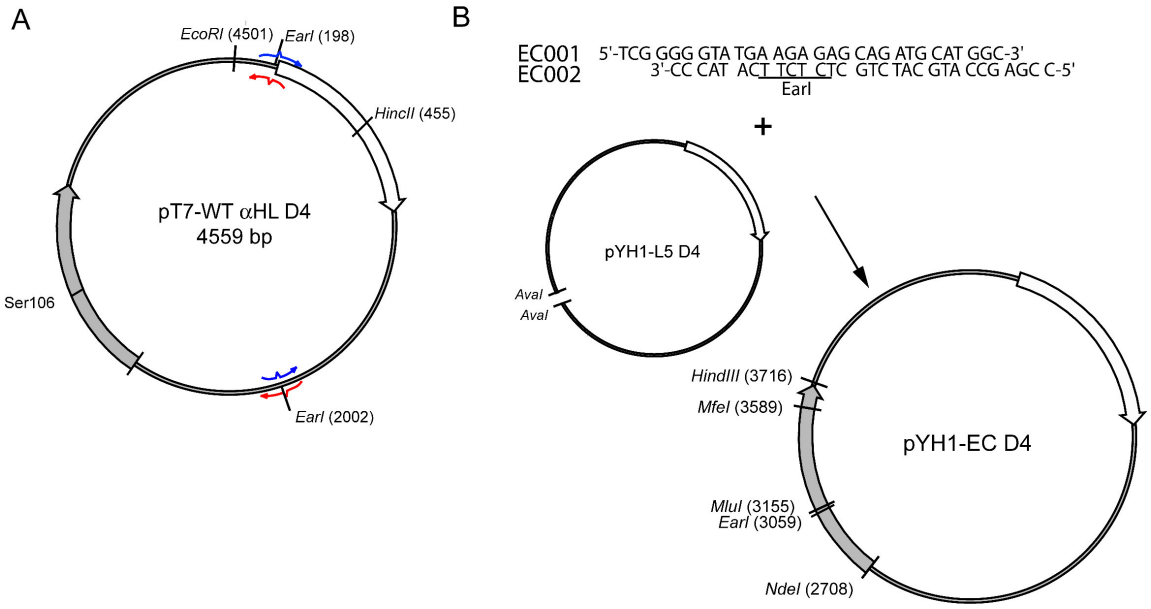

Figure 11. Generation of vectors for subcloning of the ELP repeat unit and the ELP containing-αHL.

(A) PCR- in vivo recombination for elimnation of intrinsic EarI sites iin pT7-WT αHL D4 plasmid. Four mutagenic primers were used to remove EarI sites located at 198bp and 2002 bp in the plasmid. YH001 (red, antisense) and YH003 (red, sense) primers were used in HincII-linearized pT7-WT αHL D4 template, while YH002 (blue, sense) and YH004 (blue, antisense) primers were used for EcoRI-linearized template. (B) Plasmid pYH1- EC D4 was generated to accommodate ELP concatemers using EarI and MlluI sites. Duplex DNA (EC001 and EC002) were ligated into the vector, pYH1-L5 D4 plasmid prepared by AvaI digestion, to produce the recipient vector pYH1-EC D4.

TABLE 3. List of primers and plasmids used for constructing the ELP-containing αHL genes.

Primer/ Plasmid	Description	Sequence
YH001	Reverse mutagenic primer to remove intrinsic EarI site (underlined, 198 bp position) from pT7-WT αHL D4	5'-ATACTCATACTaTTCC-TTTTTCAA-3'
YH002	Forward mutageneic primer, which is comprementary to YH001	5'-TTGAAAAAG-GAAtAGTATGAGTAT-3'
YH003	Reverse mutagenic primer to remove intrinsic EarI site (underlined, 2002 bp position of pT7-WT αHL D4)	5'-CATCAGGCGCTaTTC-CGCTTCCTC-3'
YH004	Forward mutageneic primer, which is comprementary to YH003	5'-GAGGAAGCGGAAtA-GCGCCTGATG-3'
pYH1-WT αHL D4	Plasmid containing αHL-D4 gene in T7 vector with two EarI sites (198bp, 2002bp) removed.	
pYH1-EM	Subcloning vector to generate the elastin repeat unit (ELP; VPGGGVPGGGVPGGGVPGGGVPGGG)	
pYH1-EC D4	Recipient plasmid for ELP concatemers using EarI and MluI sites	
pYH1-E(5n) D4	Plasmid containing αHL D4 gene with tandem repeats of ELP between position 105 and 106 of αHL, n= number of repeat units (1, 2, or 4)	

Footnote: The small letters in mutagenic primers indicate the base changes into the templates.

Preparation of the recipient vectors for the ELP repeat unit and the ELP concatemers

Intrinsic EarI sites of pT7-WT αHL D4 were removed by PCR in-vivo recombinations (Figure 11) (*85*). The mutagenic primers were YH001 (red, antisense) and YH003 (red, sense) for EarI site (position 198 bp) removal, and YH003 (blue, antisense) and YH004 (blue, sense) for EarI site removal (position 2002 bp) (Table 3). The PCR fragments were overlapping by 23 and 24 bp, respectively. The first PCR was performed with 150 ng of linearized pT7-WT αHL D4 (*87*) (a kind gift from Dr S.

Cheley) by HincII, as the template, 50 pmol each of YH001 and YH003 primer, 0.5 mM dNTP, 2.5 U of Expand Long Template PCR enzyme mixture (Roche Applied Science, Indianapolis, IN), 1.75 mM $MgCl_2$, and 1× Expand Long Template PCR enzyme buffer (Roche Applied Science, Indianapolis, IN) in a 50 μL reaction volume. The second PCR was performed with 150 ng of linearized pT7-WT αHL D4 by EcoRI, as the template and YH002 and YH004 as mutagenic primers. The amplification reaction consisted of a 2 min cycle at 95ºC followed by 20 cycles of 95ºC for 1 min, 50ºC for 30 s, 72ºC for 1.5 min for amplification, and a final extension at 72ºC for 5 min performed on a RoboCycler temperature cycler (Stratagene, La Jolla, CA). The PCR products were mixed together (5 μL each) and used to co-transform E. coli XL10 Gold (Stratagene, La Jolla, CA). The cells were grown for 16 h on LB-ampicillin plates. EarI digestion was used to screen for elimination of the EarI sites (198 bp and 2002bp postion). Then the sequence of the plasmid was confirmed by sequencing the plasmid. The resulting final plasmid was named pYH1-WT αHL D4 (Table 3).

The central NdeI-MfeI fragment (~800 bp) of pT7-L5 was replaced by the internal fragment (~ 790 bp) of pYH1-WT αHL D4 to introduce AvaI, MscI, and MluI sites. The resultant (pYH1-L5 D4) was linearized with AvaI followed by insertion of DNA oligonucleotides (EC001, EC002) to introduce an EarI site inbetween the AvaI sites (Table 4). The resulting vector (pYH1-EC D4) was sequenced and stored at –20ºC.

TABLE 4. List of oligonucleotides used for generation of tandem ELP repeats.

DNA	Sequence	Description
EM001	5'-TATGAACTCTTCCGTACCCGGAGGTGGCGTGCC-AGGTGGCGGTGTCCA-3'	5' half of elastin repeat unit $(VPGGG)_5$, sense
EM002	5'-GGTGGCGGAGTTCCAGGTGGAGGCGTCCCTGGCG-GAGGTGTATGAAGAGCTA-3'	3' half of elastin repeat unit, sense, 5' end phosphorylated
EM003	5'-GCCACCTGGGACACCGCCACCTGGCACGCCACC-TCCGGGTACGGAAGAGTTCA	5' half of elastin repeat, antisense, 5' end phosphorylated
EM004	5'-AGCTTAGCTCTTCATACACCTCCGCCAGGGACGC-CTCCACCTGGAACTCC	3' half of elastin repeat, antisense
EC001	5'-TCGGGGGTATGAAGAGAGCAGATGCATGGC-3'	Complementary strand of EC002
EC002	5'-CCGAGCCATGCATATGCTCTCTTCATACCC-3'	Incorporation of EarI site (underlined) on antisense strand
ETCAP001	5'-GTAGGAGGCTCCTCGGGTTCGATTGATACAAAA-GAGTA-3'	Cap DNA for ELP concatemers, sense strand
ETCAP002	5'-CGCGTACTCTTTTGTATCAATCGAACCCGAGG-AGCCTCC-3'	Cap DNA for ELP concatemers, antisense strand

Generation of a construct coding a monomermic ELP repeat unit

The monomeric repeat unit coding plasmid (pYH1-EM) was generated by ligation of two double-stranded oligonucleotides formed from synthetic DNAs, EM001, EM002, EM003, and EM004 (Table 4), into the vector pYH1-WT αHL D4 from which the central NdeI-HindIII fragment had been removed (Figure 11). Prior to ligation to the vector, 5' ends of EM002 and EM003 DNA were phosphorylated by T4 polynucleotide kinase (New England BioLab, Beverly, MA), followed by heat inactivation of the enzyme (65ºC for 20min). These DNAs encode the five tandem-repeats of VPGGG. The

EarI sites, which flank the repeat unit, are underlined in the oligonucleotide sequences. The ligated product was transformed to Sure2 ultracompetent cells (Stratagene, La Jolla, CA) to prevent any unwanted in vivo recombination. The resultanting plasmid was purified and sequenced.

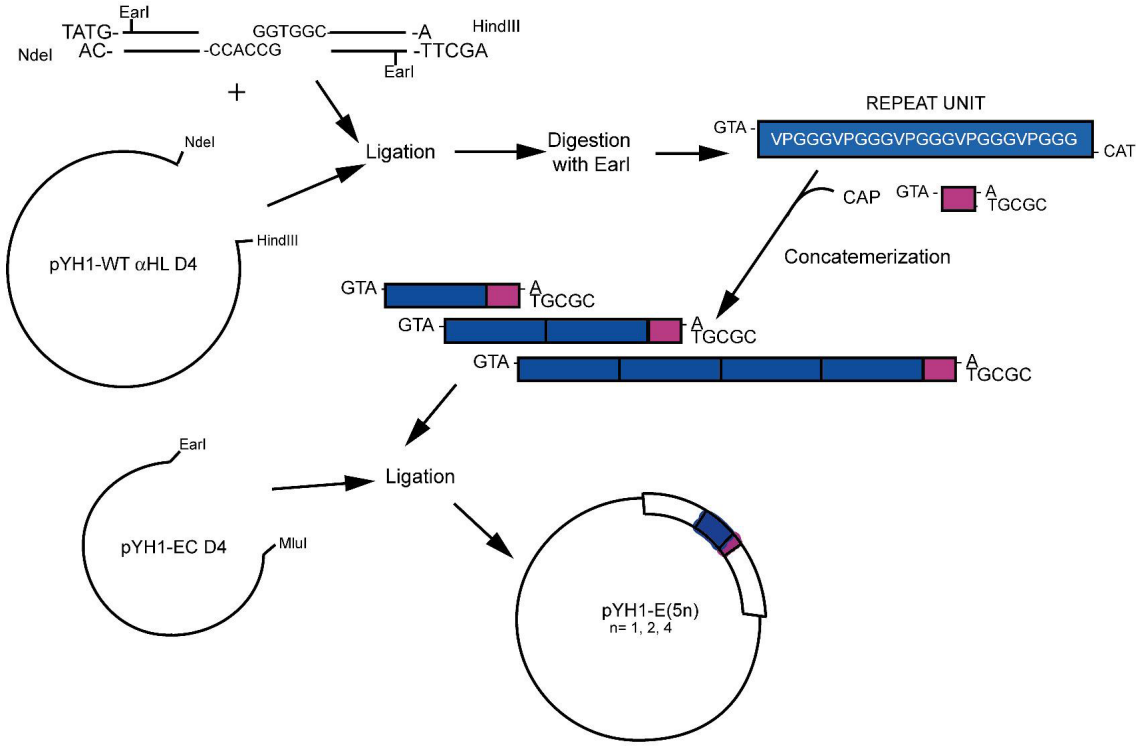

Figure 12. Construction of ELP-containing αHL gene.

DNA encoding five repeats of VPGGG was first subcloned into the pT7 vector. The purified repeat unit was then concatemerized in the head-to tail direction in the presense non-phosphorylated cap DNA. The concatemers (1, 2, and 4 repeat units) were then purified and ligated to the final recipient vector pYH1-EC-D4 with EarI and MluI.

Construction of αHL gene with tandem repeats of ELP

A series of DNA concatemers was generated by tandem ligation of the purified repeat unit in the presence of cap oligonucleotides (Figure 12) Concatemers were prepared by ligation reaction (16ºC, 16 h) of purified repeat unit and unphosphorylated cap DNA (1:20 molar ratio = repeat unit/cap) as demonstrated for Gly/Ser-loop containing αHL. Cap DNA encodes *VGGSSG*SIDTKEYA, and consists of ETCAP001 (sense) and ETCAP002 (antisense) DNA strands (Table 4). The italics indicate exogenous residues and normal letters are for endogenous residues of αHL, Ser-106 to Met-113Ala. Head-to-tail ligated concatemers with 1, 2 and 4 repeat units were purified from preparative 2.5% agarose gel followed by QIAEX II gel extraction kit procedures (Qiagen, Valencia, CA).

The concatemers were ligated into a recipient vector prepared by digestion of the pYH1-EC plasmid with EarI and MluI (Figure 12). The ligated products were transformed into E. coli Sure2 cells (Stratagene, La Jolla, CA), to prevent corruption of the repetitive genes by recombination. The final constructs contained 5 residues of linker sequence upstream (GGGSG) and downstream (GGSSG) of the ELP sequence, ELP repeats (25, 50, 100 residues) and one additional valine residue at the end of ELP sequence. The ELP-containing αHL genes were denoted as E5, E10, E20, based on the number of the pentapeptide VPGGG (i.e. 5, 10 and 20 repeats of VPGGG, respectively). At the C-terminus of the αHL gene, four residues of aspartate were added to facilitate separation of heteroheptamers (see below) (*87*). The αHL genes of all constructs were

sequenced by Lone Star Labs Co. (Houston, TX).

Construction of an αHL gene with protein kinase inhibitor fragment encoded with the inserted loop

Intrinsic SacI site removal from the vector.

Intrinsic SacI site from the plasmid pYH1-WT αHL D4 was removed by Klenow fragment using 3'exonuclease activity. pYH1-WT αHL D4 was linearized with SacI (3810 bp). Klenow fragment (2.5U) (Stratagene, La Jolla, CA) was added to the sample and incubated at 37ºC for 1h. 3' overhangs were digested by Klenow fragment exonuclease activity. Then, the Klenow enzyme was heat inactivated at 65ºC for 20 min. The modified DNA was cicularized with by T4 DNA Ligase (New England Biolabs, Beverly, MA) and then transformed in XL10-Gold competent cells. The transformed cells were pleated onto LB-Agar plate containing ampicillin for 16 h at 37ºC. Eight colonies were picked and regrown in 10 ml LB-ampicillin media for 16 h at 37ºC. Mini-DNA preparation was performed to purify plasmids for screening by digestion with SacI. A positive plasmid (pYH2-WT αHL D4) was sequenced and collected from a large culture (100 mL). The αHL gene of pYH2-WT αHL D4 (NdeI-MfeI) was replaced by the equivalent fragment of pT7-L45 or pT7-L105. The resulting constructs (pYH2-L45 D4 and pYH2-L105 D4) were isolated by mini-DNA preparation and screening by digestion with MluI, prior to sequencing and maxi-DNA preparation.

SacI-XhoI sites incorporation to the Gly/Ser loop.

The introduction of unique SacI and XhoI sites to the very end of the repetitive Gly/Ser sequence was a challenging step. Every repeat unit ended with an AvaI site. Therefore simple digestion by AvaI would remove all the Gly/Ser repeats. According to the repetitive sequences of template, a novel attempt was initiated for PCR. Instead of using the ten Gly/Ser repeats as template to incorporate unique SacI and XhoI sites, the construct with half the size of the repeat (four repeats) was used to introduce either SacI or XhoI into 5' end or 3' end of the Gly/Ser repeats, repectively (Figure 13). Then these PCR fragments were ligated with DNA strands encording PKI fragment (5-24 postion), using SacI and XhoI (Figure 13). Conventially the 3' ends of a mutagenic primer are designed to anneal to template, while the 5' ends are used for incorporation of non-complementing sequences. Here, 3' end of the mutagenic primers were designed with only 5 bp complementing sequences. However, the 5'end of the mutagenic primers were designed to anneal to template with 21 or 24 bp complementing sequences, which anneal at outside of the Gly/Ser repeats (Figure 11).

Mutagenic primers are SX001(blue, antisense) and SX002 (red, sense) and non-mutagenic primers are SC001 (blue, sense) and SC011 (red, antisense) (Table 5, Figure 13). The templates were NdeI-linearized pYH2-L45 D4 and pYH2-L105 D4, for generation of the C-terminal haves of the PKI loop-containing αHL genes, PKI115 and PKI225, respectively. For the N-terminal halves, HindIII-linearized pYH2-L45 D4 and pYH2-L105 D4 were used as template for PKI115 and PKI225, respectively (Figure 13). PCRs were perfomred at temperature using high temperature gradient (56ºC-65ºC) for

annealing step by Robo-Cycler (Staratagene, La Jolla, CA). To prevent any non-specific elongation, polymerase and antibody mixture (JumpStart AccuTaq DNA polymerase, Sigma, St Louis, MO) was used. At the initial step of denaturation, the antibody that is bound to polymerase dissociates and the polymerase is activated (*90*). The conditions for PCR were 15 cycles of denaturation for 1 min at 95ºC, annealing step for 30 s at temperature gradient (56ºC -65ºC) and extension for 1 min at 68ºC. The samples were then incubated at 68ºC for 5 min to ensure the extension. The PCR products (852 bp and 519 bp) were purified by QIAquick PCR purification kit (Qiagen, Valencia, CA).

TABLE 5. List of primers and plasmids used for PKI (5-24) loop-containing αHL.

Primer	Sequence	Description
SC001	5'-CACTATAGGGAGACCACAAC-GG-3'	Non-mutagenic forward primer, incorporation of XhoI site
SC011	5'-CCCCTCAAGACCCGTTTAGA-GGC-3'	Non-mutagenic reverse primer, incorporation of SacI site
SX001	5'-CCGAGAAATGGCGGGG-GCTCGaGtTCCGG	Mutagenic forward primer for SacI (underlined) incorporation to 3' end of the Gly/Ser repeats in pYH2-L45 D4
SX002	5'-CTCTTTTGTATCAATCGAGctcC-CCGAGC	Mutagenic reverse primer for XhoI (underlined) incorporation to 3' end of the Gly/Ser repeats in pYH2-L45 D4
pYH2-L45 D4		Plasmid with L45 αHl gene in pT7 vector with intrinsic EarI and SacI sites were removed, D4 tail on C-termini
pYH2-L105 D4		Plasmid with L105 αHl gene in pT7 vector with intrinsic EarI and SacI sites were removed, D4 tail on C-termini
pYH2-P115 D4		Plasmid withPKI loop containing αHL gene (Y102W, M113A), The loop is 115 residue- long. D4 tail on C-termini
pYH2-P206 D4		Plasmid withPKI loop containing αHL gene (Y102W, M113A), The loop is 206 residue- long. D4 tail on C-termini

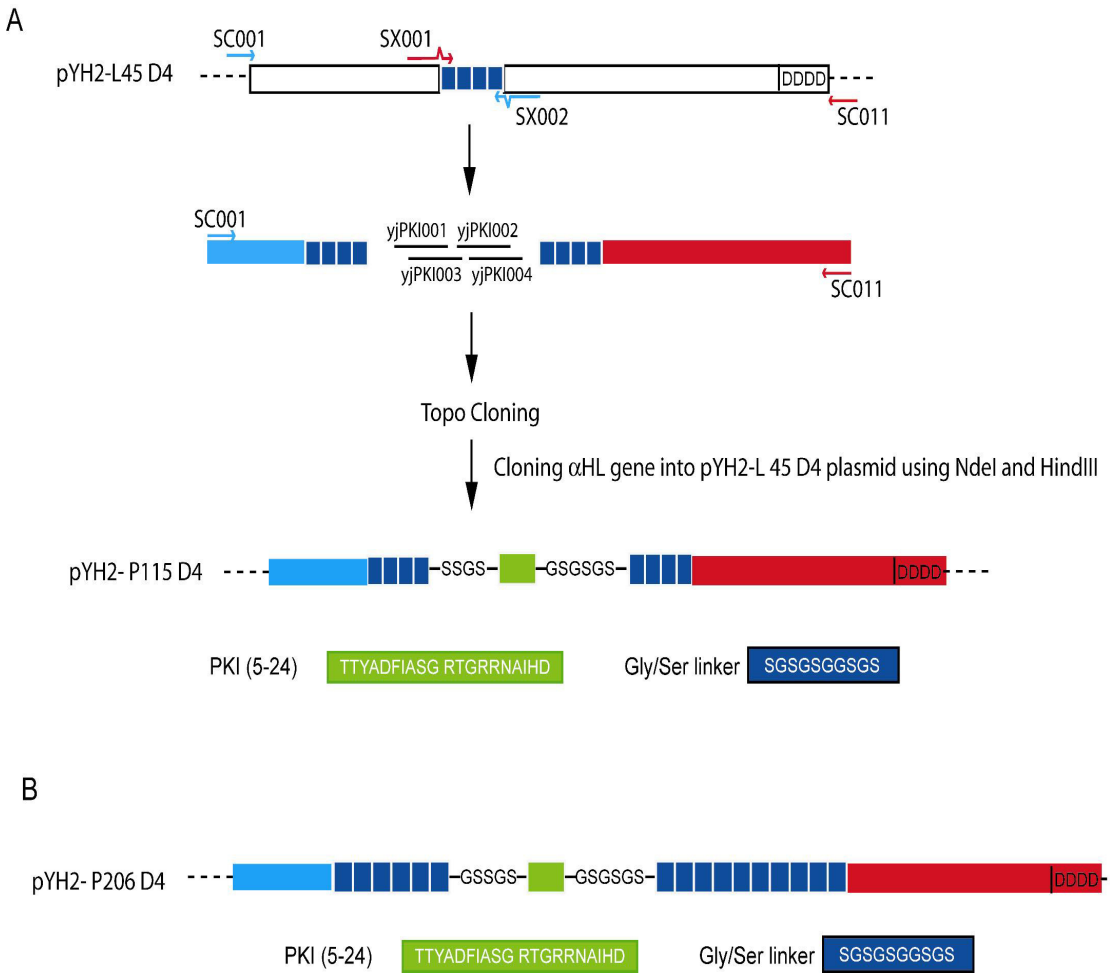

Figure 13. PKI fragment insertion to the Gly/Ser linker sequences.

(A) To incorporate a SacI site at the 3' end of the Gly/Ser repeats of L45 D4 gene, PCR was performed with non-mutagnenic primer SC001 and SX002 (light blue) with the template, HindII-linearized pYH2-L45 D4. The PCR with SC011 (non-mutagenic primer, red) and SX001 (mutagenic primer, red) was performed to incorporate an XhoI site to the 5' end of the Gly/Ser repeats of L45 D4 gene. The template was NdeI-linearized pYH2-L45 D4. The PCR products (light blue and red) was ligated with the DNA (yjPKI001-004) encoding PKI fragment (5-24) followed by second PCR with SC001 and SC011. The resulting PCR product was then subcloned into TA-TOPO vector, followed by final cloning into pYH2-EC D4 vector prepared by NdeI and HindIII digestion. The final construct is denoted as pYH2-P115 D4, which encodes the αHL gene with PKI-containg loop. (B) The same procedures were taken to generate the final construc pYH2-P206 D4. The template was either HindIII-linearized pYH2-L105 D4 or NdeI-linearized pYH2-L105 D4 for the N-terminal half or the C-terminal half, respectively, of the P206 D4 gene. The final P206 D4 gene is shown in B. Initially the DNA encoding PKI fragment was to place at the middle of the exogenous loop sequence. But during the transformation, four repeats of Gly/Ser repeat unit was lost.

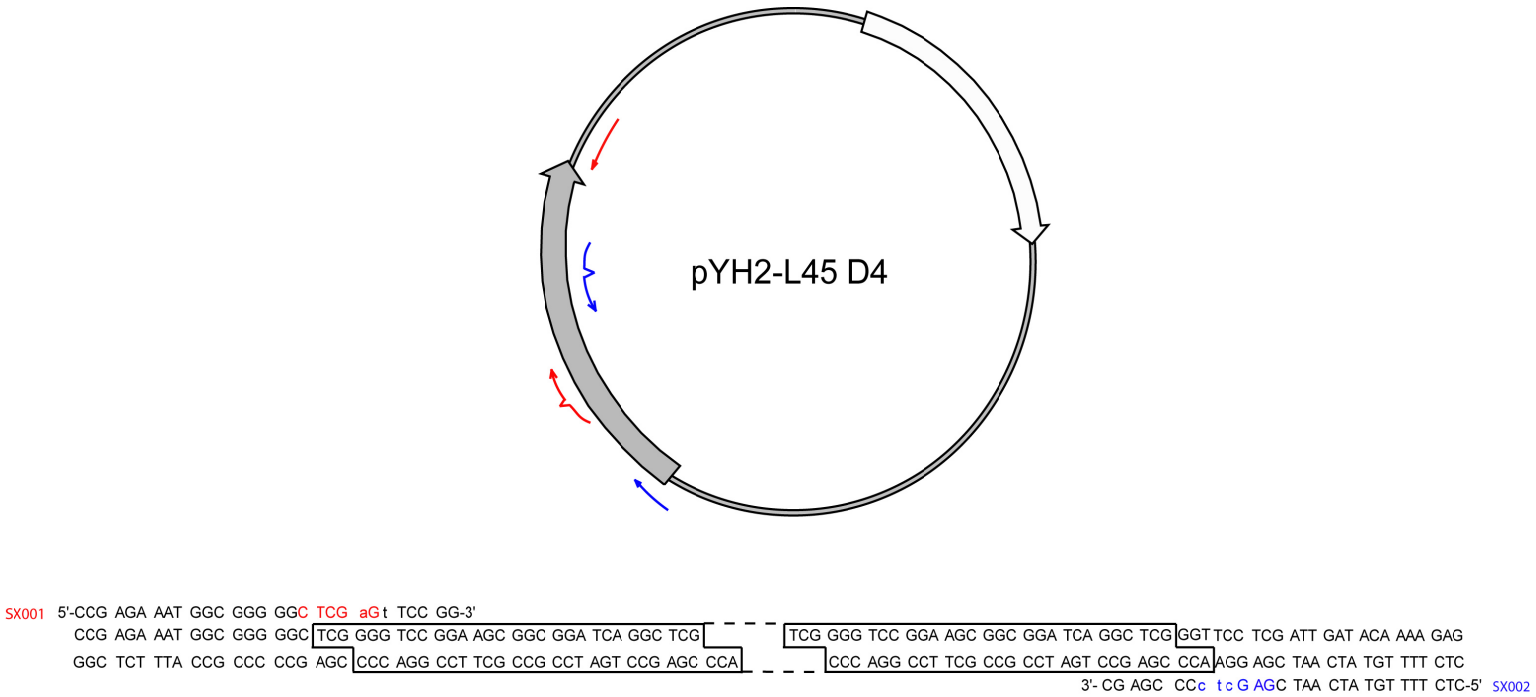

Figure 14. Diagram of pYH2-L45 D4 and mutagenic primers.

To incorporate unique SacI (red) and XhoI (blue) sites, two mutagenic primers (SX001, SX002) were designed to anneal to either the 5' end or the 3' end of repetitive sequences, respectively. The DNA sequence of Gly/Ser loop portion of pYH2-L45 D4 is shown in below. The Gly/Ser loop is boxed which repeated four times in pYH2-L45 D4 and 10 times for pYH2-L105 D4. The non-mutagenic primers (SC001 (blue) and SC011 (red)) are indicated by arrows, while the mutagenic primers are with notches. Non-complementing bases are indicated with small letters. The αHL is shown as grey box and the β-lactamase gene is in white box. These PCR reactions are to generate PKI115 D4 construct. Same primers were used for PKI225 D4 generation, whith pYH2-L105 D4 as template.

TABLE 6. List of oligonucleotides used for PKI loop containing αHL genes.

DNA	Sequence	Description
yjPKI001	5'-TATGAGCTCAGGATCGACGACCTATGCAGATTTTATCG-CATCCGGG-3'	5' half of PKI fragment, sense
yjPKI002	5'-CGTACCGGTCGTCGCAATGCAATCCATGATGGAAGCGG-ATCAGGCTCCTCGAGTA-3'	3' half of PKI fragment, sense, 5' end phosphorylated
yjPKI003	5'-ACGCCCGGATGCGATAAAATCTGCATAGGTCGTCGATC-CTGAGCTCA-3'	5' half of PKI fragment, antisense
yjPKI004	5'-AGCTTACTCGAGGAGCCTGATCCGCTTCCATCATGGATT-GCATTGCGACGACCGGT-3'	3' half of PKI fragment, antisense, 5' end phosphorylated

PKI fragment (5-24) insertion to the Gly/Ser linker sequences.

DNA fragments (yjPKI001, 5'-phosphorylated yjPKI002, 5'-phosphorylated yjPKI003, and yjPKI004) coding PKI fragment (5-24) were ligated between two PCR products (Figure 14) by T4 DNA ligase (400U, 1X buffer, 20 μL) using newly introduced SacI and XhoI sites (Table 6). Since each PCR product was from same number of Gly/Ser repeats (total 45 residues), the PKI fragment would be placed at the mid-point of the loop. Because of low yield of three-way ligation, a second set of amplification was performed using 10 cycles of PCR. The PCR conditions were the same as the first reaction condition except the primers and annealing temperautre. The primers were SC001 (sense) and SC011 (antisense) and the annealing temperature was 53ºC. The product was ligated into TOPO-TA cloning vector (pCR2.1-TOPO) according to the manufacturer (Invitrogen, Carlsbad, CA). The topoisomerase I from Vaccinia virus ligates the 3' overhang A base, which is inserted by nontemplate-dependent

terminal transferase activity of Taq polymerase, to the topo-TA vector (*91*). The circularized vector was transformed into Sure2 competent cells, instead of OneShot cells supplied with topo-TA kit, to minimize unwanted recombination of repetitive sequences. The transformed cells were spread over LB-agar-ampicillin plate at 37ºC for 16 h. Single colonies were picked and grown in an LB-ampicillin medium (10 ml) for 16h for screen of positive clones. Plasmids were purified from the cultured cells and digested with AgeI for screening. Positive clones (4 samples) were sent for sequencing. According to the sequence results, there were recombination of Gly/Ser repeats on pYH2-P215 D4 construct in all picked clones, resulting in a shorter total loop length (206 residues) and PKI fragment was located at slightly towards the C-terminus (Figure 13). The resulting construct was called as pYH2-P206 D4, due to the shortened loop length. There were no unwanted errors for pYH2-P115 D4 constructs.

Rabbit Red Blood Cell Membrane Purification

Rabbit red blood cell membranes (rRBCM) were prepared by hypotonic lysis of purified rabbit erythrocytes. After repeated washings of the lysed cell with 150 mM NaCl, 10 mM MOPS, pH 7.4, containing 1 mg/ml BSA, the membrane fraction was collected and suspended in 10 mM MOPS, 150 mM NaCl pH 7.4, containing 1 mg/ml bovine serum albumin (MBSA) at concentration of ~2.5 mg protein/ml. The concentration of membrane protein was determined with the DC-Protein Assay kit from Bio-Rad (Hercules, CA). rRBCM were stored in –80˚C until ready to use.

Preparation of Soluble Monomeric Subunits

Radiolabeled monomeric wild-type or mutant αHL polypeptides were synthesized by coupled *in vitro* transcription and translation (IVTT) in the presence of [^{35}S]methionine (10 μCi per 25 μL reaction, 1200 Ci/ mmol, ICN, Irvine, CA) and rifampicin (20 μg/ ml), with an *E. coli* T7 S30 extract System (Promega, Madison, WI) , as described previously (*14*). To inhibit transcription by *E. coli* RNA polymerase, the S30 extract was pretreated with 20 μg/ml rifampicin. A 25 μl reaction contained: 400 μg/ml DNA template (4 μl), amino acid mix minus methionine (2.5 μl), premix (10 μl), [^{35}S]methionine (1 μl, 10 μCi), S30 extract (7.5 μl). The mixture was incubated at 37°C for 1 h. The reactions were analyzed on a 10% SDS-polyacrylamide gel, which was fixed for 1 h in destaining solution (40% methanol, 40% acetic acid, 20% water) and then dried. The dried gel was visualized after exposure to BioMax MR film (Kodak, Rochester, NY) overnight.

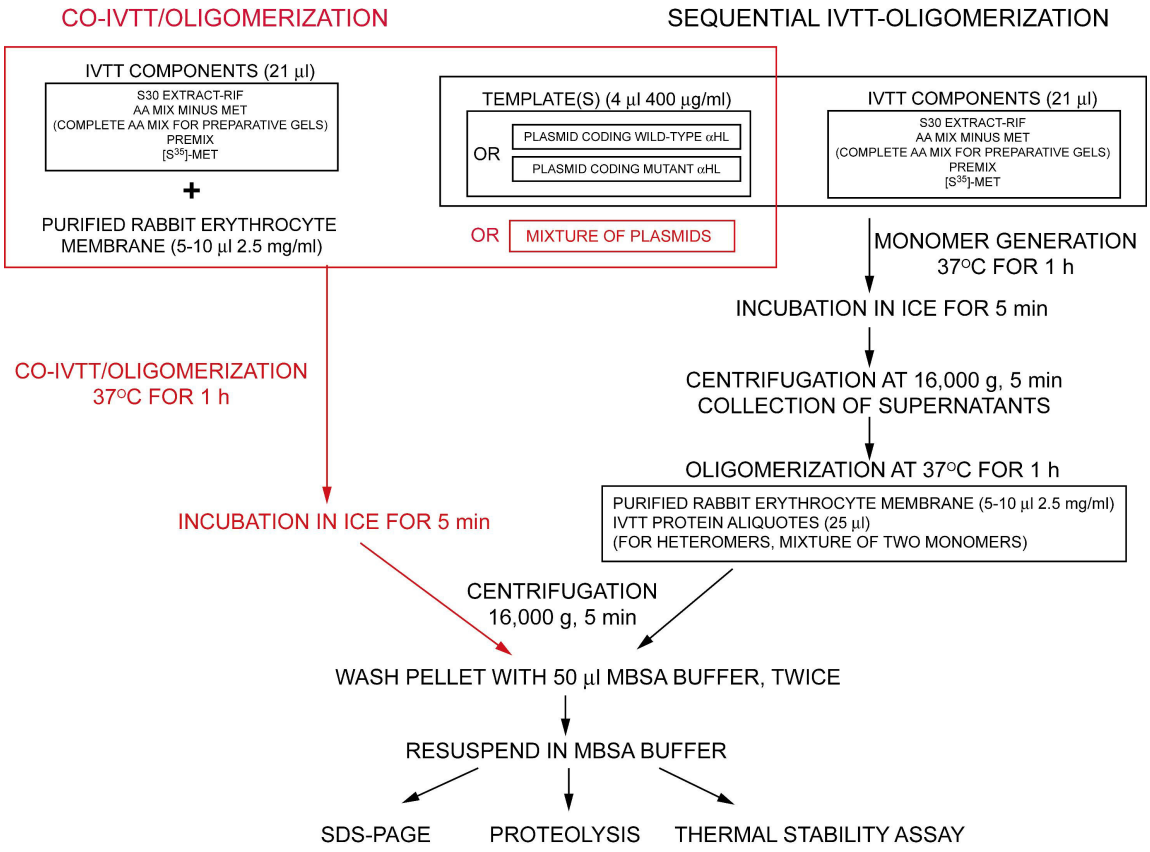

Figure 15. Flowchart of αHL oligomer formation.

αHL oligomer can be prepared by two ways: co-IVTT/oligomerization or sequential IVTT and oligomerization. With co-IVTT/oligomerization method, the templates can be either a plasmid coding wild type or mutant αHL, for homoheptamer generation. Or for heteroheptamers, mixtures of plasmids under various ratios were used. The assembled oligomer pellet was collected by centrifugation followed by washing away partially bound or non-specific bound proteins with MBSA buffer. The membrane pellet was resuspended in MBSA buffer and subjected for next step of analysis (electrophoresis, proteolysis, or thermal stability assay). With sequential method, first monomeric αHL (wild-type or mutant αHL) was prepared then assembled by mixing with purified rabbit erythrocyte membrane. For heteromers, various ratios of monomers were used. The rest of the steps were identical to co-IVTT/oligomerization method.

Oligomer Formation and Purification

Homoheptamer preparation

Radiolabeled membrane-bound wild-type or mutant αHL homoheptamers were

generated by coupled in vitro transcription and translation (IVTT) in the presence of rabbit red blood cell membranes (rRBCM), by using the S30 extract kit from Promega (Madison, WI) (*29*).Template DNA (1.6 μg) encoding either the wild-type αHL subunit (W), or an insertion mutant of αHL (L, E, or P) was incubated with rRBCM (5 μL, 2.5 mg/ ml membrane protein) and IVTT components, in the presence of [^{35}S]methionine (10 μCi) (Figure 15). To inhibit the intrinsic E. coli transcription, S30 mix was pretreated with rifampicin (20 μg/ ml). After 1 h at 37ºC, membrane pellets were collected and washed twice with MBSA (10 mM MOPS, pH 7.4, 150 mM NaCl, 1 mg/ ml BSA). The washed pellet was resuspended in MBSA (40 μL), prior to the addition of 2X Laemmli sample buffer (40 μL) (*92*). A portion of the sample (20 μL) was resolved in a 5% SDS-polyacrylamide gel. The sample was not heated, which would dissociate the subunits. The yield of oligomers was determined by phosphorimager analysis (Molecular Imager FX; Bio-Rad, Hercules CA, OptiQuant; Packard Instrument, Meriden, CT), by comparison with αHL wild-type heptamer standards run in parallel (*93*). The specific radioactivity of wild-type αHL was calculated based on the assumption that the specific hemolytic activity is 25 ng/ mL (*86*). Because no additional Met codons were introduced in the mutagenesis procedure, no correction for the number of methionine residues was required for the insertion mutants. Autoradiographs or phosphorimages were generally obtained after overnight exposure, unless otherwise indicated. For example, the gels with L25 homoheptamers were exposed for 21 d and 2 d for autoradiograms and phosphorimages, respectively.

Heteroheptamer preparation

To obtain radiolabeled heterooligomers, template DNA encoding the wild-type subunit and the insertion mutant were mixed in various ratios (W/ L (E or P) = 4: 0, 3: 1, 1: 1, 1: 3, and 0: 4) prior to IVTT. As shown previously (*29*), the presence of rRBCM during IVTT allowed the newly synthesized protein to assemble into oligomers . The IVTT reactions were carried out for 1 h at 37˚C with the molar ratios of template DNA indicated, in the presence of [^{35}S]methionine and rRBCM (5 μL, 2.5 mg protein/ml). The resulting membrane-bound heterooligomers were solubilized and purified as described for the homooligomers (Figure 15).

Heptamers for single channel recordings

For αHL pores to be used in bilayer experiments, a complete amino acid mix was used in the presence of [^{35}S]methionine to increase the yield of protein synthesis (Figure 15) (*29*). The solubilized membrane pellet was immediately separated in a preparative 5% SDS-polyacrylamide gel at 50 V for 16 h, with 0.1 mM Na thioglycolate in the cathode buffer. The gel was vacuum-dried at room temperature without fixing and exposed to X-ray film. Bands were excised from the gel by using the autoradiograph as a template. After rehydration, gel slices were crushed and soaked in water (500 μL) for 6 to 8 h. The suspension was then filtered to remove gel debris by using a cellulose acetate spin filter (Rainin, Woburn, MA). The filtrates were stored at -80ºC until required.

Limited Proteinase Assay

Membrane-bound loop-containing αHL pores ($L5_7$, $L15_7$, $L25_7$) were prepared in IVTT reactions (50 μl) in the presence of rRBCM. After 1 h at 37ºC, the membrane pellets were resuspended in MBSA (40 μL), and divided into four portions (9 μL each). Proteinase K (Roche Applied Science, Indianapolis, IN) solutions were prepared by dilution of a thawed enzyme stock (10 mg/ ml in water) and used immediately. Diluted enzyme solutions or water were added (1 μL) to the samples to give final proteinase K concentrations of 0, 5, 50, and 500 μg/ ml). After 5 min at 22°C, the reactions were stopped by treatment with phenylmethylsulfonyl fluoride (2 mM final, Roche Applied Science, Indianapolis, IN) for 5 min at 22°C, followed by the addition of 2× Laemmli sample buffer. The unheated samples were immediately resolved by electrophoresis in either 5% or 10% SDS-polyacrylamide gels. The intensity of residual bands were measured either by OptiQuant software (Packard Instrument, Meriden,CT) from phosphorimages or with ImageJ software (http://rsb.info.nih.gov/ij/, NIH, Bethesda, MD) for autoradiographs.

Thermal Stability Assay of Membrane-bound Oligomers

Radiolabeled heteromeric loop-containing αHL oligomers (L5/W, L15/W, L25/W) were synthesized by co-translation of the wild-type αHL polypeptide (W) and loop-containing αHL (L) polypeptides in the presence of [^{35}S]methionine and rRBCM.

Each washed membrane pellet obtained from translations with various molar ratios of templates (W:L = 4: 0, 3: 1, 1: 1, 1: 3, and 0: 4) was resuspended in 20 μL of MBSA. The samples were pooled, and mixed with an equal volume of 2× Laemmli buffer, and then divided into five portions (40 μL each). Each sample was overlaid with mineral oil to prevent evaporation. The samples were incubated at 22°C, 56°C, 59°C, 62°C or 65°C for 5 min in a Robocycler (Stratagene, La Jolla, CA). The treated samples were immediately separated by electrophoresis in 5% SDS-polyacrylamide gels, followed by autoradiography.

The radiolabeled homomeric loop-containing αHL oligomers (W_7, $L5_7$, $L15_7$, $L25_7$) were synthesized in IVTT reactions (100 μl) in the presence of [^{35}S]methionine and rRBCM. The washed membrane pellets were resuspended in 100 μL of MBSA, followed by the addition of an equal volume of 2X Laemmli sample buffer. The solution was then divided into five tubes (40 μL each) and incubated at 22°C, 47ºC, 50ºC, 53ºC or 56ºC for 5 min. Each sample was overlaid with mineral oil to prevent evaporation. The samples were separated by electrophoresis in 5% SDS-polyacrylamide gels, followed by autoradiography.

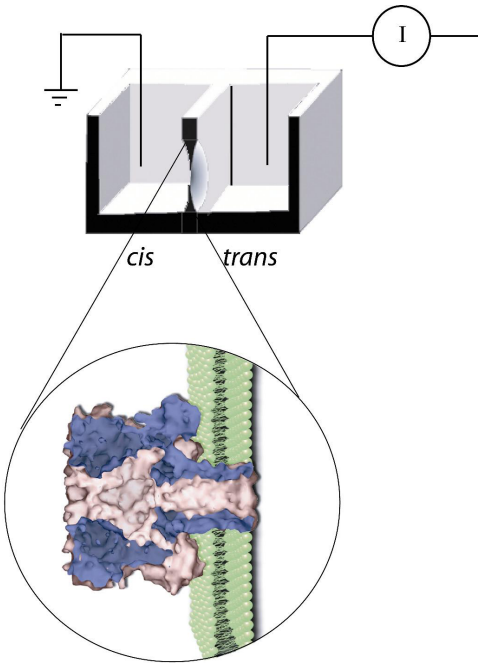

Figure 16. Illustration of planar bilayer recording apparatus with an αHL pore embedded in the lipid bilayer.

A cartoon of a typical bilayer chamber is shown. Note that the cis side, to which the protein is added, is grounded. The cap domain resides in the cis compartment.

Single-Channel Recordings

Single-channel current recordings were performed with a planar lipid bilayer generated by the method of Montal and Mueller method (*94*). Briefly, a 100 to 150 μm-diameter orifice in a 25 μm-thick Teflon film (Goodfellow Corporation, Malvern, PA) was prepared, which is separating the cis and trans compartments of the apparatus (Figure 16). The aperture was pretreated with 10% (v/v) hexadecane in n-pentane (Burdick & Jackson, Muskegon, MI). 1,2-diphytanoyl-sn-glycerophosphatidylcholine (Avanti Polar Lipds, Birmingham, AL) in highly pure pentane (Burdick & Jackson,

Allied Signal Inc., Muskegon, MI) was applied to both side of the compartment, followed by slowly elevating the solution in both compartment to generate planar lipid bilayer. Purified heptameric αHL pores (0.1 to 1.3 μg/ ml) were added to the cis compartment. A potential difference was applied across the bilayer with Ag/AgCl electrodes in 1.5% agarose (Bio-Rad, Hercules, CA) containing 3 M KCl. The cis chamber was at ground, a positive potential indicates a higher potential in the trans chamber. The current was recorded by using a patch clamp amplifier, Dagan 3900A (Dagan Co., Minneapolis, MN). The signals were stored on a DAS-75 data recorder (Dagan Co., Minneapolis, MN). After filtering with a Bessel filter (Model 900, Frequency Devices, Haverhill, MA) at 10 kHz frequency, the signals were acquired at 3 to 20 μs sampling intervals by a personal computer by using a Digidata 1200A or 1322 A/D board and Clampex 8.0 software (Axon Instruments, Union City, CA). The data are presented by using Clampfit 9.2 (Axon Instruments, Union City, CA) and Origin 6.2 (Microcal Software Inc., Northampton, MA).

SDS-PAGE Analysis

Proteins were analyzed by the method of Laemmli (*92*). Briefly, a discontinuous system composed of a lower separating gel (375 mM Tris•HCl, pH 8.8, 0.1% SDS) and an upper stacking gel (125 mM Tris•HCl, pH 6.8) was electrophoresed in running buffer (25 mM Tris•HCl, 192 mM glycine, 0.1% SDS) at a constant voltage (50 V or 100 V). Monomeric αHLs (30 kDa to 66 kDa) were resolved in 10% acrylamide gel, while heptameric αHLs (≥220kDa) were resolved in 5% acrylamide gels without prior heating

to prevent disassembly of oligomers. Electrophoresis was carried out in a Gibco BRL vertical electrophoresis system (Gibco-BRL, Gaithersburg, MD). The gels were fixed in 10% acetic acid, 40% methanol followed by drying at 80°C for analytical gels. Preparative gels were dried at room temperature without fixing. Autoradiograms of dried gels were obtained by exposure to X-ray films for 16 h, or to phosphor imaging screen for 1h. The images were analyzed by the software ImageJ (http://rsb.info.nih.gov/ij/, NIH, Bethesda, MD) and OptiQuant (Packard Instrument, Meriden, CT) or Quantity (Bio-Rad, Hercules, CA), respectively for autoradiograms and phosphoimages.

Estimation of the Cavity Volume of the αHL Pore

To determine the volume of the alpha-hemolysin cavity (Figure 17) by SPOCK 6.3 (*95*), an enclosed surface was required. The top and bottom openings of the vestibule were blocked by placing solid planes parallel to the Lys 8 and Lys 147 rings (Figure 17A, B). The software used to determine the volume cannot calculate the volume of the cavity directly, due to the large size of the αHL cavity. To overcome this, two additional planes were placed parallel to the 7-fold axis of the pore (Figure 17A). These planes isolate a "slice" of the cavity equivalent to 1/7 of the total volume. The solvent accessible surface of the αHL cavity was generated by rolling a probe with 1.4 Å diameter over the molecular surface. Then the volume of a "slice" of the cavity (Figure 17C) was calculated by SPOCK, followed by manual adjustment for the volume of the bounding plane. The total cavity volume was calculated by multiplying the volume of the slice by seven. Eight different slices were defined by rotating the vertical planes in

10 degree increments at the center of 7-fold axis. These multiple observations were made to assess the variability of the measurement.

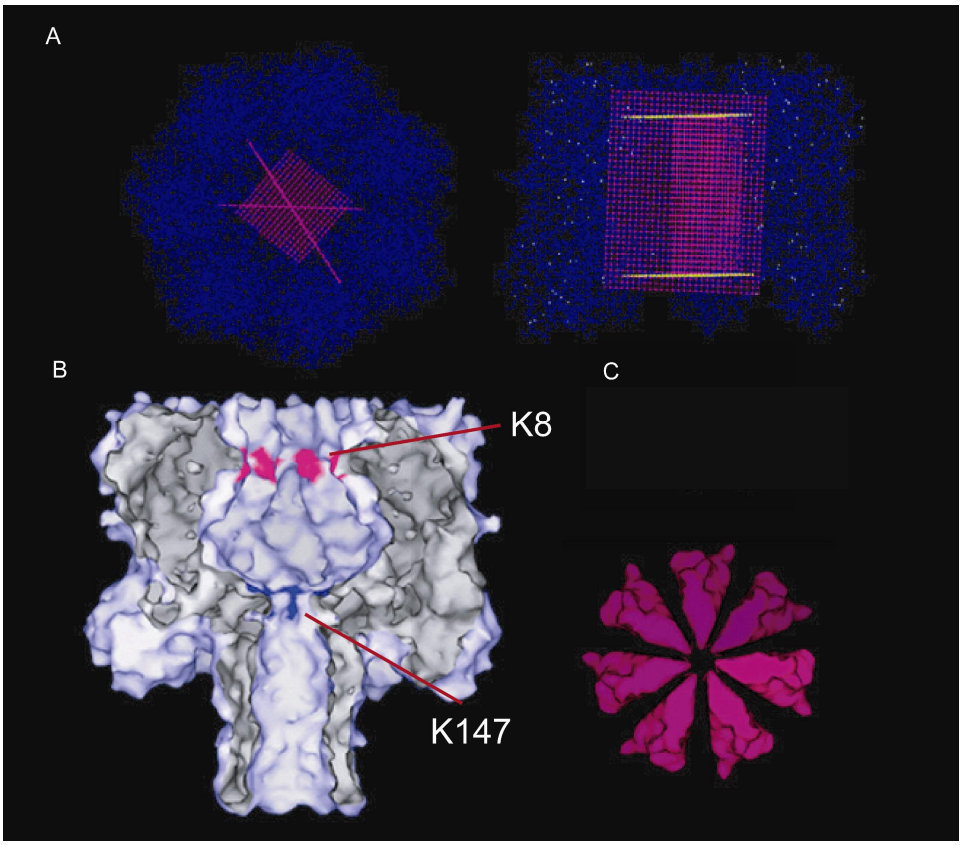

Figure 17. Calculation of the cavity volume against the solvent accessible surface of the αHL pore.

(A) The top (left) and the vertical (right) views of the αHL pore with the planes to enclose the central cavity. The horizontal planes were to seal the central lumen, and the vertical planes were to slice the cavity in 7-folds. (B) The positions where the horizontal planes were placed. (C) A slice of the cavity was arranged along the 7-fold vertical axis to demonstrate the calculation of the total cavity volume was obtained by multiplying each slice volume by seven. Manual adjustment was performed for the volume of the vertical planes.

Representations of the αHL pores and monomeric αHL subunits were generated with SPOCK 6.3. Proposed model of loop-contained αHL (L15 subunit) was generated

by Swiss-Model (*96*). The PDB coordinates of these models were superimposed to one of the wild-type αHL subunit in heptameric pore.

CHAPTER III

STUDY OF GLY/SER POLYPEPTIDE-CONTAINING ALPHA-HEMOLYSIN PORES

As for initial study work of the project, tandem repeats of flexible Gly/Ser linker sequence was placed to investigate the packing capacity of the polypeptide chain in the αHL cavity. To control the length of the insertion, Gly/Ser repeat sequences were used. Additionally, a given length of the Gly/Ser loop could be accommodated seven times, since the aHL pore is assembled by seven subunits. These insertion mutants (loop-containing subunits, L) were assembled either by themselves to form homoheptamers or with wild-type αHL subunits to form heteroheptamers. The assembled oligomers were studied in detail to provide evidence that they are assembled into stable heptamers. In addition, the oligomers were purified and used to generate pores on bilayers, which were studied with single channel recording.

The use of genetic engineering was evaluated with this initial study. The capacity of the cavity to contain polypeptide sequences was estimated. Furthermore, the dynamics of the inserted Gly/Ser loops were examined at single molecular level by observing current fluctuations through the αHL pore. These results provided fundamental informations for the next stage of the project, which was to place small functional peptides within the αHL pore.

Mutant αHL Genes Encoding Gly/Ser Loops

The peptide bond upstream from position 106 in αHL was selected as the point of insertion for Gly/Ser concatemer sequences. The selection was based on structural information and previous mutagenesis studies (*1, 6, 9, 16, 17, 20*). Optimally, the side chains adjacent to the insertion position should be exposed to solvent in both the monomeric and heptameric states of αHL for minimum perturbation of assembly and the structure of the pore.

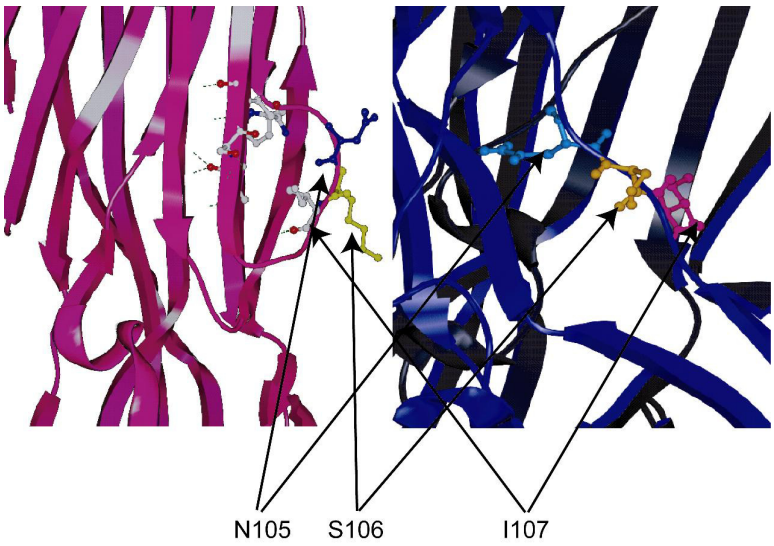

Figure 18. Accessibility of side chains near the position of insertion.

Ideally, if the side chains near the insertional position are exposed to the surface in both the monomeric (violet, left) and the heptameric state (blue, right). Therefore minimal perturbation would be caused after the loop insertion. The S106 position (yellow) is located near the widest region of equatorial axis of the pore. However, both N105 and I107 are partially facing the interior of the protein either in the monomeric or the heptameric state.

In the heptameric pore, the side chain of the wild-type residue Ser-106 is facing

towards the water-filled lumen (Figure 18) (*20*). The Gln-105 side chain of the staphylococcal leukocidin F monomer (*17*) or the Lys-99 side chain of the staphylococcal leukocidin S monomer (*9*), which correspond to residue Ser-106 in αHL, are exposed to solvent as well (Figure 18). Additionally, in the αHL pore, Ser-106 is located near the widest region of the cavity, again facilitating polypeptide insertion into the αHL backbone. In previously, polymers were tethered at position 106 without perturbing assembly (*8, 97*). Furthermore, other residues (position 104-108) located near the widest region of the cavity influenced function when cysteine mutations were performed (*20, 98, 99*) or proved to be interacting with other residues either in the monomeric or the heptameric state (*1, 100*). Therefore the position 106 would be the ideal postion for loop insertion.

Glycine and serine residues are useful amino acids for the construction of linkers (loops) between domains; the hydrophilic serine side chain allows hydrogen bonding to solvent water and glycine provides the necessary flexibility (*9, 101*). To generate the first loop-containing αHL mutant L15, a synthetic oligonucleotide encoding PRN*GGGSGSGSGGSGSSG*SIDTKEYA (the exogenous Gly/Ser-rich sequence is in italics) was inserted into pT7-WM102 from which a small fragment had been removed with MscI and MluI (Figure 10). The αHL gene in pT7-WM102 contains the mutations Tyr-102Trp and Met-113Ala to accommodate these restriction sites. During the construction of pT7-WM102, a fortuitous mutation occurred, Lys-288Glu. In the pore, position 288 is located at the top of the cap domain (Figure 19A), in the vicinity of three glutamates (Glu-287, Glu-289, Glu-290). The Lys-288Glu mutation generated a shift to

more rapid electrophoretic mobility in the assembled pores that is of the same magnitude as that seen with oligo-aspartate-tailed αHL subunits (data not shown) (*87*). Therefore, the mutation allowed the separation of loop-containing αHL oligomers from each other and from wild-type oligomers, without additional mutagenesis or chemical modification. The unitary conductance of pores formed from Y102W/M113A/K288E and the specific hemolytic activity of the mutant on rabbit red blood cells were similar to the wild-type values (Figure 19B, C).

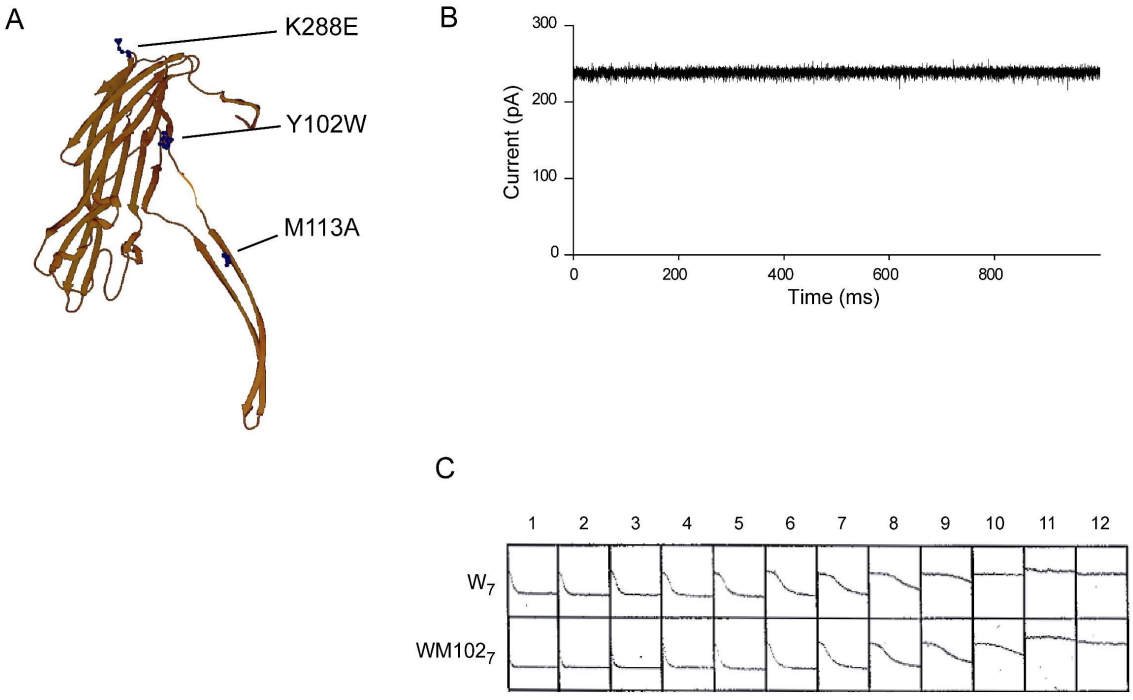

Figure 19. Functional assay of WM102.

(A) The point mutations in the WM102 αHL gene, which are proven not to interfere with the function of the αHL pore as seen by the ability to form a pore in bilayers (B) or on rabbit erythrocytes (C) . (B) Single channel recordings of triple mutant homoheptamer ($WM102_7$) at +100mV, in 2M KCl, 10mM MOPS, pH 7.4. (C) Hemolytic activity of WM102 mutant was compared with wild-type αHL (W_7). Lysis of rabbit erythrocytes was measured by scattering of intact cells at 595 nm, which decreases upon lysis of the cells.

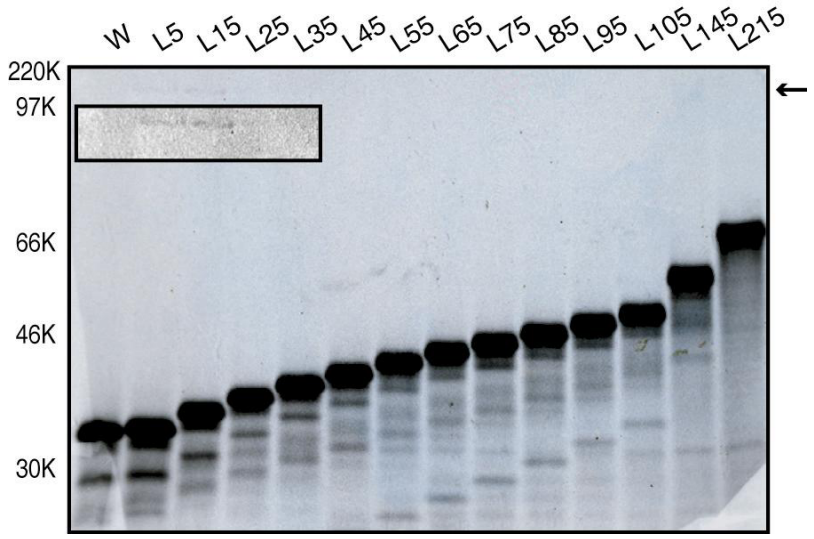

Figure 20. SDS-PAGE of monomeric Gly/Ser loop-containing αHLs.

An autoradiograph of an SDS-polyacrylamide gel showing monomeric L subunits (L5, L15, …, L145, and L215) and the W subunit. Polypeptides were synthesized by coupled in vitro transcription and translation (IVTT) in the presence of [^{35}S]methionine and resolved in a 10% gel without heating. The L subunits show decreased electrophoretic mobility that depends on the length of the loop. Preoligomerization of L5, and L15 is indicated with arrow and in inset.

Additional loop-containing subunits were designated L(10n+5), where n is the number of repeat units (Figure 9). There are several different approaches for generating genes with repeat sequences (*102, 103*). In the present work, we used a type I endonuclease (AvaI, C∨TCGG∧G) to generate non-palindromic cohesive ends on the repeat units for one-step unidirectional concatemerization (*88, 89*) and a non-phosphorylated cap DNA to control the average length of the concatemers (Figure 10). The AvaI site encodes glycine or serine, therefore only the desired amino acid sequences were introduced into the final constructs. Besides terminating concatemerization, the cap DNA provides a MluI half site. The L15 construct was used both to generate the DNA repeat unit for the construction of longer loops and as the recipient gene for the

concatemers. The recipient vector was prepared by digesting the L15 gene with AvaI and MluI (Figure 10). The 30 bp repeat unit was obtained by digesting the L15 gene with AvaI followed by preparative polyacrylamide electrophoresis. Self-ligation of the purified repeat unit by T4 DNA ligase in the presence of cap DNA generated the desired concatemers, which were gel-purified and ligated to the recipient vector. With a 1:20 molar ratio of cap to repeat unit DNA , αHL genes with up to twenty one-tandem repeats were generated (Figure 10).

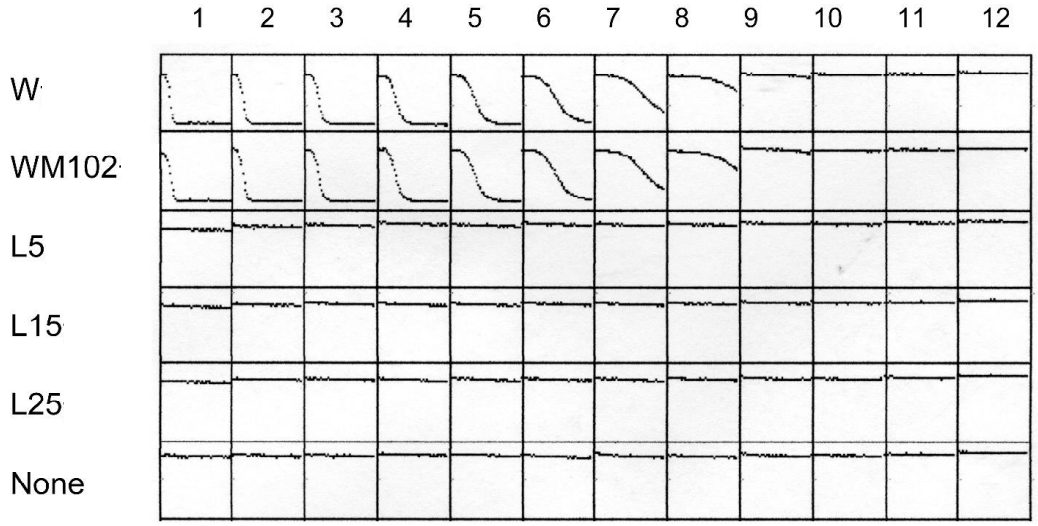

Figure 21. Hemolysis assays of short loop-containing αHLs ($0 \leq n \leq 2$) with rabbit erythrocytes.

One hour activity assays on monomeric Gly/Ser-containing subunits (L5, L15, L25) and WM102 synthesized by IVTT. The first well in each panel contained IVTT mix (5 μL) follwed by 2-fold serial dilution with 50 μL in MBSA, for the next wells. For negative control 5 μL of MBSA was added to last row. Light scattering at 595 nm was monitored at 20ºC for 1 h.

The apparent molecular masses of the L subunits ranged from 33 kDa to 59 kDa as judged by SDS-polyacrylamide gel electrophoresis; the values are somewhat higher than the calculated masses (33 kDa to 49 kDa) (Figure 20). Surprisingly, the short loop-containing mutants ($0 \leq n \leq 2$) oligomerized spontaneously after translation (arrowed, Figure 20), which accounted for lack of hemolytic activity (Figure 21). The inset is shown with a 7 d-exposure autoradiograph. Spontaneous assembly has also been noted in a mutant in which the transmembrane domain is deleted (*14*), suggesting that the kinetic barrier to assembly is readily lowered by tinkering with the junction of the cap and stem domains. However, when washed rabbit red blood cells (1%) were present during the translation of these short loop-containing subunits ($0 \leq n \leq 2$), slight lysis of red blood cells were observed in a 1 h assay. The reduced activity may partially account for low concentration of active heptameric forms (see below).

Homooligomers Containing Short Loops Resist Limited Proteolysis and are Stable at High Temperatures

To ascertain the conformational state of the oligomers, limited proteolysis was performed. The susceptibility of $L5_7$, $L15_7$, and $L25_7$ to proteinase K digestion was compared with the susceptibility of the wild-type heptamer, W_7 (Figure 22). If the oligomers were in a membrane-bound prepore state or a misassembled state, the amino-latch or other regions of the polypeptide would be accessible and therefore sensitive to proteolysis (*15, 16*).

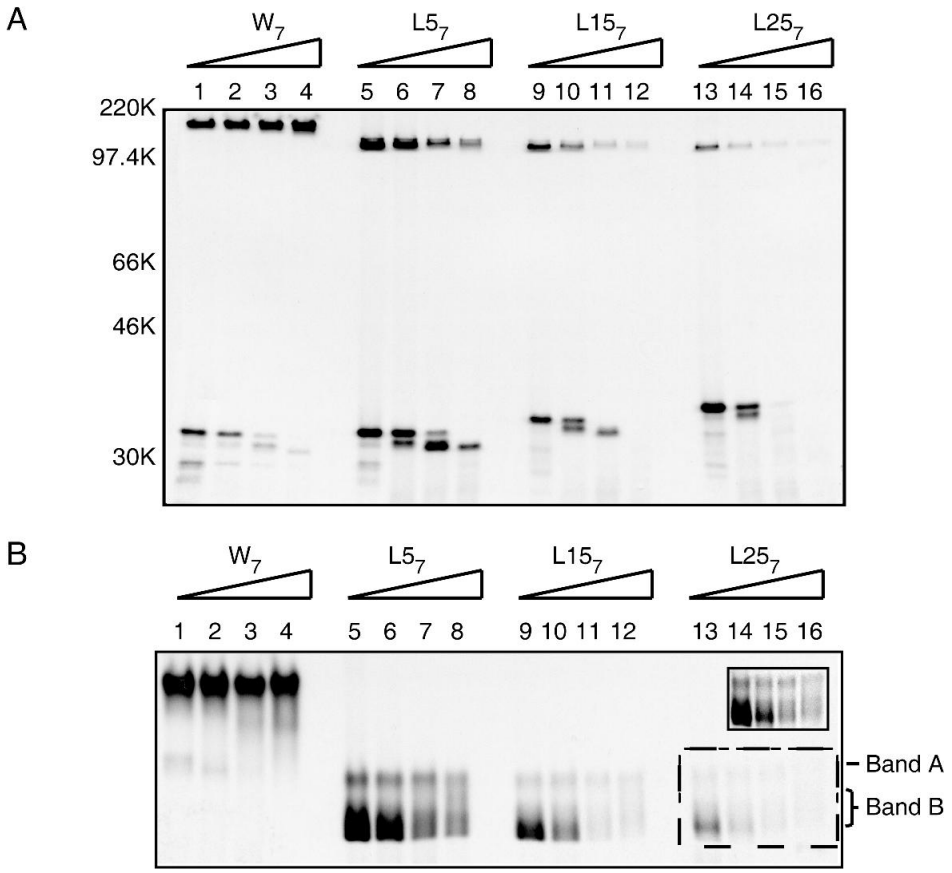

Figure 22. Limited proteolysis of homooligomers containing short Gly/Ser loops ($0 \leq n \leq 2$).

W_7, $L5_7$, $L15_7$ and $L25_7$ were treated with proteinase K for 5 min at 22°C. The homooligomers were prepared by IVTT and assembly on rRBCM. The final concentrations of proteinase K were 0 μg/ ml (lanes 1, 5, 9, and 13), 5 μg/ ml (lanes 2, 6, 10, and 14), 50 μg/ ml (lanes 3, 7, 11, and 15), and 500 μg/ ml (lanes 4, 8, 12, and 16). The proteolyzed samples were resolved in either 10% (A) or 5% (B) SDS-polyacrylamide gels without prior heating. The inset in panel B shows an autoradiograph with a longer exposure (21 d) of lanes 13 to 16. The two species of oligomers observed in 5% gels are designated band A and band B.

Initially, L subunits were assembled into homooligomers by generating monomers with an IVTT reaction, and then oligomerizing them on rabbit red blood cell membranes (rRBCM). However, when the rRBCM were present during IVTT reaction,

the yield of oligomers was increased slightly. This might be due to the preoligomerization of the loop-containing αHL. For the subsequent experiments, the IVTT reactions were performed in the presence of rRBCM.

Wild-type pores were stable (90% undigested) at up to 500 μg/ ml proteinase K as observed earlier (*14, 93*). However, the membrane-bound oligomers containing L subunits were sensitive to proteinase K treatment even at 5 μg/ ml, as visualized after electrophoresis in a 10% SDS-polyacrylamide gel (Figure 22A). Interestingly, the membrane-bound oligomers showed a more complex migration pattern in 5% gels. A fast migrating state (band B) was sensitive to digestion by proteinase K, while a slow migrating state (band A) was relatively resistant (Figure 22B). As the inserted loop became longer, the extent of formation of the membrane-bound SDS-resistant homoheptamers (band A) was reduced (as a fraction of W_7 formation under the same conditions: L5, 31%; L15, 8%,; L25, 4%). In the case of L5, band A was resistant to proteinase K treatment at up to 500 μg/ ml (89% undigested). Band A from the L15 or L25 subunits were partly digested under the same conditions (~70% undigested).

The fully assembled αHL pore (W_7) is known to be stable in 4.3% SDS at up to 65°C (*13, 20, 29*). The thermostability of the homoheptamers W_7, $L5_7$, $L15_7$, and $L25_7$ were compared by incubation at various temperatures (22°C, 47°C, 50°C, 53°C, 56°C) in electrophoresis sample buffer containing 4.3% SDS (*92*) for 5 minutes, followed by immediate separation in a 5% SDS-polyacrylamide gel (Figure 23). Band A was stable at all the temperatures tested, while band B underwent breakdown to monomers at

temperatures higher than 22°C.

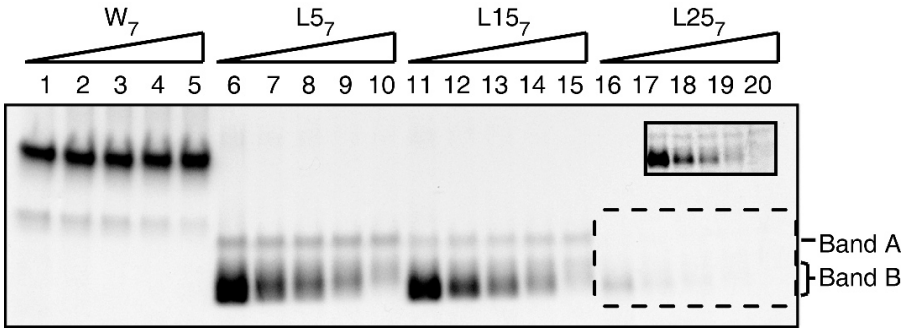

Figure 23. Thermal stability of homooligomers with short ($0 \leq n \leq 2$) Gly/Ser loops.

Homoheptamers (W_7, $L5_7$, $L15_7$, and $L25_7$) were synthesized by IVTT in the presence of rRBCM (4 reactions, 37ºC, 1 h, 100 μL total). The washed membranes were resuspended in MBSA buffer (100 μL) followed by the addition of 2X Laemmli sample buffer (100 μL). The solution was then divided into five portions (40 μL) and incubated with a mineral oil overlay at various temperatures for 5 min. The samples were immediately resolved in a 5% SDS-polyacrylamide gel. Lanes 1, 6, 11, 16: 22°C; lanes 2, 7, 12, 17: 47°C; lanes 3, 8, 13, 18: 50°C; lanes 4, 19, 14, 19: 53°C; and lanes 5, 10, 15, 20: 56°C. The inset shows an autoradiograph with a longer exposure (21 d) of lanes 16 through 20.

L Subunits with Short Loops ($n \leq 2$) Can Form Heptamers

To determine number of L subunits in the oligomeric form, L subunits were co-translated with W subunits at various ratios in the presence of rRBCM. The K288E mutation resided only in the L subunits and generated pores of increased electrophoretic mobility, with similar gel shifts to those observed with αHL pores containing subunits with four aspartate residues at the C terminus (*5, 87*). If there is no change of stoichiometry with loop insertions, heteromers with eigth different combinations would be observed, as illustrated in the left panel of Figure 24. For each W/L combination, we identified nine bands upon electrophoresis (Figure 24). As shown above, band B was

sensitive to digestion by proteinase K and was unstable above room temperature (Figure 22, 23). Further, the protein in band B failed to form pores in planar lipid bilayers and may comprise misfolded and/or misassembled pores. Therefore, band B was not investigated further and not counted as a distinct subunit combination. Band A was separated into a ladder of eight species, each stepwise shift in electrophoretic mobility corresponding to the incorporation of one L subunit into the αHL oligomer (*5, 87, 93*). The results indicate that the homooligomers formed by L5, L15 and L25 are indeed heptamers and that all possible combinations of W and L subunits can associate.

In a control experiment, heteromers formed from W subunits and subunits obtained by IVTT of pT7-WM102 (containing the gene for Y102W/M113A/K288E with no encoded loop) were resolved in a 5% gel. Eight bands were again observed, in this case without a band B species (data not shown). The band A components for L5, L15 and L25 (the presumed homoheptamers) co-migrated with homoheptamers of the pT7-WM102 protein.

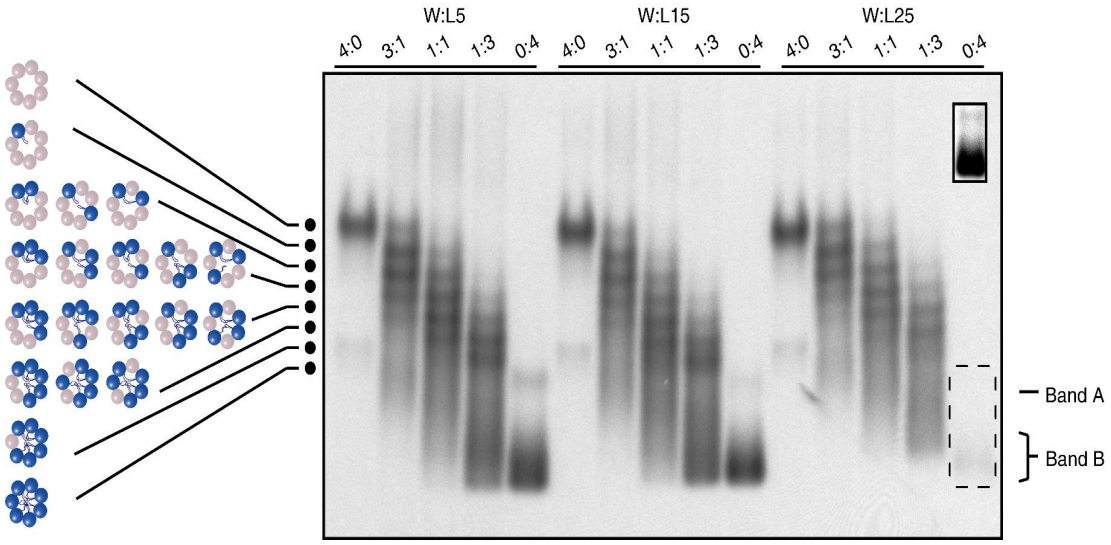

Figure 24. Assembly of heteromeric αHL pores with short Gly/Ser loop-containing subunits ($0 \leq n \leq 2$).

Separation by SDS-polyacrylamide gel electrophoresis of heteromers formed from the W subunit and L subunits (L5, L15, and L25). L5, L15, and L25 DNA templates were mixed with wild-type DNA template (W) in the ratios indicated above the lanes and the washed membranes were solubilized in MBSA buffer (40 μL), mixed with an equal volume of 2X Laemmli sample buffer and subjected to electrophoresis without heating. The autoradiogram shows the electrophoretic ladders generated by the K288E mutation in the L subunits. The magnitude of the shift towards greater mobility depends on the number of L subunits in an oligomer. The black dots show the eight bands, indicative of a heptamer, that were formed in addition to band B. The inset shows an autoradiogram with a longer exposure (21 d) of the boxed region. Graphic representation of the heteromers are shown in the left panel corresponding to the species resolved in gel. All possible permutations of L subunit and W subunits are illustrated. The various permutations of each combination are not separated.

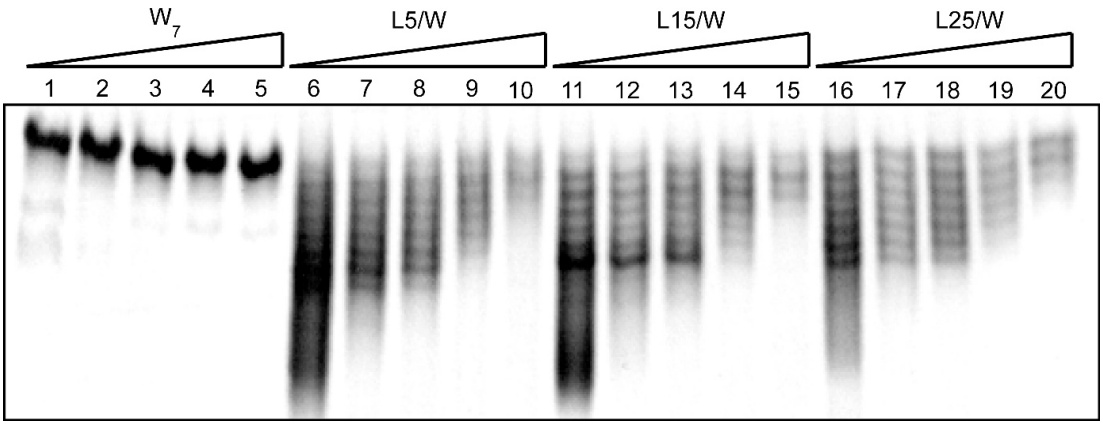

Figure 25. Thermal stability of heteromers with short Gly/Ser loops ($0 \leq n \leq 2$) in the lumen.

Heteroheptamers (L5/W, L15/W, and L25/W) were obtained by co-translation (37ºC, 1 h) from the W and L subunit DNA templates (L5, L15, or L25) in various ratios (W to L = 4: 0, 3: 1, 1: 1, 1: 3, 0: 4) in the presence of rRBCM. The oligomers obtained at the different ratios were pooled and treated at various temperatures as described in Figure 23. Lanes 1, 6, 11, 16: 22°C; lanes 2, 7, 12, 17: 56°C; lanes 3, 8, 13, 18: 59°C; lanes 4, 19, 14, 19: 62°C; lanes 5, 10, 15, 20: 65°C.

Heterooligomers Containing Short Loops Are Stable at High Temperatures

Heteromers made with wild-type subunits and loop-containing subunits (L5/W, L15/W, and L25/W) showed similar stability regardless of the length of the inserted loop (Figure 25). By contrast, the number of loops in a pore did affect its stability: heteromers with six L subunits ($L(10n+5)_6W_1$ n = 0, 1, 2) were stable at up to ~60°C, heteromers with three to five L subunits ($L(10n+5)_{3\text{ to }5}W_{4\text{ to }2}$ n = 0, 1, 2) were stable at up to ~63°C, while $L(10n+5)_1W_6$, and $L(10n+5)_2W_5$, (n = 0, 1, 2) were as stable as the W_7 pore.

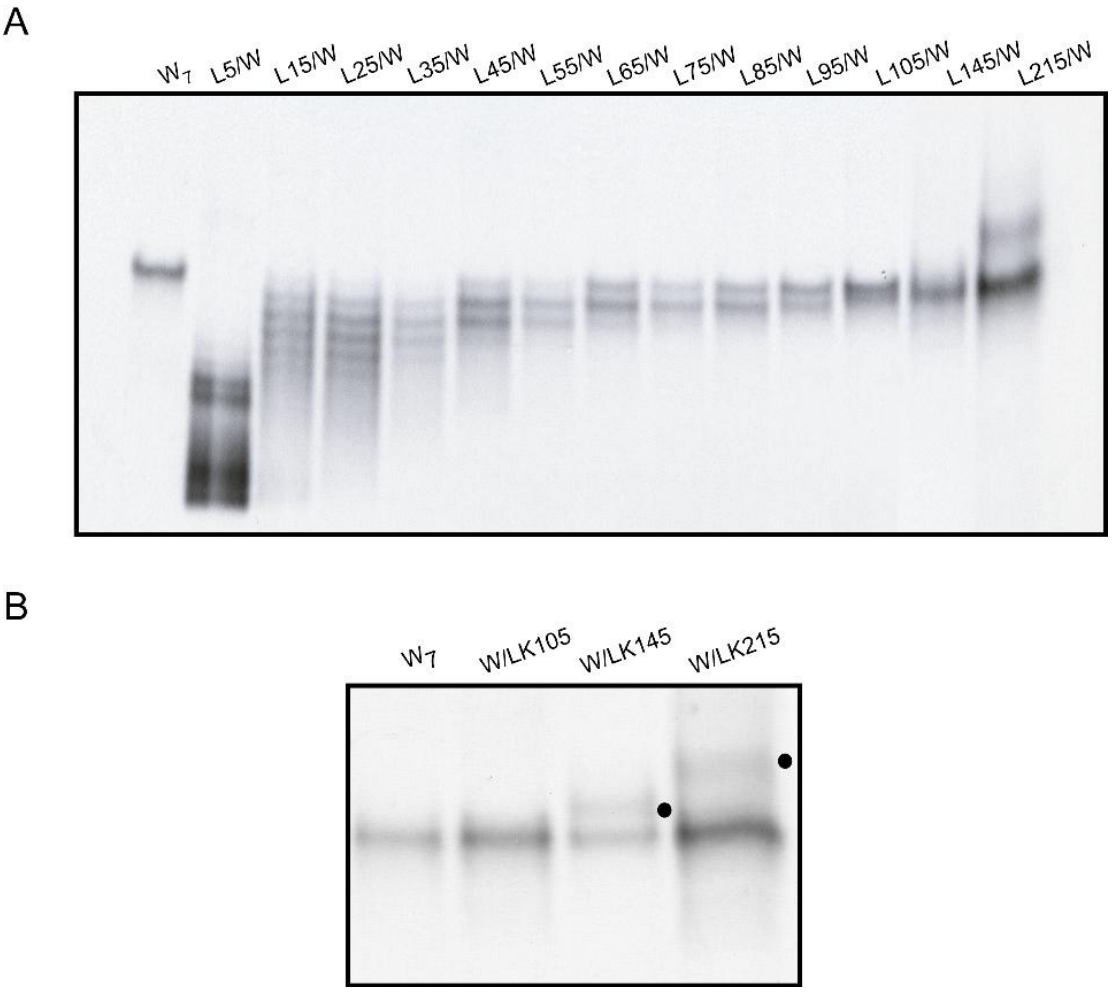

Figure 26. Maximum allowed number of L subunits in the heteroheptameric pores.

(A) Heteroheptamers (L5/W, L15/W, …, L145/W, L215/W) were synthesized by IVTT in the presence of rRBCM for 1 h at 37ºC. The templates were mixtures of W subunit DNA and L subunit DNA in a 1: 1 ratio. Membrane-bound oligomers were resolved in 5% SDS-polyacrylamide gels without prior heating. (B) Heteromers formed from the K288E revertants (L105K/W, L145K/W, L215K/W) were generated by co-translation in the presence of rRBCM and resolved in a 5% gel without prior heating. The templates were mixtures of W subunit DNA and L(10n+5)K subunit DNA in a 1: 1 ratio.

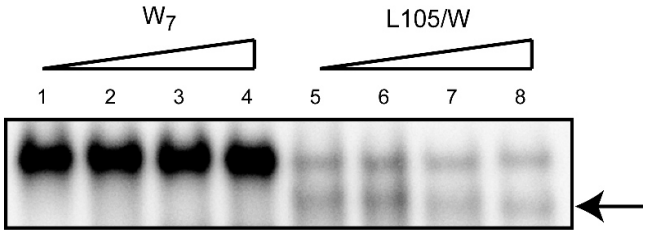

Figure 27. Limited proteolysis of heteromeric αHL pore with one long loop of 105 residues.

W_7, and heteromers of L105 and W subunits (L105/W) were treated with proteinase K for 5 min at 22°C. The oligomers were prepared by IVTT and assembled on rRBCM. The final concentrations of proteinase K were 0 μg/ ml (lanes 1, and 5), 5 μg/ ml (lanes 2, and 6), 50 μg/ ml (lanes 3, and 7), and 500 μg/ ml (lanes 4, and 8). The proteolyzed samples were resolved in a 5% SDS-polyacrylamide gel without prior heating. The protease resistant heteromer $L105_1W_6$ is shown (arrow).

Subunits Containing Longer Loops Form Heteroheptamers with Wild-Type αHL Subunits, but Not Homoheptamers

To explore the capacity of the cavity in the αHL pore for L subunits with longer loops ($n \geq 3$), additional heteromers were assembled with W subunits (Figure 26). For short loops ($0 \leq n \leq 2$), pores with seven L subunits could form (Figure 24). However, if the loops were longer than 25 residues ($n \geq 3$), the L subunits could not assemble by themselves (data not shown), but they did form heteromers with W subunits (Figure 26). Four subunits of L35 ($n = 3$) were able to assemble with three W subunits, while up to three subunits of L45 ($n = 4$) were incorporated into heptamers. For longer loops ($n = 5$ or 6), up to two L subunits were tolerated. For loops with more than seven repeats ($7 \leq n \leq 10$, $n = 14$ or 21), only one L subunit was incorporated. The L105/W heteromers (67 % at 500 μg/ml proteinase K treatment) were proteinase-resistant (Figure 27). When higher ratios of L: W were tested (up to 6 to 1), no additional L subunits were incorporated.

Longer exposure (21 d) of the dried gels to X-ray films failed to demonstrate the incorporation of additional L subunits.

The electrophoretic mobility of the L_1W_6 heptamers was reduced when the length of the loop was longer than 95 residues. In these cases, the effect of the loop on electrophoretic mobility outweighed that of the K288E mutation. For example, $L105_1W_6$ migrated slightly more slowly than L_1W_6 for L5 through L95, while $L215_1W_6$ migrated more slowly than even W_7 (Figure 24). When the K288E mutation was reversed (to "E288K"), the ladders caused by the incorporation of L subunits were not observed, but the decrease in electrophoretic mobility caused by the insertions in $L145_1W_6$ and $L215_1W_6$ were clearly visible (Figure 26B), suggesting that the additional polypeptide chain protrudes out of the lumen. This assumption was further substantiated by the electrical behavior of pores in bilayer experiments (see below).

Single-Channel Recordings of Loop-Containing Pores

The properties of gel-purified loop-containing oligomers were examined by planar bilayer recording in 2 M KCl, 10 mM MOPS, pH 7.4 (Figure 28). Unitary conductance values for $L5_7$ and $L15_7$ were 1.91 ± 0.02 nS (N = 4) and 1.90 ± 0.02 nS (N = 3), respectively, at +100 mV. Under the same conditions, the unitary conductance of W_7 was 2.18 ± 0.21 nS (N = 7). Like W_7, the currents were devoid of substates. By contrast, when the cavity was fully packed with polypeptide loops, the residual current was greatly reduced relative to W_7: $L35_4W_3$, 1.10 ± 0.04 nS (N = 3); $L25_6W_1$, 1.01 ± 0.15 nS (N = 4); $L25_7$, 0.67 ± 0.02 nS (N = 5) (Figure 28).

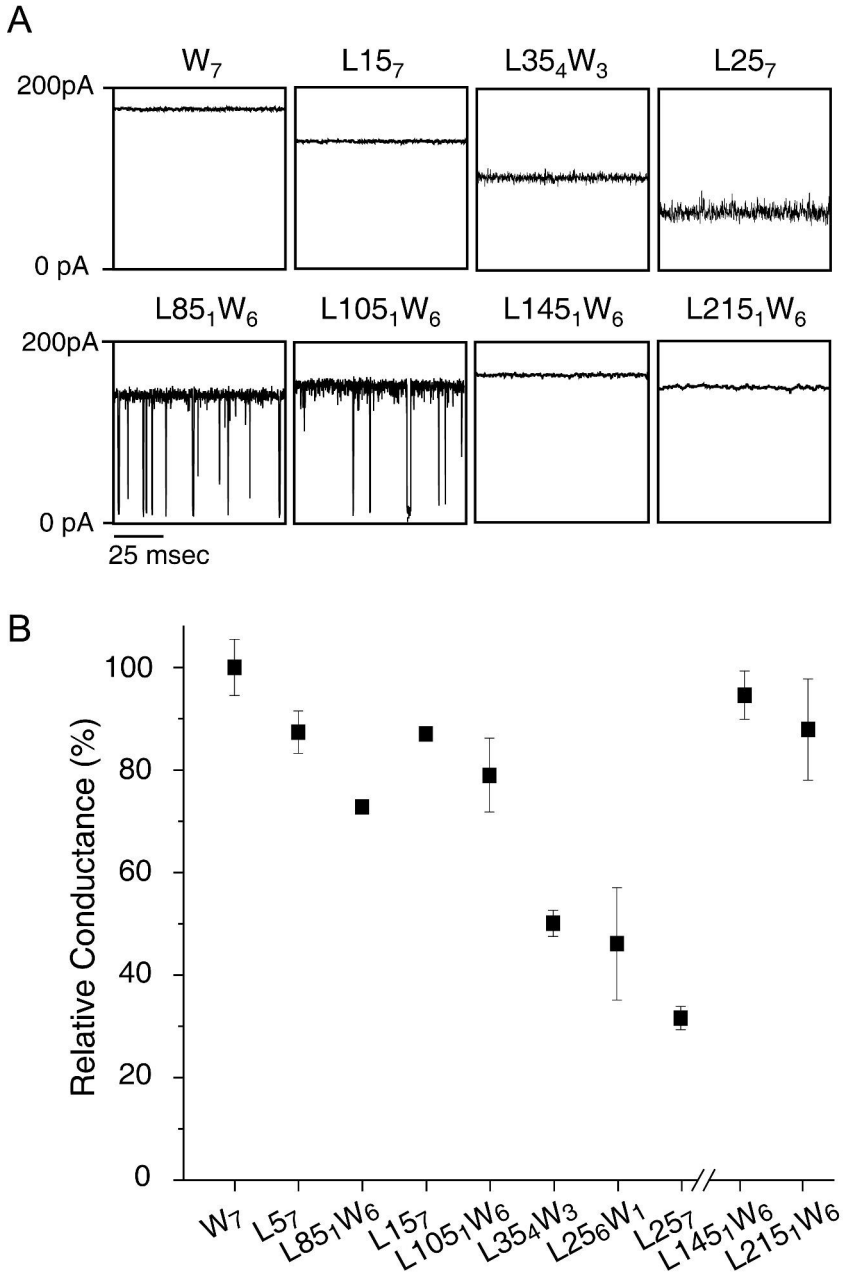

Figure 28. Single-channel recordings of αHL pores containing Gly/Ser loops.

(A) Single-channel recordings were performed at +100mV in 2 M KCl, 10 mM MOPS, pH 7.4. The currents were filtered at 10 kHz. Each heteromer was obtained by IVTT (37ºC, 1 h) in the presence of rRBCM and purified from a preparative 5% gel. (B) The single-channel current values were determined and expressed as a percentage of the W_7 current. Error bars indicate standard deviations of the mean (N = 8 for W_7, N = 3 to 5 for the rest). The recording conditions are same as in (A). The total number of inserted amino acids in the examined pore increases along the x-axis, except for $L145_1W_6$ and $L215_1W_6$, in which a portion of the loop is presumed to be outside the lumen.

With a single long loop (n = 8 or 10), transient partial closures of the pore were observed at positive applied potentials, but not at negative potentials (Figure 29). The closures are similar to those seen with αHL pores with PEG chains covalently attached within the cavity (*8*). The lifetimes of the closures were 99 ± 7 μs for $L85_1W_6$ and 593 ± 63 μs for $L105_1W_6$. The unitary conductance values were 1.59 ± 0.01 nS and 1.72 ± 0.08 nS, respectively, for $L85_1W_6$ and $L105_1W_6$ and the amplitude of the blockade in the closed state was ~1.53 nS in both cases. Unlike $L85_1W_6$ and $L105_1W_6$, $L145_1W_6$ and $L215_1W_6$, the pores with the longest loops, exhibited high unitary conductance values and no closures at both positive and negative applied potentials. Hence, they were similar to W_7, $L5_7$ and $L15_7$. The conductance values were: $L145_1W_6$, 2.06 ± 0.11 nS (N = 4) and $L215_1W_6$, 1.92 ± 0.04 nS (N = 4). Again, this observation suggests that a inserted long loop (n=14 or 21) resides mainly outside the pore, and does not affect the overall current flow (no blockade, no reduction of conductance).

Summary

Here, an unusual piece of protein engineering is described, in which an internal cavity within a transmembrane protein pore has been filled with additional polypeptide sequences. The engineered heptameric pores contain either seven short polypeptide loops ($0 \leq n \leq 2$) or a smaller number of long loops ($3 \leq n \leq 21$). The pores are stable as judged by protease-sensitivity and thermolability, and functional as judged by their ability to form pores in planar lipid bilayers.

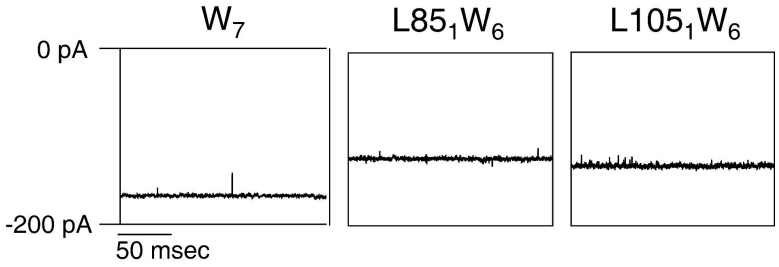

Figure 29. Single-channel recordings of long loop-containing αHL pores at negative potentials.

Electrical current of W_7, $L85_1W_6$ and $L105_1W_6$ pores were measured at –100 mV, in 2 M KCl, 10 mM MOPS, pH 7.4.

$L25_7$ was the homomeric pore that contained the largest amount of foreign sequence: 175 residues. The electrophoretic mobility of $L25_7$ (E288K reverted) was identical to that of W_7, suggesting that its hydrodynamic properties are unaltered and therefore that the additional polypeptide chains are contained within the protein. The conductance of $L25_7$ was 31% of that of W_7; therefore hydrated ions are still free to pass through it (Figure 28). The current passing through the pore exhibited excess noise, which might arise from movement of the loops near the constriction or from destabilization of the structure (Figure 28).

The accessible volume of the cavity in the cap domain is 32,600 $Å^{3,}$ as calculated by the slice of the enclosed central cavity, which divides the volume by seven (Figure 17). The pore that contained the most foreign residues, 175, was $L25_7$. To estimate the accessible volume take by the L25 loops, molecular graphic model of a L25 loop was generated by Swiss-Model. By rolling a probe, whose radius is 1.4, along the molecular surface of the L25 loop, the accessible volume taken up by a L25 loop was 8,330 $Å^3$,

which generated the total volume of seven L25 loops were 23,200 $Å^3$. Therefore, they must remain highly hydrated within the cavity, in agreement with the ability of the $L25_7$ pore to conduct ions, based on single-channel recordings. Furthermore, since there are no interaction with each other, the total volume taken up by the loop would be larger than the estimated accessible volume deduced from the L25 loop model.

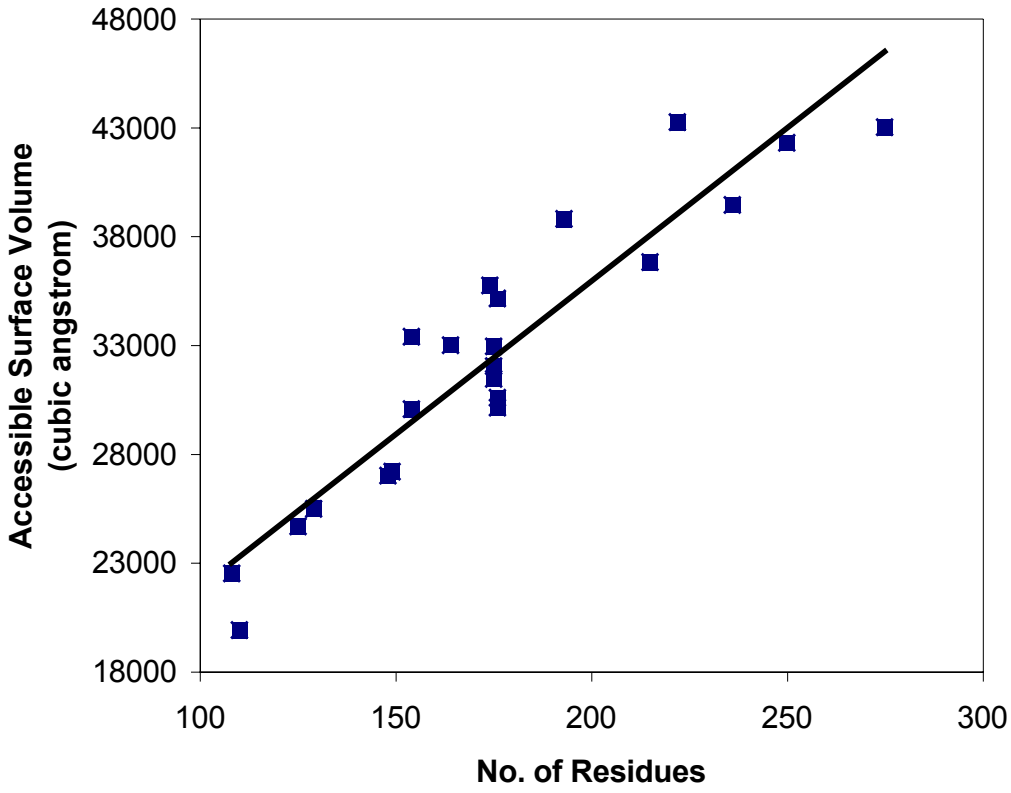

Figure 30. Accessible surface volumes of proteins from protein data bank.

Solvent accessible volumes of twenty two sample proteins were plotted against the number of residues. These proteins are globular, monomeric proteins with 100-300 residues, defined by X-ray analysis at 2.7A resolution or better (1CHH, 1A2P, 2PYP, 132L, 1A29, 1A2T, 1D1M, 1F18, 142L, 1CV8, 1AHN, 1FAJ, 1WBA, 1BG7, 1KHI, 1L4U, 1JUV, 1ATK, 1AQ7, 1C4F, 1AG1, 1DUI). The data were fitted to a straight line, to determine the corresponding number of residues for 32,600 $Å^3$ accessible surface volume.

The accessible volumes of twenty two proteins (1CHH, 1A2P, 2PYP, 132L, 1A29, 1A2T, 1D1M, 1F18, 142L, 1CV8, 1AHN, 1FAJ, 1WBA, 1BG7, 1KHI, 1L4U, 1JUV, 1ATK, 1AQ7, 1C4F, 1AG1, 1DUI) containing 108 to 275 residues were determined by SPOCK and then plotted versus the number of residues. From a linear fit, the number of residues corresponding to an accessible volume of 32,600 $Å^3$ is 176 (Figure 30). With these results, we can speculate that the cavity of the αHL pore could be packed with a folded protein with ~175 residues. Given the consideration of surface charges and the shape of a protein, the actual maximum limit would be less than 175 residues. An attempt to place a folded protein (98 residues plus 17 residues of linkers) in the αHL central cavity is currently investigate.

Only one copy of the largest loops (more than 75 amino acids) could be incorporated per heptamer, which is reminiscent of attempts to place covalently-attached PEG chains within the pore (*8*). For example, only one copy of a 5-kDa PEG could be placed within the cap domain. Pores with more than one PEG chain failed to assemble. The unitary conductance of pores of the form L_1W_6 did not differ greatly from W_7. For example, the conductance of $L105_1W_6$ was 79% of W_7. Interestingly, $L105_1W_6$ and similar pores (n = 8 to 10), exhibited transient closures (Figure 28A), suggesting that the loop was able to move into the constriction and almost completely block the pore. When the loop was larger still (n = 14 and 21), no closures were seen ($L145_1W_6$ and $L215_1W_6$, Figure 28A), suggesting that in these cases the loop is extruded through the cis entrance into the medium in keeping with the altered electrophoretic mobility of these pores. In the cases of $L145_1W_6$ and $L215_1W_6$, but not $L105_1W_6$, the electrophoretic mobility was

significantly reduced compared to W_7 (Figure 26B).

Table 7. Single-channel current recordings of a Gly/Ser loop-containing αHL pores.

αHL pore	Molecular weight of polymer (kDa)	Closed event duration (μs)	Closed event frequency (s^{-1})
$L65_1W_6$	4.7	65 ± 7	155 ± 129
$L85_1W_6$	6.1	269 ± 50	122 ± 7
$L105_1W_6$	7.5	593 ± 63	85 ± 5
αHL-PEG-3K*	3.0	132 ± 10	26 ± 10
αHL-PEG-5K*	5.0	13700 ± 2200	0.20 ± 0.02

The values are the mean ± SD for at reast five single-channel recordings.
*The electrical signatures of PEG-tethered αHL pores were adapted from the work by Movileanu et al. (*7*).

This finding is again reminiscent of the properties of pores containing covalently-attached PEG chains (*7,8*). For example, a pore containing a 3.4 kDa chain, terminated at the free end with biotin, comigrated with unmodified heptamer (W_7) and exhibited numerous spikes towards lower conductance, like $L105_1W_6$. When the PEG chain was captured in the cis compartment with streptavidin, the current became quiet, like that of $L215_1W_6$, suggesting that a portion of $L215_1W_6$ loop is protruding out of the lumen. Furthermore, the electrical signature of the modified αHL pore with a polymer (Gly/Ser loop or PEG) showed similar results (Table 7). As the length of the attached polymer lengthened, the dwell time of the events increased, while their frequency reduced.

CHAPTER IV

INTRODUCTION OF A TEMPERATURE-RESPONSIVE GATING MECHANISM INTO THE ALPHA-HEMOLYSIN PORE

Molecular Design of the αHL Subunit Containing an ELP Insertion

Based on the work in previous chapter, three different lengths of elastin-like polypeptide repeats (ELP repeats, (ELP=$(VPGGG)_n$, where n is 5, 10, and 20) were inserted before αHL residue S106 by cassette mutagenesis. It has previously been shown that the modification at S106 of αHL does not interfere with the protein assembly (*8*). We designed ELP loops of 5, 10, and 20 tandem repeats of the VPGGG pentapeptide, plus one valine (as a result of cloning) and ten residues of Gly/Ser linker sequences. The resulting αHL constructs containing these inserts (E) are E5, E10, and E20, respectively, which contain 36, 61, and 111 amino acid residues (Figure 31).

The given sequence of ELP at salt concentration was anticipated to have a transition temperature (Tt) at ~35ºC where single channel measurements are performed (1 - 2 M NaCl), according to extensive studies by Urry's group (*32*). However, the bulkiness or hydrophobicity of the inserted ELP residues could interfere with the folding of water-soluble αHL. Furthermore, the insert might interfere with the assembly process, especially the prepore to pore transition (*6, 20*). To facilitate the detection and analysis of the temperature effect on the αHL pore, it would be better to have the current

fluctuation (i.e. close and open states) with engineered ELP containg αHL pore. From the initial work with Gly/Ser loop-containing αHL pores (chapter III), the length dependence of the electrical current fluctuation and the number of L subunits in the heptamer were observed. Three different lengths (36, 61, 111 residues) of ELP loop were selected, which were generating partially closed states with the Gly/Ser-loop containing αHL pores with similar loop length (35, 65, 105 residues).

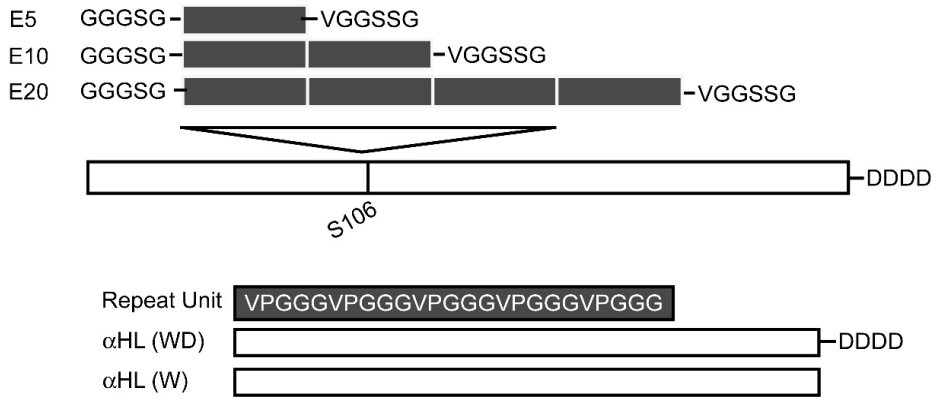

Figure 31. Diagram of ELP-containing αHL genes.

Concatamerized ELP repeat unit with flanking glycine-serine linkers were inserted by cassette mutagenesis between N105 and S106 in a wild-type αHL subunit with a polyaspartate tail (WD). The ELP-containing subunits were denoted as E5, E10, and E20, where the number represents the total number of inserted VPGGG repeats. Each repeat unit consists of five tandem repeats of VPGGG.

Instead of cloning an ELP repeat encoding one VPGGG motif, a tandem penta-repeat of VPGGG was cloned into the pYH1-αHL D4 vector (Table 3) using NdeI and HindIII sites, to facilitate concatemer formation of the desired length (Figure 11). By comparison, the earlier Gly/Ser repeat unit was composed of the 10 residues (SGSGSGGSGS). To produce a concatemer with ten tandem repeats of SGSGSGGSGS,

many trials were attempted. Not only was the yield of concatemers with a high number of repeats low, but the resolution of purification gel was poor since there is only a 30bp difference between neighboring concatemers. Here, by designing a longer the repeat unit (75 bp, $(VPGGG)_5$), both yield and resolution of higher concatemers were improved.

The repeat units from the pYH1-EM D4 vector were purified after digestion with EarI, which is a type II endonuclease. Type II enzymes digest DNA at sites outside the recognition sequences. Therefore the repeat unit would code only the ELP sequences without insertion of any unnecessary sequences. The 5' ends of purified repeat units were phosphorylated to facilitate head-to-tail ligation. Due to EarI cohesive ends, one additional residue of valine was added to the C-terminus of each ELP repeat, giving the final ELP sequence as $(VPGGG)_{5n}V$, where n is 1, 2 or 4. Each concatemer was flanked with 5 residues of flexible Gly/Ser linker sequences (Figure 31) to minimze any structural perturbation to main body of αHL. Purified concatemers of the desired length (5, 10, 20 repeats of VPGGG) were cloned into the recipient vector (pYH1-EC D4) using EarI and MluI sites, to generate the ELP-containing αHL genes (E5, E10, and E20) (Figure 12).

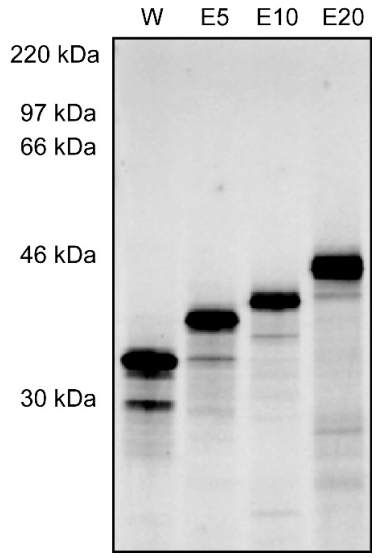

Figure 32. SDS-PAGE of monomeric E subunits with different lengths of a ELP loop

An autoradiogram of an SDS-polyacrylamide gel is shown for monomeric ELP containing subunits (E5, E10, E20) and the monomeric W subunit. Polypeptides were synthesized by coupled in vitro transcription and translation (IVTT) in the presence of [^{35}S]methionine and resolved in a 10% gel.

Generation of Heteromeric ELP-containing αHL Pore

The molecular masses of the subunits E5, E10, and E20 were approximately 35 kDa, 37 kDa and 45 kDa, respectively, as determined by SDS-PAGE, which is in good accordance with the calculated molecular masses (36.4 kDa, 38.2 kDa, and 41.9 kDa for E5, E10 and E20, respectively) (Figure 32). Heteroheptamers of W and E subunits were prepared by in vitro transcription and translation (IVTT) in the presence of purified rabbit red blood cell membranes (*29*). The templates were 1:1 molar ratio mixtures of plasmids encoding W subunit and E subunit, which generated the best resolution for all the possible heteromers. No additional incorporation of E subunits to a heptamer were detected even at higher W/E template molar ratio (data not shown). As fully assembled

heptamers are known to be stable in SDS if not heated (*6*), washed membrane bound heptamers were resolved in SDS-PAGE without heating (Figure 33).

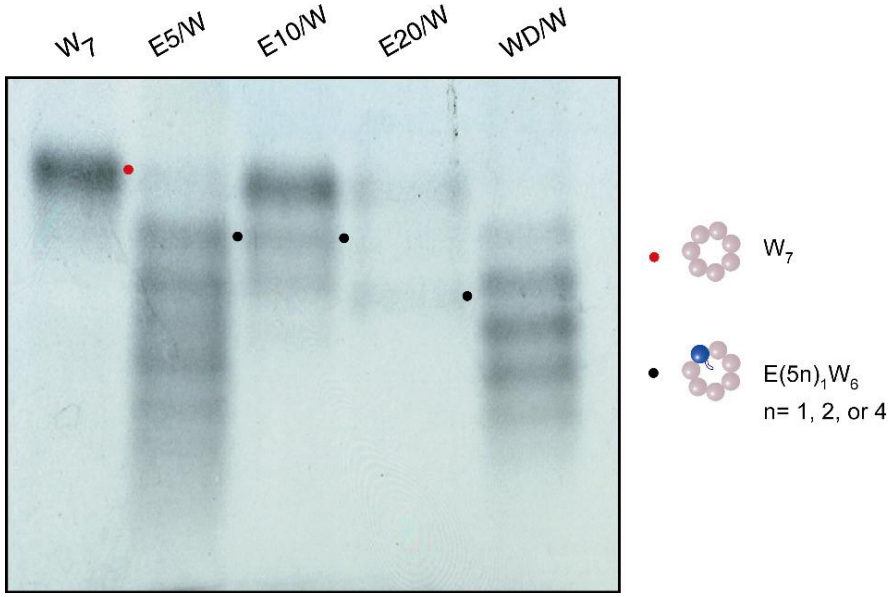

Figure 33. Heteromers by E subunits with different length of inserted ELP.

An autoradiograph shows electrophoretic shifts generated by polyaspartate tail (D4) on C-terminus of E subunits. The dotted bands (red for W_7 and black for E_1W_6 heteromers) were excised from a preparative gel for single-channel recordings.

Heteromers with E and W subunits showed downward electrophoretic shifts according to the number of subunits with oligoaspartate tail (D4) (Figure 33). Up to five E5 subunits were tolerated in E5/W heteromers, whereas only four L35 subunits were tolerated in L35/W heteromers (Figure 26). These findings might account for less probability to confine more flexible Gly/Ser- loops in the cavity than ELP-loops during oligomerization. Interestingly, we found different electrophoretic migration patterns for large ELP-inserted loop ($E20_1W_6$, dotted), which were similar to pores with a long

Gly/Ser loop insertion ($L145_1W_6$ and $L215_1W_6$, Figure 26), but in reverse direction (slower migration). The $L145_1W_6$ and $L215_1W_6$ exhibited slower migration while $E20_1W_6$ showed faster migration in 5% gel. Since there are no extra charged residues in the ELP loop, we can assume that the disposition of the loops contributes to the additional shifts, as observed previously with PEG-modified αHL pores (*8*). Heteromers with one loop $(E(5n)_1W_6$ (n=1, 2,4) or $(Ln)_1W_6$ (n=35, 65, 115, chapter III), were purified from polyacrylamide gels and subjected to a second SDS-PAGE analysis after heating to disassemble heptamer into monomers. The relative intensity reading of E subunit to W subunits were approximately 1:6 for three different trials ($E5_1W_6$; 1:6.3 ± 0.8 (N=3), $E10_1W_6$; 1:5.8 ± 0.48 (N=3), $E20_1W_6$; 1:6.5 ± 0.7 (N=3)). These heteromers were further studied with single-channel electrical recordings.

Insert Length-dependent Electrical Behaviors

Currents flowing through individual αHL pores were recorded at +80 mV in 2 M KCl, 10 mM potassium phosphate, pH7.5 (Figure 34). These conditions were chosen to maximize the signal to noise ratio over a wide temperature range. At room temperature (23 ± 0.5 °C), the current flowing through a single wild-type αHL pore (W_7) was 164 ± 6 pA (N=7). Advantageously for this study, W_7 pore remained opened for an indefinite period of time even at elevated temperatures. The open-state current amplitude through individual ELP-containing αHL pores (E_1W_6) were significantly reduced and decorated by transient short-lived current blockade events (closed states).

As the inserted loop was lengthened, the amplitudes of both the open state and

the closed state were reduced (Figure 34B-D). For heteromers with one short ELP loop ($E5_1W_6$, M_w=2.6 kDa, 36 amino acids), we observed an open-state current of 139 ± 8 pA (N=4), which is a 15.2 ± 2.5 % reduction (Figure 34B) comparing to the open-state of the W_7 pore. The very short-lived negative spikes are characterized by a duration, current amplitude and frequency of 108 ± 12 μs (N=4), 98 ± 11 pA (70.5 % of open state, n=4) and 140 ± 9 s^{-1} (N=4), respectively. Similar results were observed when a flexible poly(ethylene glycol) (PEG-3 kDa) chain was covalently attached through a disulfide bond to S106C of an αHL subunit (*7, 8*). The duration and frequency were 130 ± 10 μs and 26 ± 10 s^{-1}, for single PEG-3 kDa modified αHL pore assayed in 300 mM KCl, 5 mM Tris-HCl (pH 7.0), 100 μM EDTA. The short-lived negative spikes were interpreted as excursions of the peptide loop across the constriction of the αHL pore.

For heteromeric pores with a medium-sized ELP loop ($E10_1W_6$), the open-state current amplitude is further reduced to 123 ± 5 pA (N=14). The transient current blockades were also augmented (95 ± 2 % of open state, N=14), less frequent (61 ± 7 s^{-1}, N=14) and of longer duration (2.6 ± 0.28 ms, N=14) (Figure 34C). This result was anticipated; in the limited volume of the cavity, a longer loop is expected to be less mobile than a shorter loop, as the volume occupied by the hydrated longer ELP loop would be larger than the shorter one. Similar length dependent current behavior was observed with single PEG-5 kDa chain modified αHL pores (*7*). The duration (13.7 ± 2.2 ms) was lengthened and the frequency (0.20 ± 0.02 s^{-1}) was reduced compared to the PEG-3 kDa modified αHL pores.

In case of a long ELP-loop-containing αHL pore ($E20_1W_6$), a substantial reduction in the open-state current amplitude (104 ± 5 pA (N=3)) was observed (Figure 32D), which was accompanied by full current blockades (99 ± 1 %, N=3) of long duration (45.0 ± 5.3 ms, N=3) and lowered frequency (19 ± 2.7 s^{-1}, N=3) (Table 8). Substantially increased noise levels observed at both the open and closed states might account for the movement of the loops near the constriction or for the destabilization of αHL pore.

Table 8: Single-channel electrical signatures of ELP-containing αHL pores.

αHL pore	No. of residues in loop	Molecular mass of loop (kDa)	I_c/I_o*	Closed event frequency (s^{-1})	Closed event duration (μs)
$E5_1W_6$	36	2.6	0.29 ± 0.4 (4)	140 ± 9 (4)	108 ± 12 (4)
$E10_1W_6$	61	4.4	0.05 ± 0.02 (14)	61 ± 7 (14)	2600 ± 280 (14)
$E20_1W_6$	111	8.1	0.01 ± 0.01 (3)	19.0 ± 2.7 (3)	45000 ± 5300 (3)
$L65_1W_6$	65	4.7	0.14 ± 0.03 (3)	155 ± 12 (3)	65 ± 7 (3)

The values are the mean ± SD for at least three distinct single-channel experiments.
*I_c/I_o is the normalized amplitude of the closed state by the amplitude of the open-state.

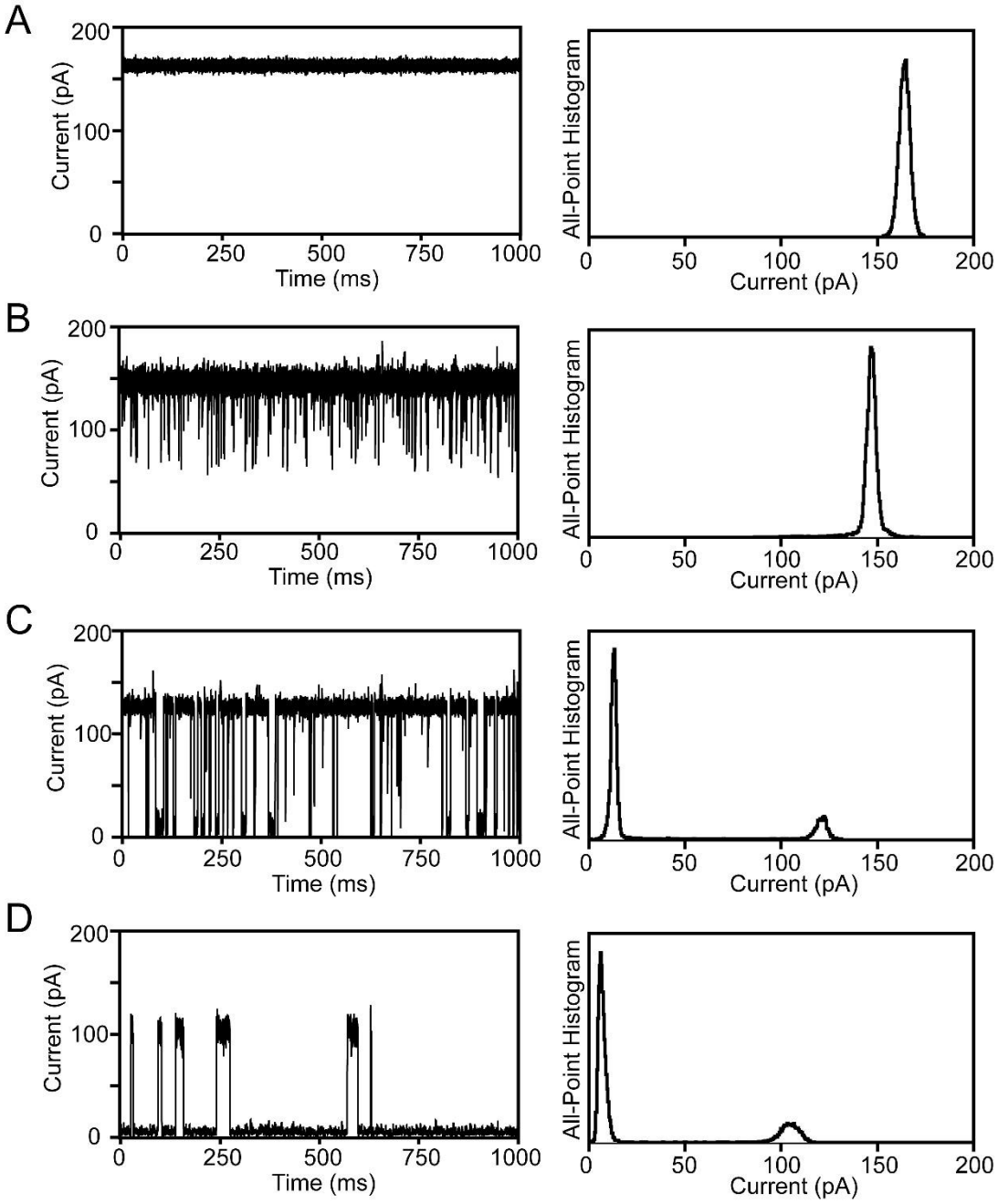

Figure 34. Effect of ELP loop length on currents of αHL pores.

Single channel recordings of W_7 (A), $E5_1W_6$ (B), $E10_1W_6$ (C), and $E20_1W_6$ (D) were analyzed at room temperature (23 ± 0.5ºC) in 2 M KCl, 10 mM K-phosphate buffer, pH 7.5. The transmembrane potential was +80 mV. The recorded current was low-pass 8-pole Bessel filter 20 kHz and sampled at 50 kHz. The right hand panels are representative the traces for each pore and the left hand panels are the all-point histograms corresponding to the single-channel recordings. Note that as the loop lengthens the currents of open and closed states are reduced and the duration of the closed states lengthened.

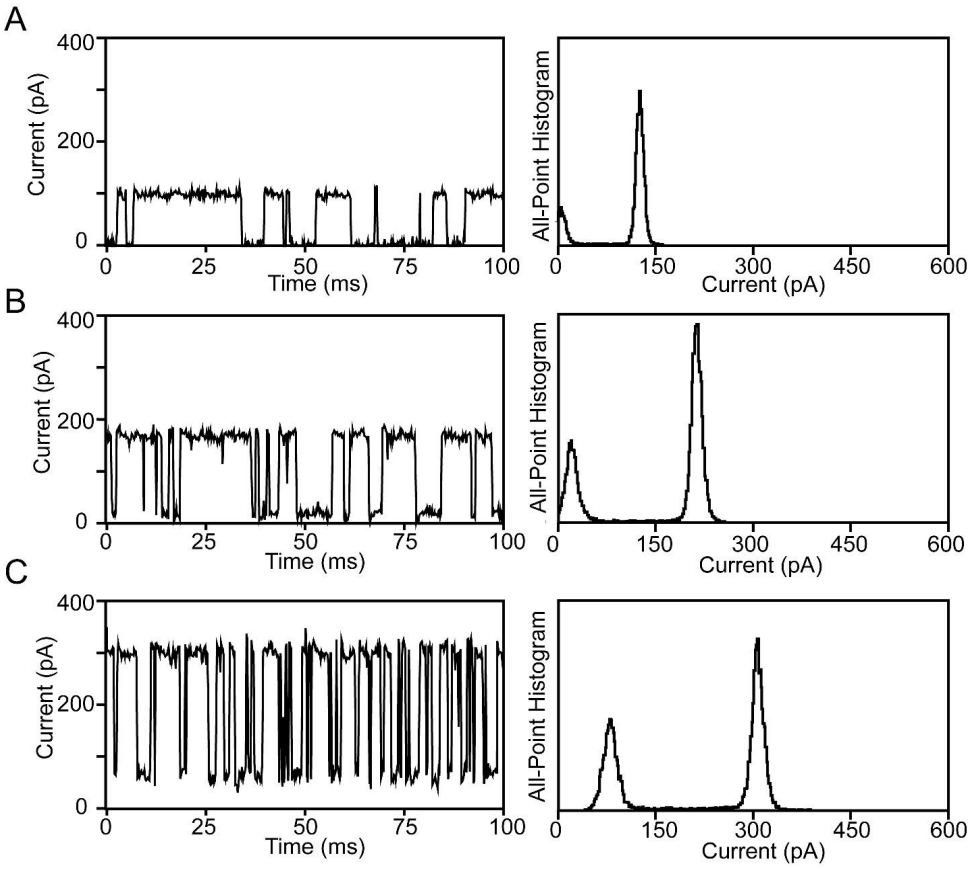

Figure 35. Single-channel recordings of the $E10_1W_6$ pore at different temperatures.

The electrical current through the $E10_1W_6$ pores were studied at 20ºC (A), 40ºC (B), and 60ºC (C). The holding potential was +80 mV. The temperature was controlled by connected PC, through an external command connection via Digidata 1322A, which converts the analog data to the digital data. The current and the temperature were simultaneously monitored by the Clampex 9.2 software. Other experimental conditions are the same as those presented in Figure 34.

Table 9: Single-channel electrical signatures of $E10_1W_6$ pores at different temperatures.

Temperature (ºC)	P_1	P_2	Duration of short occupied states (μs)	Duration of long occupied states (μs)	Total event duration (μs)
20	0.05 ± 0.02	0.95 ± 0.02	390 ± 36	4200 ± 240	4000 ± 380
40	0.67 ± 0.03	0.33 ± 0.03	231 ± 27	1800 ± 160	750 ± 91
60	0.95 ± 0.02	0.05 ± 0.02	120 ± 16	720 ± 83	150 ± 21

The values are the mean ± SD for at reast five single-channel recordings.
P_1 and P_2 are the probability of the short and long occupied states, respectively.

Electrical Recordings of an ELP-containing αHL Pore at Different Temperatures

The heteromer, $E10_1W_6$, was further studied with single-channel recordings to seek evidence for temperature-dependent gating mechanisms. With the other ELP loops, the electrical signals were either too short to resolve or too infrequent to analyse. $E5_1W_6$ produced very short-lived transient events at room temperature, with an average duration of 108 μs (Figure 34B, Table 8), but the individual current blockade events were hardly resolvable at elevated temperatures (data not shown). The main state of the $E20_1W_6$ pore was the closed state with probability of 0.80 ± 0.06 (N=3) at room temperature, which required longer recording time to obtain the significant data. However, $E10_1W_6$ produced full current blockade events at 20°C, and the signals were resolvable throughout the temperature range examined in this work (20 – 60°C) (Figure 35).

The characteristics of both the open-state current amplitude and individual current blockade events are highly temperature-sensitive. First, the open-state current amplitude of the $E10_1W_6$ pore increases with temperature from 119 ± 7 pA (N=8) at 20 °C to 189 ± 11 (N=5) and 301 ± 12 pA (N=5) at 40 and 60 °C, respectively (Figure 35), as expected due to the increase in conductivity of the bulk solution. There were two types of closing events, one of short duration and another of long duration. For example, at 20 °C, we observed complete transient blockades with a duration of 390 ± 36 μs (the probability P_1=0.05 ± 0.02, the short occupied states) and 4.20 ± 0.24 ms (P_2=0.95 ± 0.02, the long occupied states) (N=8). The total event frequency recorded at this temperature was 43.0 ± 5.7 s^{-1}. The total event frequency of events (both short and long

occupied states) increased substantially with the temperature while the duration of the events were reduced. At 40ºC and 60ºC, the total closed state event frequencies were 165 ± 17 s^{-1} and 475 ± 38 s^{-1}, respectively. The duration of events was 750 ± 91 μs (N=5) and 150 ± 21 μs (N=5) at 40 °C and 60 °C, respectively (Table 9).

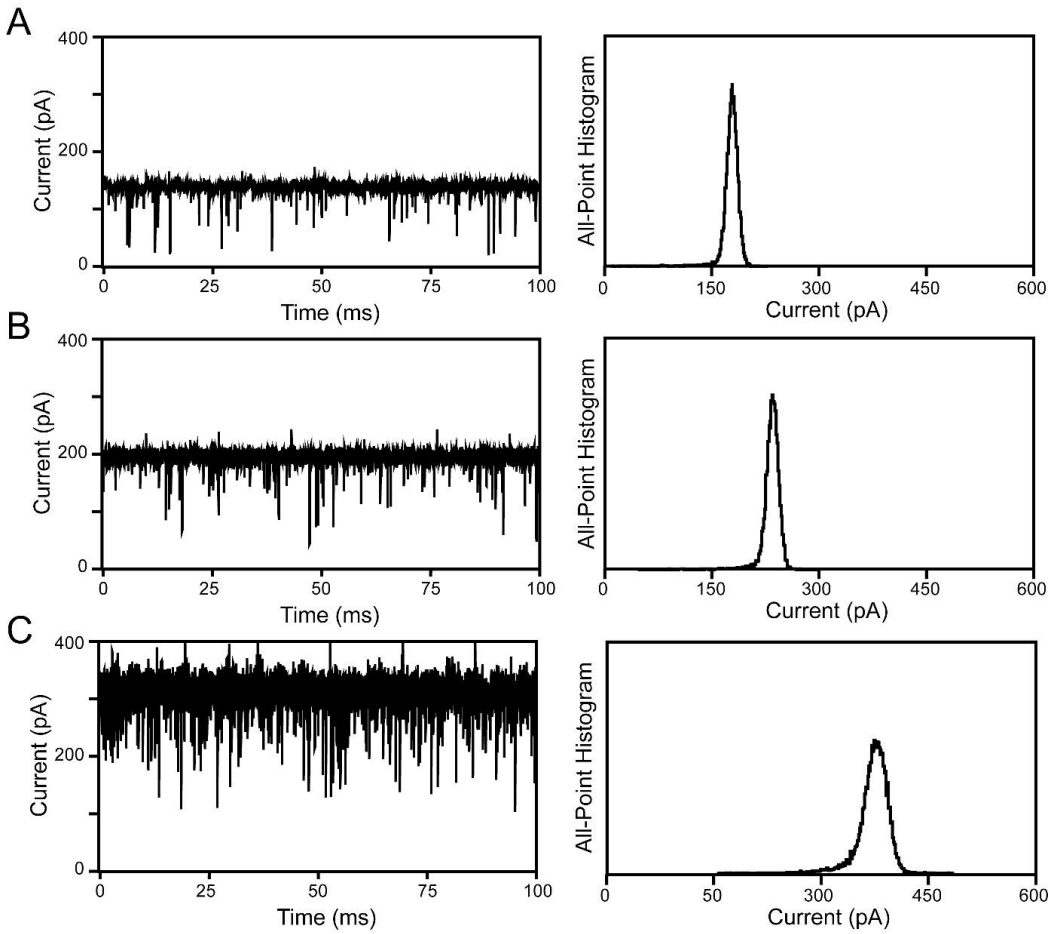

Figure 36. Single channel recordings of a Gly/Ser loop-containing αHL pore ($L65_1W_6$) at different temperatures.

As the $L65_1W_6$ pore accommodates a similar number of exogenous amino acid residues in the central cavity of the αHL pore as $E10_1W_6$, single channel recordings were conducted at 20ºC (A), 40ºC (B), and 60ºC (C), for comparison with the $E10_1W_6$ pore (Figure 35) at same temperatures. All the conditions for the recording and analysis are same as in Figure 33.

To verify the identity of the temperature-dependent responses of $E10_1W_6$, we carried out single-channel electrical recordings for a pore with Gly/Ser loop ($L65_1W_6$) of closely similar length (Figure 36) in similar conditions to those presented in Figure 33. Gly/Ser loop sequence is expected not to follow an inverse structural transition as the temperature increases, since the ELP sequence and the abductin sequence are known to be the only polypeptides that exhibit temperature-dependent inverse transitions. At 20°C, the single-channel electrical recordings of $L65_1W_6$ pore revealed very short-lived negative current spikes (65 ± 7 μs, N=3). At 20°C, the open-state current amplitude of $L65_1W_6$ was 135 ± 7 pA (N=3), while the closed state amplitude was only 17 ± 11 pA (N=3) (Figure 34A). At 60 °C, the open-state and closed state amplitudes were 336 ± 12 pA (N=3) and 50 ± 12 pA (N=3) (Figure 36C). The event duration was very short compared to that of $E10_1W_6$ pore, under the same conditions (Figure 35), suggesting the Gly/Ser loop is more flexible than the ELP loop in the cavity.

Due to the increase of the bulk solution conductivity with the temperature (*104*), the amplitude of the currents through $L65_1W_6$ and $E10_1W_6$ were observed for both the open and closed states (Figure 37). To cancel out the effect of solution conductivity, the amplitude of the closed state current was normalized by that of the open state current and then plotted against temperature (Figure 37B). When the data points were fitted with sigmoidal curve, $E10_1W_6$ showed two-state transitions with the mid point located at 38.1 ± 0.4 °C (N=5), while the $L65_1W_6$ did not show any changes with temperature. With extensive study by Urry's group(*32, 38, 40*), this transition temperature was estimated as ~ 32°C with VPGGG repeat.

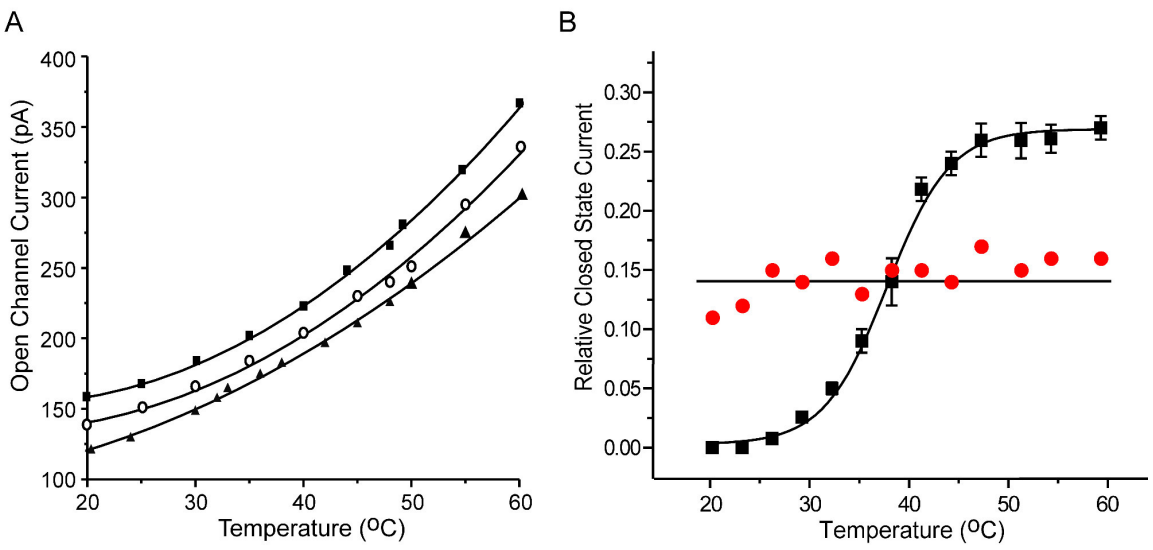

Figure 37. Temperature-dependent conductance of the αHL pores.

(A) The conductance of αHL pores, W_7, $L65_1W_6$, and $E10_1W_6$ were measured at +80 mV in 10 mM K-phosphate buffer, 2 M KCl, pH 7.5 at different temperatures. The net conductivity of the solution is increasing with the increase of temperature. Filled square (■) is for W_7 pore, open circle (○)$L65_1W_6$ pore; and filled triangle (▲) $E10_1W_6$ pore. (B) The closed state current of $E10_1W_6$ (black) or $L65_1W_6$ (red) was divided by the open state current of the corresponding pore to cancel out the bulk solution effect and plotted against temperature. All the data measured at +80 mV and repeated at least with five distinctive single-channel recordings. All point were fitted with sigmoidal curve.

A simple model with four states, which illustrates the temperature-induced changes in the open-state and the closed state, is presented in Figure. 38. States I and II represent the open and closed states, respectively, of the ELP-containing αHL pore at temperature below Tt. States III and IV indicate the open and closed states, respectively, of the ELP-inserted αHL pore at temperature above Tt. The transition between the I and II states to the III and IV states requires energy, in this case heat. Therefore at given temperature, only the state with low residual current (states I and II) or the state with high residual current (state III and IV) was observed.

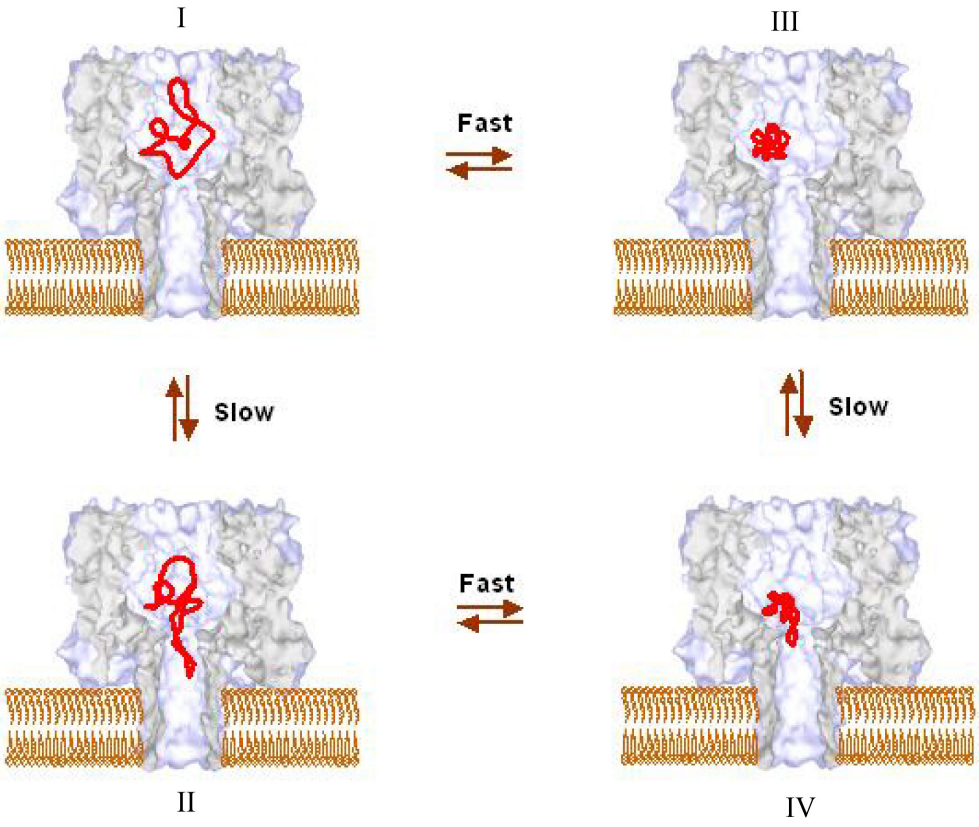

Figure 38. Model of temperature-responsive gating mechanism for an ELP-containing αHL pore.

The low conductance states account for the state of inserted ELP in the lumen at below the transition temperature (I and II states). The high conductance states account by the hydrophobic collapsed ELP insert in the lumen at above Tt (III and IV states). At positive potentials, some parts of the loop may be jammed in the constriction region, which is responsive for closed states (II and IV states). At above Tt, the ELP portion is more compactly packed than the state below Tt. The rigidity and the reduced volume of the ELP accounts for shorter blockade duration at above Tt.

Summary

Staphylococcal αHL pores was engineered to exhibit a temperature-responsive gating mechanism. Controlled number of ELP repeats with defined length were located in the central cavity of the αHL pore. The amplitude and the frequency of the transient blockades increased as the temperature increased from 20ºC to 60ºC, while their duration decreased. When the amplitude of blockade was normalized with that of the fully open state, a sigmoidal two-state transition was found, with the midpoint at 38.1 ± 0.4ºC. As the estimated transition temperature for VPGGG repeat was ~ 32ºC , according to Urry, this observation was proposed as the result of the ELP inverse transition. Different guest residue in the ELP sequence, which changes the transition temperature would provide further evidence fot the identity of the temperature-dependent behavior of the engineered αHL pore. In the future, ELP sequences within αHL pores might be engineered further to allow, for example, the temperature-controlled release of drugs from lipid vesicles or the permeabilization of mammalian cells for the introduction of cryoprotectants.

CHAPTER V

PROTEIN ANALYTES DETECTED WITH AN αHL PORE

Generation of an αHL with an Encoded PKI Loop

Based on the work with the Gly/Ser loop- containing αHL pores, a loop length of 115 residues was determined to be a candidate for PKI fragment (TTYADFIASGRTGRRNAIHD, 5-24 residues) insertion at near the mid region of the loop. From electrophoretic migration assays and single-channel recordings with long Gly/Ser loop containing αHL pores, ($L105_1W_6$, $L145_1W_6$, and $L215_1W_6$), the minimal length of an inserted loop that will protude out of the lumen is ~ 105 residues. Also conformational changes of 20 residues of PKI fragment (5-24) was observed when it is bound to the PKA catalytic subunit, indicating some extra residues might be needed to ease the interaction. Therefore a 115 residue-long loop would serve as the adequate length to make the loop move in and out of the lumen without any struggle and for the PKI fragment to interact with the PKA catalytic subunits.

Initially, the pYH2-L105 D4 and pYH2-L45 D4 constructs were generated to place single cysteine residue at the mid point of the Gly/Ser loop. By modifying the cysteine with commercially available iodoacetyl biotin (biotinyl-iodoacetamidyl-3,6-dioxaoctanediamine, Pierce, Rockford IL), an attempt to evaluate the topology of a Gly/Ser loop (105 residues and 215 residues) and/or the frequency of its availability at

outside of the lumen (mainly at cis side) were tried. This iodoacetyl biotin has shortest spacer arm (polyethylene oxide, 24.7Å) in commercially available cysteine-specific biotins. The electrical traces of biotin tethered αHL pores were decorated with 6 extra substates (data not shown). These result might account for the the fast transitions of the polymer due to the flexibility of the spacer arm. Furthermore, addition of wild-type streptavidin to the cis side of the chamber failed to show changes in any of 6 substates, indicating the distance of the biotin probe might be too far away from the cis mouth of the pore. Due to the complexity of the signals, this constructs were not further studied.

Four strands of single strand DNA, encoding *SSGS*TTYADFIASGRTGRRNA-IHD*GSGSGSS* (PKI fragment (5-24) and Gly/Ser linker sequences (italic)), were ligated between SacI and XhoI sites of the PCR fragments, which represents N-terminal (light blue) and C-terminal (red) halves of the αHL gene (Figure 14). The PKI fragment was placed near the mid point of the PKI 115 loop (115 residue-long loop with PKI fragment) as intended, while it was shifted towards N-terminus during cloning for PKI 206 loop (206 residue-long loop with PKI fragment) (Figure 39). The αHL subunit with PKI sequence is denoted as Pn subunit, where n is for the number of exogenous loop residues (115 or 206) (Figure 39).

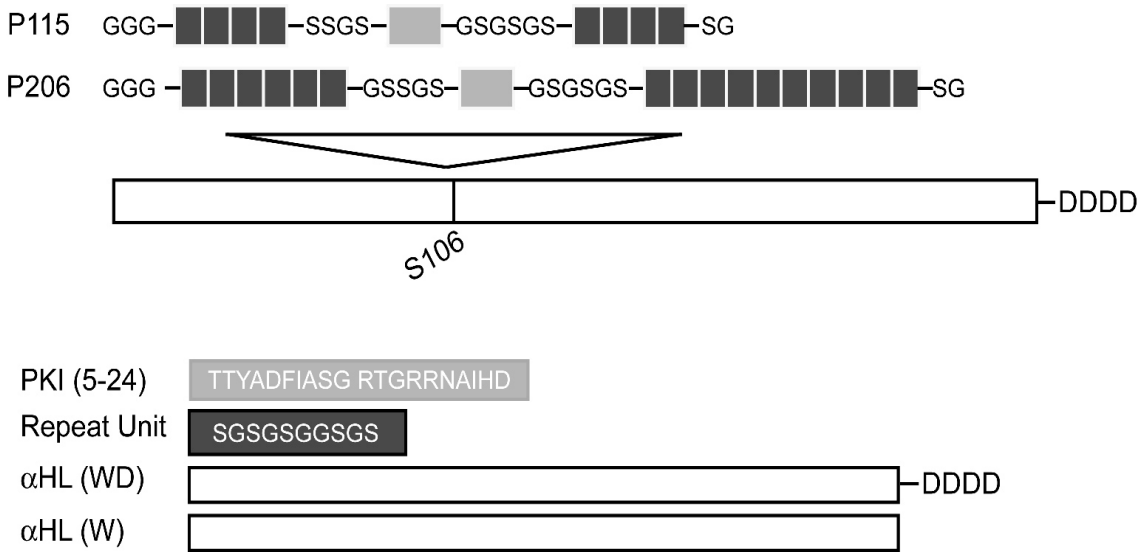

Figure 39. Diagram of protein kinase inhibitor fragment (5-24) containing alpha-hemolysin subunits

Protein kinase inhibitor fragment (5-24) was inserted approximately at mid-point of Gly/Ser-rich loops to generate P115 and P215 constructs, respectively. For P215 construct, fortuitous recombination of repetitive Gly/Ser segments were observed for final clone. Therefore, the final constructs were named as P115 and P206 for αHL subunits with a PKI fragment-containing loop, which are 115 residues and 206 residues, respectively. The entire exogenous loop segments were placed upstream of S106 position of wild-type αHL. For separation of the αHL pores with P115 or P206 subunit from the wild-type αHL pores, four aspartate residues were attached to C-terminus of the gene.

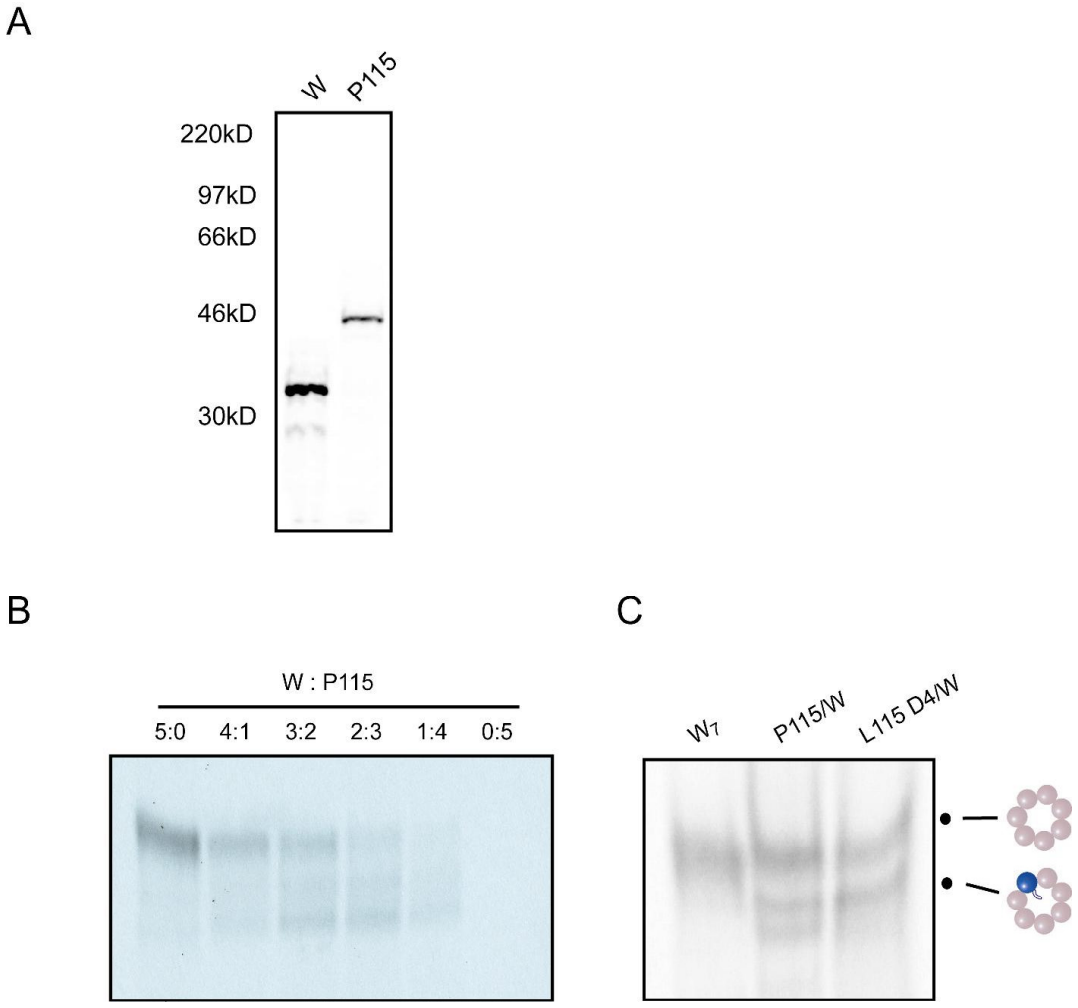

Figure 40. Autoradiographs of the monomeric P115 subunit and heteromeric αHL pore with P115 subunit.

(A) [^{35}S]Methionine-labeled monomeric P115 was resolved in 10% SDS-polyacrylamide gel. P115 constructs were migrating according to the calculated molecular weights (42 kDa) in 10% gel. As for the control, monomeric W subunits were applied in first lane. (B). An autoradiograph of heteromers of P115 and W subunits formed by IVTT in the presence of rRBCM, under different molar ratio of templates (W:P115). The identity of third band of P115/W is unknown and not further studied. (C). To compare the electrophoretic migration pattern of the membrane bound oligomers, the homoheptameric wild-type αHL pore (first lane) and the heteroheptamers of L115 D4 subunit and W subunit are also shown (third lane). Dotted band indicates the oligomers subjected for single channel recordings. As illustrated on the left side of the autoradiogram, the first band indicates homoheptameric wild-type αHL pore, and the second band for P115/W heteromers with only one P115 subunit and six W subunits, as confirmed by relative intensity of each subunits, after re-resolved in 10% gel prior to heating (data not shown).

Heteromer Formation

Radiolabeled monomeric P115 subunit was generated by IVTT in the presence of [^{35}S]-methionine. The calculated molecular weight of P115 subunit is 42 kDa, which was in good accordance with SDS-PAGE (Figure 40A). Heteromeric P115/W αHLs were generated by IVTT in the presence of [^{35}S]methionine and purified rRBCM. There were 3 bands in total for the P115/W lane (Figure 40B).The second (heteromer type 1) and the third bands (heteromer type 2) were purified subjected for second SDS-PAGE analysis after heating. Interestingly both samples gave roughly 1:6 ratio of P115/W subunit intensity (data not shown). Furthermore the extent of gel shift for heteromer type 2 varied from gel to gel (Figure 40C), indicating it might be the $P115_1W_6$ heteromer with its loop threading out. The P115/W heteromer migration pattern was compared with P115/W heteromer (Figure 40C). Charge of the loop (net two positive charges at pH 6.8) might contribute for the third band, assuming that same extent of both P115 and L115 loop were protruding out of the αHL lumen. However this heteromer type 2 was not further studied.

The dotted P115/W heteromer ($P115_1W_6$) was purified from preparative acrylamide gel and the ability to bind protein kinase catalytic subunit was determined by single channel recordings. The purity of $P115_1W_6$ heteromer was confirmed by second SDS-PAGE (10% acrylamide) after heating the sample (data not shown). P206 construct was not investigated further, since the heteromeric pore ($P206_1W_6$) generated no changes with PKA presence (Figure 41). However, a correlation was observed between the length of the inserted loop with the electrical signals, which is similar to Gly/Ser-loop

containing αHL pores (see below).

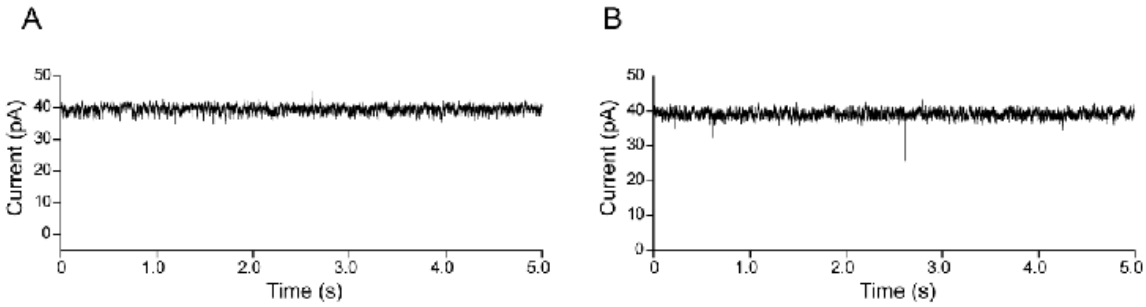

Figure 41. Traces of $P206_1W_6$ heteromeric pore with and without PKA in the chamber.

The single-channel recording of $P206_1W_6$ pores (two channels) in 300 mM KCl, 50 mM MOPS pH 6.8, 1 mM $MgCl_2$, 100 μM ATP at +80 mV without (A) and with (B) PKA (80 nM, cis) addition.

Single-molecular Binding Events of PKA to PKI Fragment-containing Loop

As described earlier, the $P206_1W_6$ pore failed to show the PKA binding (Figure 41), and not assyed further. The single channel recordings of $P115_1W_6$ showed PKA catalytic subunit binding events at single molecular level, in the presence of 100 μM ATP and 1 mM $MgCl_2$. Without the presence of PKA catalytic subunits, the pore exhibited high noise electrical signals with an open state amplitude of 14.22 ± 0.01 pA (N=5). However, when PKA catalytic subunits were added to the cis chamber (100 nM), two types (I and II) of more open states were observed, as shown in Figure 42. The dwell time of these events are 3.27 ± 0.67 s (N=27) and 5.16 ± 1.2 s (N=18), with the amplitude of 18.45 ± 0.1pA and 17.36 ± 0.01 pA, respectively for the I and II states.

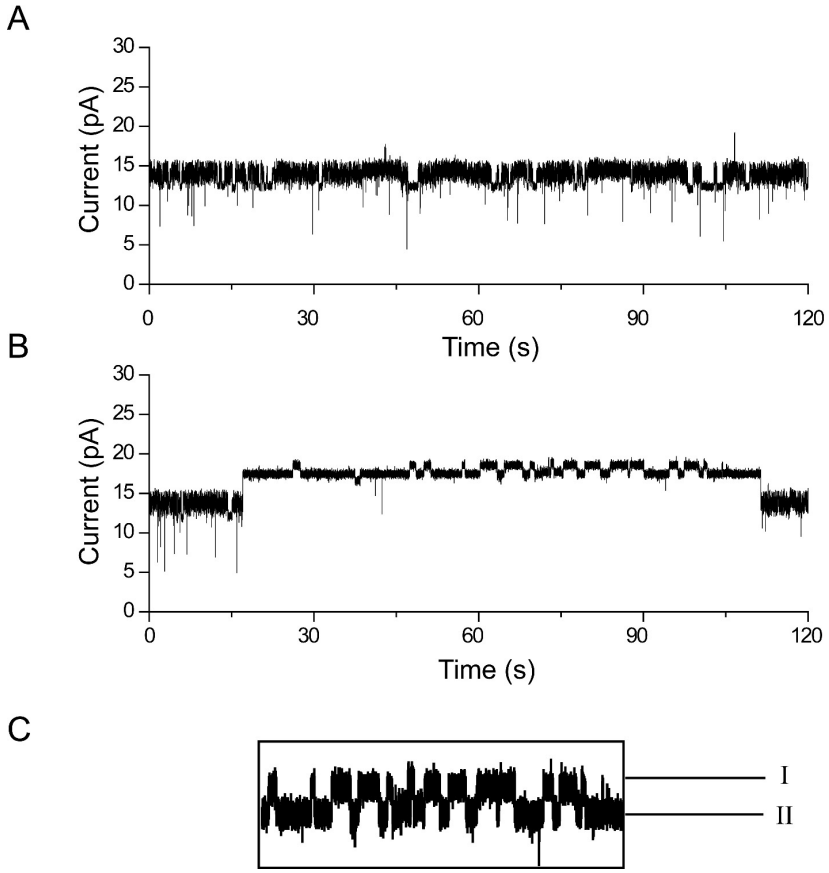

Figure 42. Single molecular binding events of PKA to PKI sequence of $P115_1W_6$.

Electrical current flow (A) through the $P115_1W_6$ pore was recorded at +80 mV in 5 mM MOPS pH 6.8, 300 mM NaCl. The signals were acquired at 200 μs intervals and filtered with 3.0kHz Bessel filter. (B) Upon addition of the PKA catalytic subunits (100 nM) to cis compartment of the chamber with 1 mM $MgCl_2$, 100 μM ATP, two types (I and II) of more open states were observed. A zoomed section of these two events was shown in C.

The dwell time of type I event was in good accordance with that of the αHL (T129C-PKI αHL) pore, which is chemically modified by single PKI fragment (5-24) polypeptide at the trans mouth. The dwell time of T129C-PKI αHL pore is ~ 3.5 s at –80 mV, in 300 mM KCl, 15 mM MOPS (pH 6.8) (*61*). Unlike T129C-PKI αHL pore, upon binding of PKA catalytic subunits, the current through the $P115_1W_6$ pore was increased

6.3%. This is interpleted as the result of loop threading out from the αHL lumen. Similar increase of current was observed with $L145_1W_6$ and $L215_1W_6$ pore, whose loop is believed to be out side of the lumen. Other similar characteristics of $P115_1W_6$ pore to $L145_1W_6$ and $L215_1W_6$ are, upon binding to the PKA catalytic subunits, the channel traces became quiet like the wild-type αHL pore (no substates and the size of the amplitude) (Figure 42).

Since it is known that the binding of MgATP to catalytic subunit changes PKI affinity to high affinity, the current through $P115_1W_6$ pore was measured with and without MgATP in the chamber. Without MgATP, weak binding of PKA to PKI-loop was observed (29.8 ± 3.2 μs dwell time with 3.9 Hz frequency), as shown with very short binding events (arrowed, Figure 43B,C). With increased concentration of PKA, from 50 nM to 100 nM, more frequent short binding events were detected but with similar duration (22.1 ± 1.7 μs dwell time with 6.35 Hz frequency). When 100 μM ATP and 1 mM $MgCl_2$ were added to cis side of the chamber, more longer binding events were detected (3.1 ± 0.1 s) but in scarce frequency (0.5 Hz) This observation account for high affinity interaction (dissociation constant Kd = 0.3 nM) of PKA catalytic subunit with PKI, when ATP and divalent metal ions were present.

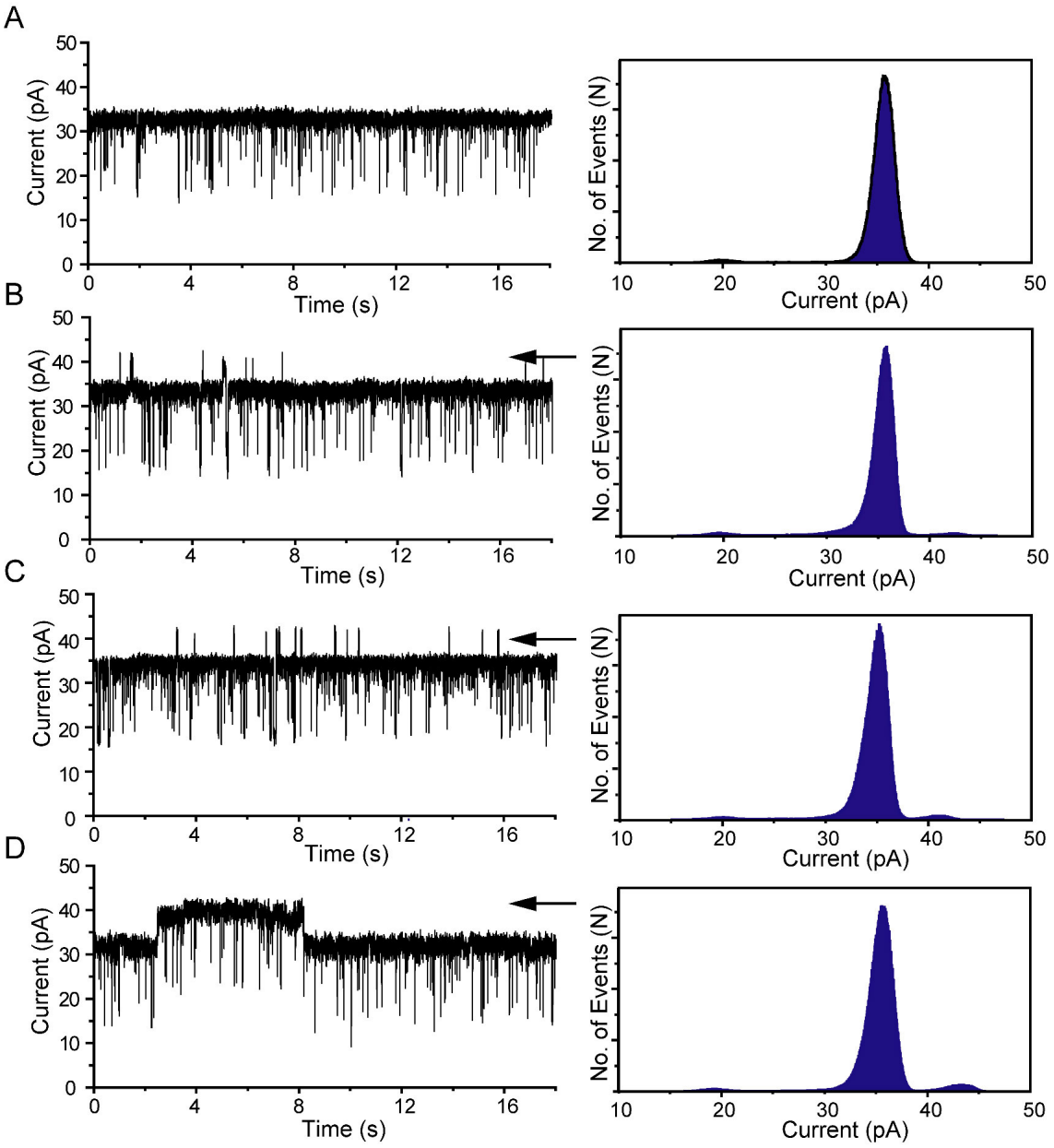

Figure 43. The effect of ATP on the interaction of PKA-PKI fragment of $P115_1W_6$ pore.

Electrical current flow (A) through $P115_1W_6$ (two channels) was recorded at +80 mV in 5 mM MOPS pH 6.8, 300 mM NaCl. The signals were acquired at 100 μs intervals and filtered with 3.0 kHz Bessel filter. Traces are shown on the left panels and the all-point histograms are shown on the right. To show the binding event of PKA (arrowed) from cis side of the pore, 50 nM PKA (B) and 100 nM PKA (C) was added to cis chamber. When 100 μM ATP and 1 mM $MgCl_2$ were added to the channel in C, longer binding events were observed (D).

Summary

By introducing a heat stable protein kinase fragment (5-24) into αHL pore as a part of the exogenous loop (115 residues), the interaction of cAMP-dependent protein kinase catalytic subunit and PKI sequences was detected in single molecular level. The transient closure of the pore, interpreted as the dynamics of loop near the constriction region, was stopped by binding to PKA molecule from outside of αHL lumen. The increase of the current amplitude and the dampening of the noise upon binding indicate that the loop was stretched out from the cavity. The $P115_1W_6$ pore generated different kinetic model (Figure 44) with the recently reported T129C-PKI αHL pores (*62*). For the time allowed, this construct was studied in terms of the evidence for the length dependent loop encapsulation.

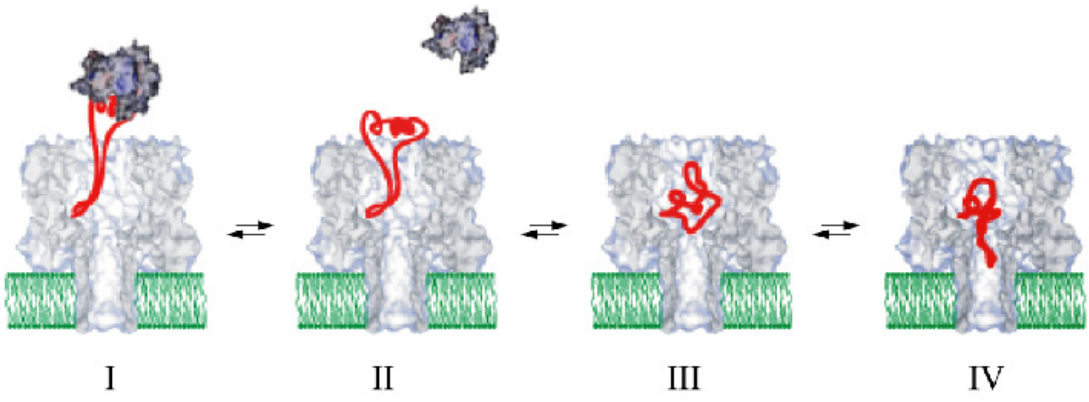

Figure 44. Model of PKA capture events of PKI loop-containing αHL pore.

Capture of PKI fragment by PKA catalytic subunit (I) from the cis side of chamber dampens the electrical noise of PKI-containing αHL pore ($P115_1W_6$). If the loop is protruding out of the lumen (II), the channel shows open state (type II), as the loop becomes stretched and less available in the lumen. However, when the loop resides mainly inside the lumen (III and IV), the pores generated fast fluctuation of the current, indicating the loop movement near the constriction (IV).

The electrophoretic shift and the characteristics of electrical current (the amplitude and the current fluctuation) suggested that the loop with ~115 residues are protruding out of the αHL lumen. As seen with Gly/Ser loop-containing αHL heteroheptamers, the loop length of 145 or 215 residues generated high conductivity state without any substates or noise. This characteristic was interpreted as the Gly/Ser loop resided mainly outside of the αHL lumen. Similar effect was observed with $P115_1W_6$ and $P206_1W_6$ αHL pores. The electrical current of $P115_1W_6$ pores was decorated with transient closed states, similar to $L105_1W_6$ pore (Figure 28). When the PKA catalytic subunits were added to the cis compartment, the signal of this transient closure was dampened, indicating capture of inserted PKI fragment sequence by PKA catalytic subunits. This result was similar to the interaction of the PEG-tethered αHL pore with the streptavidin (*7*). Interestingly, the amplitude of the current was increased when the signal was dampened, indicating the loop is stretched out thus generating less occlusion effect of the current flow. Capturing event of the tethered PEG molecule from cis side of the lumen, failed to generate the current amplitude changes (*7*). The volume occupied by the hydrated PEG molecue in the αHL central cavity would be smaller than the loop of $P115_1W_6$, as the reduction of the conductivity was only ~5% with the PEG 3.4 kDa, whereas it was ~32% with the loop of $P115_1W_6$. Therefore, by threading and stretching out the loop of make more ionic flow through the αHL pore than with the PEG.

As anticipated, the $P206_1W_6$ pore generated unitary high open conductance states (Figure 41), simlar to $L145_1W_6$ and $L215_1W_6$ pore (Figure 28). The pores with these

length (≥ 145 residues) of the polypeptide loop are likely to assemble into the heptamers with most of the inserted loop already threading out through the cis mouth fo the pore. It is supprising to be able to assemble at all, since the amino-latch region, together with stem, is where most conformational changes occur during the pre-pore to the pore transition. It is not determined that the $P115_1W_6$, $L145_1W_6$, and $L215_1W_6$ pores are in the identical conformational state as the wild-type αHL pores. But they formed SDS stable oligomer and pores in the lipid bilayer with the similar size of conductance (Figure 28, 29, 42). It would be entropically unfavorable to wrap back a protruding loop into the confined cavity, as no reversible occurrence of trasient closure was observed for all tested pores. On the contrary, the $P115_1W_6$ pore exhibited frequent reversible occurrence of the transient closed states, even after the loop was stretched out of the lumen due to the binding events. It might suggest that it unfavors to be pulled by PKA catalytic subunit by producing strain force to αHL mainbody of P115 subunit. More detailed study might prove this assumption.

CHAPTER VI

SUMMARY

In the present work, unusual fusion proteins were tested, in which the exogenous polypeptide chain (here, loop) was filled into the empty cavity of αHL pore. To evaluate the capacity of the central lumen with polypeptide chain, tandem repeat of Gly/Ser linker sequence was placed by genetic approaches. With the engineered pores, basal information (length dependence L subunit incorporation to oligomers, dynamics of the Gly/Ser loop assayed with single channel recordings, and topology of the loop with long loop) were obtained. Amazingly, the αHL was able to form heptamers even with 175 residues of exogenous sequence.

Based on these results, temperature-responsive polypeptide (ELP sequence) was introduced to the αHL pore. As the ELP undergoes inverse temperature transition, $E10_1W_6$ pores showed the mostly closed states to the mostly open states. By introducing different residue for guest residue or different length of the loop, the αHL pores can be engineered to gate at different temperatures, or different environmental factors (pH, pressure). These results provide fascinating possibilities to develop a simple pore to a tool for drug delivery or for delivery of cryoprotectants.

Lastly, the possibility to detect analyte from outside of the lumen was demonstrated. Designed PKI fragment (5-24)-containing loop was fluctuating in and out of the αHL lumen reversibly. Upon addition of the PKA catalytic subunits to the cis compartment of the chamber, the interaction with the PKI fragment and the PKA was observed. This result demonstrates that the αHL pores could be engineered with polypeptide based loops to detect the analytes in and out of the pore. For example, the small analytes (20 Å in diameter) could be detected in the lumen, while the large analytes (above 20 Å in diameter) will be detected outside of the lumen.

To extend these projects to the next level, a functional protein (truncated photoactive yellow protein (28-125, 98 residues) was engineered into the αHL gene with short flanking Gly/Ser linkers (3 residues for N-termini, and 14 residues for C-termini of PYP) to located in the αHL central cavity. The number of the total exogenous residues were 115. The photoactive yellow protein (PYP) is covalently attached to a chromophore (p-coumaric acid), which facilitates the study of the chimera protein the folding and the function. The maximum absorbance of the chromophore changes from 335 nm to 450 nm in the light cycle of the native PYP. When the PYP was inserted in the αHL gene between postions 105 and 106, the similar absorbance change (from 315 nm to 432 nm) was observed at the monomeric stage of the chimera protein (PYP-HL), suggesting the fusion into the αHL gene was not interfering with the PYP function. This result stimulated to generate the heteromers of with the PYP-HL subunit and the W subunit. As anticipated, the PYP-HL subunit was incorporated once in the αHL

heptamer, as seen with the $P115_1W_6$ pore reported in chapter IV. Several different approaches were performed to purify the $(PYP\text{-}HP)_1W_6$ heteromers. However there were complications with the purification, since the monomeric chimera protein was aggregating constantly. Currently, the improvement for the purificaion conditions is investigaing. This unfinished work would generate a possibility to convert a substrate to product during the passage through the pore, in future.

REFERENCES

1. Song, L., Hobaugh, M. R., Shustak, C., Cheley, S., Bayley, H., and Gouaux, J. E. (1996) Structure of staphylococcal alpha-hemolysin, a heptameric transmembrane pore, *Science 274*, 1859-66.

2. Montoya, M., and Gouaux, E. (2003) Beta-barrel membrane protein folding and structure viewed through the lens of alpha-hemolysin, *Biochim. Biophys. Acta 1609*, 19-27.

3. Bayley, H., and Cremer, P. S. (2001) Stochastic sensors inspired by biology, *Nature 413*, 226-30.

4. Eroglu, A., Russo, M. J., Bieganski, R., Fowler, A., Cheley, S., Bayley, H., and Toner, M. (2000) Intracellular trehalose improves the survival of cryopreserved mammalian cells, *Nat. Biotechnol. 18*, 163-7.

5. Shin, S. H., Luchian, T., Cheley, S., Braha, O., and Bayley, H. (2002) Kinetics of a reversible covalent-bond-forming reaction observed at the single-molecule level, *Angew. Chem. Int. Ed. Engl. 41*, 3707-9.

6. Walker, B., and Bayley, H. (1995) Restoration of pore-forming activity in staphylococcal alpha-hemolysin by targeted covalent modification, *Protein Eng. 8*, 491-5.

7. Movileanu, L. , Howorka, S., Braha, O., and Bayley, H. (2000) Detecting protein analytes that modulate transmembrane movement of a polymer chain within a single protein pore, *Nat. Biotechnol. 18*, 1091-5.

8. Howorka, S., Movileanu, L., Lu, X., Magnon, M., Cheley, S., Braha, O., and Bayley, H. (2000) A protein pore with a single polymer chain tethered within the lumen, *J. Am. Chem. Soc. 122*, 2411-6.

9. Guillet, V., Roblin, P., Werner, S., Coraiola, M., Menestrina, G., Monteil, H., Prevost, G., and Mourey, L. (2004) Crystal structure of leucotoxin S component: new insight into the staphylococcal beta-barrel pore-forming toxins, *J. Biol. Chem. 279*, 41028-37.

10. Gouaux, E., Hobaugh, M., and Song, L. (1997) alpha-Hemolysin, gamma-hemolysin, and leukocidin from Staphylococcus aureus: distant in sequence but similar in structure, *Protein Sci. 6*, 2631-5.

11. Galdiero, S. , and Gouaux, E. (2004) High resolution crystallographic studies of alpha-hemolysin-phospholipid complexes define heptamer-lipid head group interactions: implication for understanding protein-lipid interactions, *Protein Sci. 13*, 1503-11.

12. Valeva, A., Walev, I., Pinkernell, M., Walker, B., Bayley, H., Palmer, M., and Bhakdi, S. (1997) Transmembrane beta-barrel of staphylococcal alpha-toxin forms in sensitive but not in resistant cells, *Proc. Natl. Acad. Sci. U S A 94*,

11607-11.

13. Valeva, A., Weisser, A., Walker, B., Kehoe, M., Bayley, H., Bhakdi, S., and Palmer, M. (1996) Molecular architecture of a toxin pore: a 15-residue sequence lines the transmembrane channel of staphylococcal alpha-toxin, *EMBO J. 15*, 1857-64.

14. Cheley, S., Malghani, M. S., Song, L., Hobaugh, M., Gouaux, J. E., Yang, J., and Bayley, H. (1997) Spontaneous oligomerization of a staphylococcal alpha-hemolysin conformationally constrained by removal of residues that form the transmembrane beta-barrel, *Protein Eng. 10*, 1433-43.

15. Walker, B., Braha, O., Cheley, S., and Bayley, H. (1995) An intermediate in the assembly of a pore-forming protein trapped with a genetically-engineered switch, *Chem. Biol. 2*, 99-105.

16. Olson, R., Nariya, H., Yokota, K., Kamio, Y., and Gouaux, E. (1999) Crystal structure of staphylococcal LukF delineates conformational changes accompanying formation of a transmembrane channel, *Nat. Struct. Biol. 6*, 134-40.

17. Pedelacq, J. D., Maveyraud, L., Prevost, G., Baba-Moussa, L., Gonzalez, A., Courcelle, E., Shepard, W., Monteil, H., Samama, J. P., and Mourey, L. (1999) The structure of a Staphylococcus aureus leucocidin component (LukF-PV) reveals the fold of the water-soluble species of a family of transmembrane pore-

forming toxins, *Structure Fold Des. 7*, 277-87.

18. Miles, G., Cheley, S., Braha, O., and Bayley, H. (2001) The staphylococcal leukocidin bicomponent toxin forms large ionic channels, *Biochemistry 40*, 8514-22.

19. Walker, B., Krishnasastry, M., Zorn, L., and Bayley, H. (1992) Assembly of the oligomeric membrane pore formed by Staphylococcal alpha-hemolysin examined by truncation mutagenesis, *J. Biol. Chem. 267*, 21782-6.

20. Walker, B., and Bayley, H. (1995) Key residues for membrane binding, oligomerization, and pore forming activity of staphylococcal alpha-hemolysin identified by cysteine scanning mutagenesis and targeted chemical modification, *J. Biol. Chem. 270*, 23065-71.

21. Krishnasastry, M., Walker, B., Braha, O., and Bayley, H. (1994) Surface labeling of key residues during assembly of the transmembrane pore formed by staphylococcal alpha-hemolysin, *FEBS Lett. 356*, 66-71.

22. Walker, B., Kasianowicz, J., Krishnasastry, M., and Bayley, H. (1994) A pore-forming protein with a metal-actuated switch, *Protein Eng. 7*, 655-62.

23. Braha, O., Gu, L. Q., Zhou, L., Lu, X., Cheley, S., and Bayley, H. (2000) Simultaneous stochastic sensing of divalent metal ions, *Nat. Biotechnol. 18*, 1005-7.

24. Gu, L. Q., Braha, O., Conlan, S., Cheley, S., and Bayley, H. (1999) Stochastic sensing of organic analytes by a pore-forming protein containing a molecular adapter, *Nature 398*, 686-90.

25. Gu, L. Q., Cheley, S., and Bayley, H. (2001) Capture of a single molecule in a nanocavity, *Science. 291*, 636-40.

26. Cheley, S., Gu, L. Q., and Bayley, H. (2002) Stochastic sensing of nanomolar inositol 1,4,5-trisphosphate with an engineered pore, *Chem. Biol. 9*, 829-38.

27. Howorka, S., Movileanu, L., Braha, O., and Bayley, H. (2001) Kinetics of duplex formation for individual DNA strands within a single protein nanopore, *Pro.c Natl. Acad. Sci. U S A 98*, 12996-3001.

28. Howorka, S., Nam, J., Bayley, H., and Kahne, D. (2004) Stochastic detection of monovalent and bivalent protein-ligand interactions, *Angew. Chem. Int. Ed. Engl. 43*, 842-6.

29. Cheley, S., Braha, O., Lu, X., Conlan, S., and Bayley, H. (1999) A functional protein pore with a "retro" transmembrane domain, *Protein Sci. 8*, 1257-67.

30. Sanchez-Quesada, J., Saghatelian, A., Cheley, S., Bayley, H., and Ghadiri, M. R. (2004) Single DNA rotaxanes of a transmembrane pore protein, *Angew. Chem. Int. Ed. Engl. 43*, 3063-7.

31. Sandberg, L. B., Soskel, N. T., and Leslie, J. G. (1981) Elastin structure,

biosynthesis, and relation to disease states, *N. Engl. J. Med. 304*, 566-79.

32. Urry, D. W. (1993) Molecular machines - how motion and other functions of living organisms can result from reversible chemical-changes, *Angew. Chem. Int. Ed. Engl. 32*, 819-41.

33. Meyer, D. E. , and Chilkoti, A. (2004) Quantification of the effects of chain length and concentration on the thermal behavior of elastin-like polypeptides, *Biomacromolecules 5*, 846-51.

34. Urry, D. W. (1997) Physical chemistry of biological free energy transduction as demonstrated by elastic protein-based polymers, *J. Phys. Chem. 101*, 11007-28.

35. Yamaoka, T., Tamura, T., Seto, Y., Tada, T., Kunugi, S., and Tirrell, D. A. (2003) Mechanism for the phase transition of a genetically engineered elastin model peptide (VPGIG)40 in aqueous solution, *Biomacromolecules 4*, 1680-5.

36. Gosline, J. M., and French, C. J. (1979) Dynamic mechanical properties of elastin, *Biopolymers 18*, 2091-103.

37. Li, B., and Daggett, V. (2003) The molecular basis of the temperature- and pH-induced conformational transitions in elastin-based peptides, *Biopolymers 68*, 121-9.

38. Urry, D. W., Gowda, D. C., Parker, T. M., Luan, C. H., Reid, M. C., Harris, C. M., Pattanaik, A., and Harris, R. D. (1992) Hydrophobicity scale for proteins

based on inverse temperature transitions, *Biopolymers 32*, 1243-50.

39. Meyer, D. E. , and Chilkoti, A. (2002) Genetically encoded synthesis of protein-based polymers with precisely specified molecular weight and sequence by recursive directional ligation: examples from the elastin-like polypeptide system, *Biomacromolecules 3*, 357-67.

40. Urry, D. W. (1992) Free energy transduction in polypeptides and proteins based on inverse temperature transitions, *Prog. Biophys. Mol. Biol. 57*, 23-57.

41. Urry, D. W., Haynes, B., and Harris, R. D. (1986) Temperature dependence of length of elastin and its polypentapeptide, *Biochem. Biophys. Res. Commun. 141*, 749-55.

42. Luan, C. H., Parker, T. M., Prasad, K. U., and Urry, D. W. (1991) Differential scanning calorimetry studies of NaCl effect on the inverse temperature transition of some elastin-based polytetra-, polypenta-, and polynonapeptides, *Biopolymers 31*, 465-75.

43. Urry, D. W., Hayes, L. C., Gowda, D. C., Harris, C. M., and Harris, R. D. (1992) Reduction-driven polypeptide folding by the delta Tt mechanism, *Biochem. Biophys. Res. Commun. 188*, 611-7.

44. Trabbic-Carlson, K., Liu, L., Kim, B., and Chilkoti, A. (2004) Expression and purification of recombinant proteins from Escherichia coli: comparison of an

elastin-like polypeptide fusion with an oligohistidine fusion, *Protein Sci. 13*, 3274-84.

45. Urry, D. W. (1999) Elastic molecular machines in metabolism and soft-tissue restoration, *Trends Biotechnol. 17*, 249-57.

46. Meyer, D. E. , Kong, G. A., Dewhirst, M. W., Zalutsky, M. R., and Chilkoti, A. (2001) Targeting a genetically engineered elastin-like polypeptide to solid tumors by local hyperthermia, *Cancer Res. 61*, 1548-54.

47. Chilkoti, A., Dreher, M. R., and Meyer, D. E. (2002) Design of thermally responsive, recombinant polypeptide carriers for targeted drug delivery, *Adv. Drug Deliv. Rev. 54*, 1093-111.

48. Gill, G. N., and Garren, L. D. (1970) A cyclic-3',5'-adenosine monophosphate dependent protein kinase from the adrenal cortex: comparison with a cyclic AMP binding protein, *Biochem. Biophys. Res. Commun. 39*, 335-43.

49. Hauer, J. A., Barthe, P., Taylor, S. S., Parello, J., and Padilla, A. (1999) Two well-defined motifs in the cAMP-dependent protein kinase inhibitor (PKIalpha) correlate with inhibitory and nuclear export function, *Protein Sci. 8*, 545-53.

50. Wen, W., Taylor, S. S., and Meinkoth, J. L. (1995) The expression and intracellular distribution of the heat-stable protein kinase inhibitor is cell cycle regulated, *J. Biol. Chem. 270*, 2041-6.

51. Tash, J. S., Welsh, M. J., and Means, A. R. (1980) Protein inhibitor of cAMP-dependent protein kinase: production and characterization of antibodies and intracellular localization, *Cell 21*, 57-65.

52. Whitehouse, S., and Walsh, D. A. (1983) Mg X ATP2-dependent interaction of the inhibitor protein of the cAMP-dependent protein kinase with the catalytic subunit, *J. Biol. Chem. 258*, 3682-92.

53. Herberg, F. W., and Taylor, S. S. (1993) Physiological inhibitors of the catalytic subunit of cAMP-dependent protein kinase: effect of MgATP on protein-protein interactions, *Biochemistry 32*, 14015-22.

54. Herberg, F. W., Doyle, M. L., Cox, S., and Taylor, S. S. (1999) Dissection of the nucleotide and metal-phosphate binding sites in cAMP-dependent protein kinase, *Biochemistry 38*, 6352-60.

55. Zheng, J., Knighton, D. R., ten Eyck, L. F., Karlsson, R., Xuong, N., Taylor, S. S., and Sowadski, J. M. (1993) Crystal structure of the catalytic subunit of cAMP-dependent protein kinase complexed with MgATP and peptide inhibitor, *Biochemistry 32*, 2154-61.

56. Zheng, J. H. , Knighton, D. R., Xuong, N. H., Parello, J., Taylor, S. S., and Sowadski, J. M. (1992) Crystallization studies of the catalytic subunit of cAMP-dependent protein kinase: crystals of murine recombinant catalytic subunit and a mutant, Cys 343-Ser, diffract to 2.7 A resolution, *Acta Crystallogr. B 48*, 241-4.

57. Prade, L., Engh, R. A., Girod, A., Kinzel, V., Huber, R., and Bossemeyer, D. (1997) Staurosporine-induced conformational changes of cAMP-dependent protein kinase catalytic subunit explain inhibitory potential, *Structure 5*, 1627-37.

58. Hauer, J. A., Taylor, S. S., and Johnson, D. A. (1999) Binding-dependent disorder-order transition in PKI alpha: a fluorescence anisotropy study, *Biochemistry 38*, 6774-80.

59. Scott, J. D., Fischer, E. H., Demaille, J. G., and Krebs, E. G. (1985) Identification of an inhibitory region of the heat-stable protein inhibitor of the cAMP-dependent protein kinase, *Proc. Natl. Acad. Sci. U S A 82*, 4379-83.

60. Cheng, H. C., Kemp, B. E., Pearson, R. B., Smith, A. J., Misconi, L., Van Patten, S. M., and Walsh, D. A. (1986) A potent synthetic peptide inhibitor of the cAMP-dependent protein kinase, *J. Biol. Chem. 261*, 989-92.

61. Xie, H., Braha, O., Gu, L. Q., Cheley, S., and Bayley, H. (2005) Single-Molecule Observation of the Catalytic Subunit of cAMP-Dependent Protein Kinase Binding to an Inhibitor Peptide, *Chem. Biol. 12*, 109-20.

62. Murray, P. R., Rosenthall, K. S., Kobayashi, G. S., and Pfaller, M. A. (2002) *Medical Microbiology*, Fourth edition, Mosby, St. Louis.

63. Honeyman, A. L., Friedman, H., and Bendinelli, M. (2001) *Staphylococcus*

aureus Infection and Disease, First edition, Kluwer Academic/ Plenum Publishers, New York.

64. Rogolsky, M. (1979) Nonenteric toxins of Staphylococcus aureus, *Microbiol. Rev. 43*, 320-60.

65. Foster, T. J. (2004) The Staphylococcus aureus "superbug", *J. Clin. Invest. 114*, 1693-6.

66. Fey, P. D., Said-Salim, B., Rupp, M. E., Hinrichs, S. H., Boxrud, D. J., Davis, C. C., Kreiswirth, B. N. , and Schlievert, P. M. (2003) Comparative molecular analysis of community- or hospital-acquired methicillin-resistant Staphylococcus aureus, *Antimicrob. Agents Chemother. 47* , 196-203.

67. Balaban, N., Giacometti, A., Cirioni, O., Gov, Y., Ghiselli, R., Mocchegiani, F., Viticchi, C., Del Prete, M. S., Saba, V., Scalise, G., and Dell'Acqua, G. (2003) Use of the quorum-sensing inhibitor RNAIII-inhibiting peptide to prevent biofilm formation in vivo by drug-resistant Staphylococcus epidermidis, *J. Infect. Dis. 187*, 625-30.

68. Costerton, J. W., Stewart, P. S., and Greenberg, E. P. (1999) Bacterial biofilms: a common cause of persistent infections, *Science 284*, 1318-22.

69. Leid, J. G., Shirtliff, M. E., Costerton, J. W., and Stoodley, A. P. (2002) Human leukocytes adhere to, penetrate, and respond to Staphylococcus aureus biofilms,

Infect. Immun. 70, 6339-45.

70. Parker, M. W., Pattus, F., Tucker, A. D., and Tsernoglou, D. (1989) Structure of the membrane-pore-forming fragment of colicin A, *Nature 337*, 93-6.

71. Li, J. D., Carroll, J., and Ellar, D. J. (1991) Crystal structure of insecticidal delta-endotoxin from Bacillus thuringiensis at 2.5 A resolution, *Nature 353*, 815-21.

72. Choe, S., Bennett, M. J., Fujii, G., Curmi, P. M., Kantardjieff, K. A., Collier, R. J., and Eisenberg, D. (1992) The crystal structure of diphtheria toxin, *Nature 357*, 216-22.

73. Minn, A. J., Velez, P., Schendel, S. L., Liang, H., Muchmore, S. W., Fesik, S. W., Fill, M., and Thompson, C. B. (1997) Bcl-x(L) forms an ion channel in synthetic lipid membranes, *Nature 385*, 353-7.

74. Parker, M. W., Buckley, J. T., Postma, J. P., Tucker, A. D., Leonard, K., Pattus, F., and Tsernoglou, D. (1994) Structure of the Aeromonas toxin proaerolysin in its water-soluble and membrane-channel states, *Nature 367*, 292-5.

75. Li, J., Koni, P. A., and Ellar, D. J. (1996) Structure of the mosquitocidal delta-endotoxin CytB from Bacillus thuringiensis sp. kyushuensis and implications for membrane pore formation, *J. Mol. Biol. 257*, 129-52.

76. Lindeberg, M., Zakharov, S. D., and Cramer, W. A. (2000) Unfolding pathway of the colicin E1 channel protein on a membrane surface, *J. Mol. Biol. 295*, 679-

92.

77. Tosteson, D. C., Cook, P., Andreoli, T., and Tieffenberg, M. (1967) The effect of valinomycin on potassium and sodium permeability of HK and LK sheep red cells, *J. Gen. Physiol. 50*, 2513-25.

78. Pinkerton, M., Steinrauf, L. K., and Dawkins, P. (1969) The molecular structure and some transport properties of valinomycin, *Biochem. Biophys. Res. Commun. 35*, 512-8.

79. Ohnishi, M., Fedarko, M. C., and Baldeschwieler, J. D. (1972) Fourier transform C-13 NMR analysis of some free and potassium-ion complexed antibiotics, *Biochem. Biophys. Res. Commun. 46*, 312-20.

80. Urry, D. W., and Kumar, N. G. (1974) Affirmation of critical proton magnetic resonance data on the solution conformation of the valinomycin-potassium ion complex, *Biochemistry 13*, 1829-31.

81. Duax, W. L., Langs, D. A., Pangborn, W. A., Smith, G. D., Pletnev, V. Z., and Ivanov, V. T. (1989) Molecular conformation and ion transport of cyclic and linear ionophores, *J. Mol. Graph. 7*, 82-6.

82. Pressman, B. C. (1965) Induced active transport of ions in mitochondria, *Proc. Natl. Acad. Sci. U S A 53*, 1076-83.

83. Kovacs, F., Quine, J., and Cross, T. A. (1999) Validation of the single-stranded

channel conformation of gramicidin A by solid-state NMR, *Proc. Natl. Acad. Sci. U S A 96*, 7910-5.

84. Klebe, R. J., Harriss, J. V., Sharp, Z. D., and Douglas, M. G. (1983) A general method for polyethylene-glycol-induced genetic transformation of bacteria and yeast, *Gene 25*, 333-41.

85. Howorka, S., and Bayley, H. (2002) High-throughput scanning mutagenesis by recombination polymerase chain reaction , *Methods Mol. Biol. 182*, 139-47.

86. Walker, B., Krishnasastry, M., Zorn, L., Kasianowicz, J., and Bayley, H. (1992) Functional expression of the alpha-hemolysin of Staphylococcus aureus in intact Escherichia coli and in cell lysates. Deletion of five C- terminal amino acids selectively impairs hemolytic activity, *J. Biol. Chem. 267*, 10902-9.

87. Howorka, S., Cheley, S., and Bayley, H. (2001) Sequence-specific detection of individual DNA strands using engineered nanopores, *Nat. Biotechnol. 19*, 636-9.

88. Hartley, J. L., and Gregori, T. J. (1981) Cloning multiple copies of a DNA segment, *Gene 13*, 347-53.

89. Liaw, G. J. (1994) Improved protocol for directional multimerization of a DNA fragment, *Biotechniques 17*, 668-70.

90. Kellogg, D. E., Rybalkin, I., Chen, S., Mukhamedova, N., Vlasik, T., Siebert, P. D., and Chenchik, A. (1994) TaqStart antibody: "hot start" PCR facilitated by a

neutralizing monoclonal antibody directed against Taq DNA polymerase, *Biotechniques 16*, 1134-7.

91. Shuman, S. (1994) Novel approach to molecular cloning and polynucleotide synthesis using vaccinia DNA topoisomerase, *J. Biol. Chem. 269*, 32678-84.

92. Laemmli, U. K. (1970) Cleavage of structural proteins during the assembly of the head of bacteriophage T4, *Nature 227*, 680-5.

93. Miles, G., Movileanu, L., and Bayley, H. (2002) Subunit composition of a bicomponent toxin: staphylococcal leukocidin forms an octameric transmembrane pore, *Protein Sci. 11*, 894-902.

94. Montal, M., and Mueller, P. (1972) Formation of bimolecular membranes from lipid monolayers and a study of their electrical properties, *Proc. Natl. Acad. Sci. U. S. A. 69*, 3561-6.

95. Christopher, J. A. (1998) *SPOCK: The Structural Properties Observation and Calculation Kit (Program* Manual), Version 6.3, Center for Macromolecular Design, Texas A&M University, College Station, TX.

96. Guex, N., and Peitsch, M. C. (1997) SWISS-MODEL and the Swiss-PdbViewer: an environment for comparative protein modeling, *Electrophoresis 18*, 2714-23.

97. Movileanu, L., Cheley, S., Howorka, S., Braha, O., and Bayley, H. (2001) Location of a constriction in the lumen of a transmembrane pore by targeted

covalent attachment of polymer molecules, *J. Gen. Physiol. 117*, 239-52.

98. Chang, C. Y., Niblack, B., Walker, B., and Bayley, H. (1995) A photogenerated pore-forming protein, *Chem. Biol. 2*, 391-400.

99. Kawate, T., and Gouaux, E. (2003) Arresting and releasing Staphylococcal alpha-hemolysin at intermediate stages of pore formation by engineered disulfide bonds, *Protein Sci. 12*, 997-1006.

100. Panchal, R. G., and Bayley, H. (1995) Interactions between residues in staphylococcal alpha-hemolysin revealed by reversion mutagenesis, *J. Biol. Chem. 270*, 23072-6.

101. Huang, F., and Nau, W. M. (2003) A conformational flexibility scale for amino acids in peptides, *Angew. Chem. Int. Ed. Engl. 42*, 2269-72.

102. Blachinsky, E., Marbach, I., Cohen, R., Grably, M. R., and Engelberg, D. (2004) Procedure for controlling number of repeats, orientation, and order during cloning of oligonucleotides, *Biotechniques 36*, 933-6.

103. Wright, E. R., and Conticello, V. P. (2002) Self-assembly of block copolymers derived from elastin-mimetic polypeptide sequences, *Adv. Drug Deliv. Rev. 54*, 1057-73.

104. Kuyucak, S., and Chung, S. H. (1994) Temperature dependence of conductivity in electrolyte solutions and ionic channels of biological membranes, *Biophys.*

Chem. 52, 15-24.

VITA

Yun Hee Jung
Department of Medical Biochemistry and Genetics
440 Joe H. Reynolds Medical Building
1114 TAMU
College Station, TX 77843

Education

Ph.D.	Medical Biochemistry and Genetics Texas A&M University System Health Science Center College Station, Texas Dissertation Advisor: Dr. Hagan Bayley	1999-2005
M.S.	Agricultural Chemistry College of Life Science and Agriculture Seoul National University Republic of Korea	1993-1995
B.S.	Agricultural Biology College of Life Science and Agriculture Seoul National University Republic of Korea	1989-1993